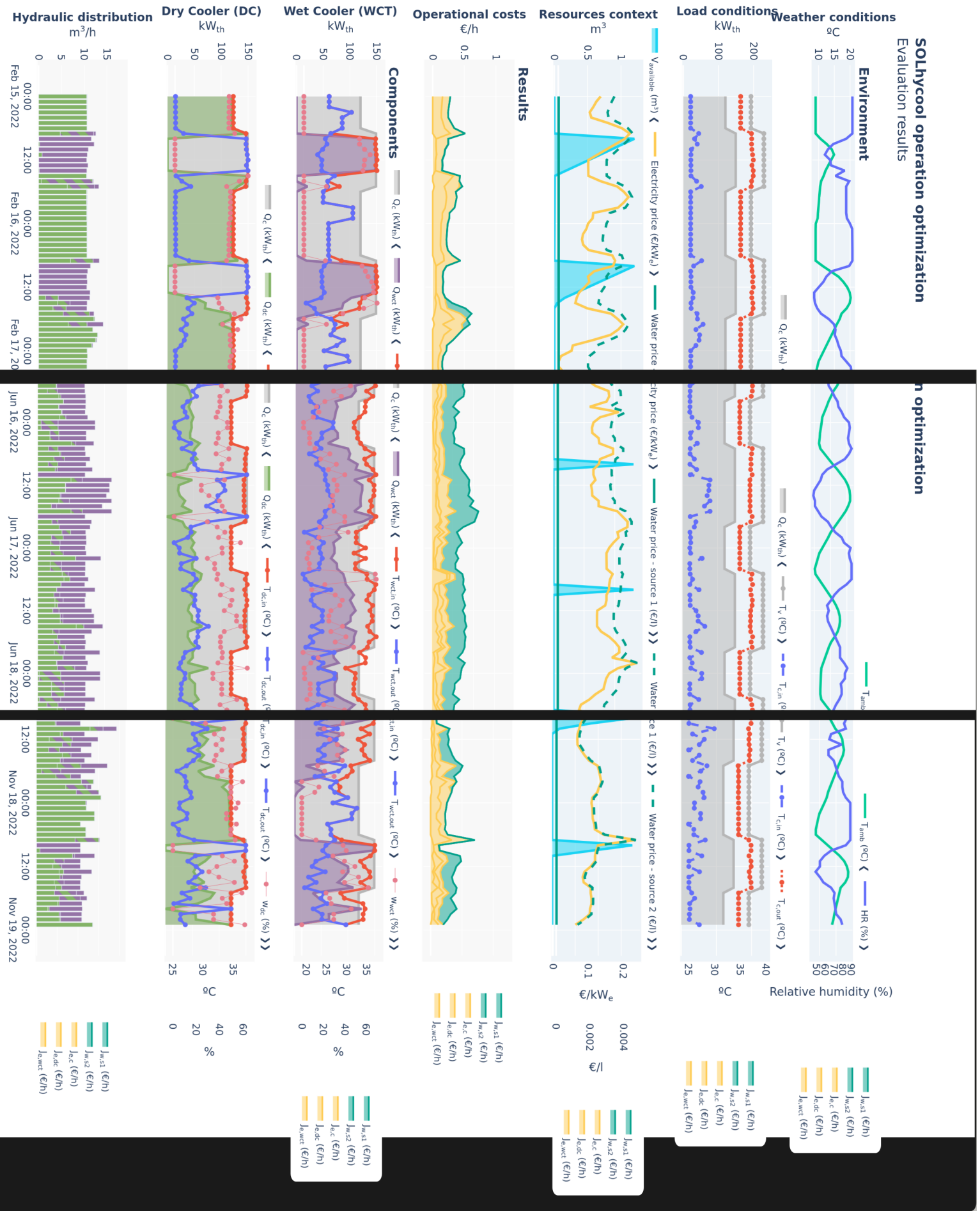




Esta sección no está terminada. Siquieres puedes echarle un ojo para ver la estructura y cómo encaja con el resto pero no merece la pena revisarla en detalle en el estado actual.

SOHycool operation optimization

Evaluation results



Model 0.1: Test

$T_{cc,out}, C_e, C_w, T_{c,out} = \text{combined cooler model}(q_c, R_p, R_s, \omega_{dc}, \omega_{wct}, T_{amb}, HR_i, T_v, \dot{m}_v)$
 $T_{cc,in} = T_{c,out}$
 $T_{dc,in} = T_{cc,in}$
 $q_{dc} = q_c \cdot (1 - R_p)$
 $q_{wct,p} = q_c \cdot R_p$
 $q_{wct,s} = q_{dc} \cdot R_s$
 $T_{dc,out}, C_{e,dc} = \text{dc model}(q_{dc}, \omega_{dc}, T_{amb}, T_{dc,in})$
 $q_{wct}, T_{wct,in} = \text{mixer model}(q_{wct,p}, T_{cc,in}, q_{wct,s}, T_{dc,out})$
 $T_{wct,out}, C_{e,wct}, C_{w,wct} = \text{wct model}(q_{wct}, \omega_{wct}, T_{amb}, HR, T_{wct,in})$
 $T_{c,in}, T_{c,out} = \text{condenser model}(q_c, \dot{m}_v, T_v)$
 $q_{cc}, T_{cc,out} = \text{mixer model}(q_{wct}, T_{wct,out}, q_{dc}, T_{dc,out})$
 $C_e = C_{e,dc} + C_{e,wct} + C_{e,c}$
 $C_w = C_{w,wct}$

As can be seen in Model 0.1, the counter is working.

Problem .1: Test

Hello, here is some text without a meaning. This text should show what a printed text will look like at this place. If you read this text, you will get no information. Really? Is there no information? Is there a difference between this text and some nonsense like "Huardest gefburn"? Kjift – not at all! A blind text like this gives you information about the selected font, how the letters are written and an impression of the look. This text should contain all letters of the alphabet and it should be written in of the original language. There is no need for special content, but the length of words should match the language.

$$\min_{\mathbf{x}, \mathbf{e}; \theta} J = f(\mathbf{x}, \mathbf{e}; \theta) = f(x)$$

with:

- Model name model

$$out_1, out_2 = f(in_1, in_2, \dots, in_N)$$

- Decision variables

$$\mathbf{x} = [x_1, x_2]$$

- Environment variables

$$\mathbf{e} = [e_1, e_2, \dots, e_3]$$

- Fixed parameters

$$\theta = [\theta_1 = X, \theta_2 = Y]$$

subject to:

- Box-bounds

$$\cdot x_1 \in [\underline{x}_1, \bar{x}_1]$$

- $x_2 \in [\underline{x}_2, \bar{x}_2]$
- Constraints
 - $|out_X - out_Y| \leq \epsilon_1$
 - $out_X \leq out_Z - \Delta Z$

As can be seen in Problem .1, the counter is working.

TL;DR

test test

Problem: Test

$$\min_{\mathbf{x}, \mathbf{e}; \theta} J = f(\mathbf{x}, \mathbf{e}; \theta) = f(x)$$

with:

- Model name model
 - $out_1, out_2 = f(in_1, in_2, \dots, in_N)$
- Decision variables
 - $\mathbf{x} = [x_1, x_2]$
- Environment variables
 - $\mathbf{e} = [e_1, e_2, \dots, e_3]$
- Fixed parameters
 - $\theta = [\theta_1 = X, \theta_2 = Y]$

subject to:

- Box-bounds
 - $x_1 \in [\underline{x}_1, \bar{x}_1]$
 - $x_2 \in [\underline{x}_2, \bar{x}_2]$
- Constraints
 - $|out_X - out_Y| \leq \epsilon_1$
 - $out_X \leq out_Z - \Delta Z$

the heat definition of efficiency

In process heat driven system, plants that produce the same final product, the most efficient one that uses the least amount of heat. While given two plants that produce the same amount of waste heat, the one is the one that produces given that heat.

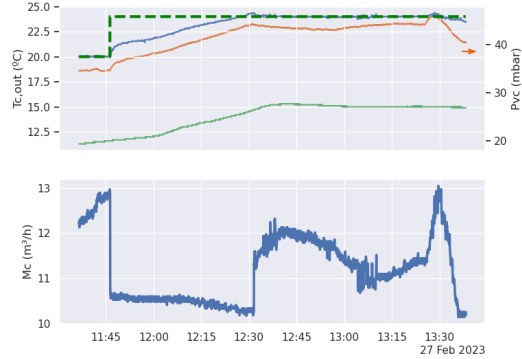
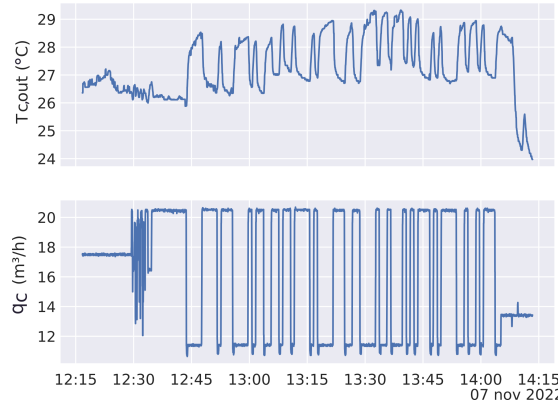


Figure 2: Condenser outlet temperature control implementation. To tune the controller, the system was excited with a PRBS signal. An ARX model ($n_a = 20$, $n_b = 4^{\text{th}}$ order fit) was extracted in MATLAB, which allowed to extract the first-order dynamic with which to tune the controller.

The kaobook class

PhD Thesis

**Towards optimal resource management in solar thermal applications:
desalination and CSP**

Juan Miguel Serrano Rodríguez

July 2, 2025

University of Almería

The kaobook class

Disclaimer

You can edit this page to suit your needs. For instance, here we have a no copyright statement, a colophon and some other information. This page is based on the corresponding page of Ken Arroyo Ohori's thesis, with minimal changes.

No copyright

 This book is released into the public domain using the CC0 code. To the extent possible under law, I waive all copyright and related or neighbouring rights to this work.

To view a copy of the CC0 code, visit:

<http://creativecommons.org/publicdomain/zero/1.0/>

Colophon

This document was typeset with the help of KOMA-Script and \LaTeX using the kaobook class.

The source code of this book is available at:

<https://github.com/fmarotta/kaobook>

(You are welcome to contribute!)

Publisher

First printed in May 2019 by University of Almería

The harmony of the world is made manifest in Form and Number, and the heart and soul and all the poetry of Natural Philosophy are embodied in the concept of mathematical beauty.

– D'Arcy Wentworth Thompson

Acknowledgements

Test test test

Federico Marotta

Summary

I am of the opinion that every \LaTeX geek, at least once during his life, feels the need to create his or her own class: this is what happened to me and here is the result, which, however, should be seen as a work still in progress. Actually, this class is not completely original, but it is a blend of all the best ideas that I have found in a number of guides, tutorials, blogs and tex.stackexchange.com posts. In particular, the main ideas come from two sources:

- ▶ [Ken Arroyo Ohori's Doctoral Thesis](#), which served, with the author's permission, as a backbone for the implementation of this class;
- ▶ The [Tufte-Latex Class](#), which was a model for the style.

The first chapter of this book is introductory and covers the most essential features of the class. Next, there is a bunch of chapters devoted to all the commands and environments that you may use in writing a book; in particular, it will be explained how to add notes, figures and tables, and references. The second part deals with the page layout and design, as well as additional features like coloured boxes and theorem environments.

I started writing this class as an experiment, and as such it should be regarded. Since it has always been intended for my personal use, it may not be perfect but I find it quite satisfactory for the use I want to make of it. I share this work in the hope that someone might find here the inspiration for writing his or her own class.

Resumen

Contents

Acknowledgements	v
Summary	vii
Resumen	ix
Contents	xi
How to read this thesis	1
About the author	3
INTRODUCTION	5
1 Context and motivation	7
2 Modelling overview	9
2.1 Performance metrics	9
2.2 First principle modelling	9
2.3 Data-driven modelling	9
2.3.1 Gaussian Process Regression	10
2.3.2 Artificial Neural networks	10
2.3.3 Random Forest	12
2.3.4 Gradient Boosting	12
2.4 Hybrid modelling	12
2.5 Data-driven from first-principles models. Sample generation	12
3 Sensitivity analysis	13
4 Control overview	15
4.1 PID controllers	15
4.2 Hierarchical control	15
5 Optimization overview	17
5.1 NLP problems	17
5.2 MINLP problems	17
5.3 Multi-objective optimization	17
5.4 Optimization algorithms	17
6 Research plan	19
6.1 Hypothesis	19
6.2 Objectives	19
7 Contributions	21
OPTIMAL WATER AND ELECTRICITY MANAGEMENT IN A COMBINED COOLING SYSTEM	23
Derived scientific contributions	25
8 CSP overview	27
8.1 Cooling and water use	27
9 Modelling of a combined cooling system	29
9.1 Wet cooler	29
9.1.1 Poppe model	30
9.1.2 Samples generation for first-principles to data-driven models	32
9.1.3 Model interface	32

9.2	Dry cooler	33
9.2.1	Physical model	33
9.2.2	Samples generation for first-principles to data-driven models	33
9.2.3	Model interface	33
9.3	Other components	34
9.3.1	Electrical consumption	34
9.3.2	Surface condenser	34
9.3.3	Mixers	35
9.4	Complete system	35
10	Optimization of a combined cooling system	37
10.1	Environment definition	37
10.2	Static optimization	38
10.2.1	Dry cooler	39
10.2.2	Wet cooler	39
10.2.3	Combined cooler	40
10.3	Horizon optimization	41
10.3.1	A discussion on solving the optimization problem	42
10.3.2	Proposed solution: Decomposition-based multi-objective optimization with trajectory planning	43
11	Combined cooling pilot plant at Plataforma Solar de Almería	47
11.1	Plant description	48
11.2	Experimental campaigns	49
11.3	Experimental campaigns for the wet cooling tower	49
11.3.1	Experimental campaign 1	49
11.3.2	Experimental campaign 2	50
11.3.3	Experimental campaign 3	51
11.3.4	Experimental campaigns for the dry cooler	51
12	Validation in the combined cooling pilot plant	53
12.1	Modelling	53
12.1.1	Wet cooler model alternatives comparison and validation	53
12.1.2	Dry cooler model alternatives comparison and validation	54
12.1.3	Main components modelling conclusions	57
12.1.4	Condenser model validation	59
12.1.5	Complete system model validation	60
12.2	Control and optimization results	62
12.2.1	Choosing an optimization algorithm	62
12.2.2	Comparing the static and horizon optimization strategies	63
12.2.3	Validation at pilot plant	64
13	Annual analysis: ANDASOL-II CSP plant	67
13.1	Limitations	67
13.2	Environment definition	68
13.2.1	Water context	68
13.2.2	Thermal load	68
13.2.3	Costs context	69
13.3	Optimization strategies comparison	69
13.4	Alternatives comparison	72
ENERGY MANAGEMENT IN MED PROCESSES DRIVEN BY VARIABLE ENERGY SOURCES	75	
Derived scientific contributions	77	
14	Thermal desalination	79
15	SolarMED pilot plant	81
15.1	Heat generation and storage subsystem	81
15.2	Separation subsystem	81
16	Performance evaluation in Multi-Effect Distillation (MED) processes: standard methodology proposal	85
16.1	Process analysis	87

16.2	Performance metrics	88
16.2.1	Separation metrics	88
16.2.2	Energetic metrics	89
16.2.3	Exergetic metrics	90
16.3	Instrumentation	92
16.3.1	Key process variables	92
16.3.2	Instrumentation requirements	93
16.3.3	Uncertainty determination	94
16.4	Monitoring and process control	95
16.4.1	Monitoring: steady-state identification	95
16.4.2	Control system	95
16.5	Methodology application in an experimental campaign	97
16.5.1	Implementation results	98
16.5.2	Results analysis	102
CONCLUSIONS AND OUTLOOK		105
	Conclusions	107
	Outlook and future work	107
	Derived scientific contributions	107
Bibliography		109

List of Figures

1	A rotated figure	2
2	Condenser outlet temperature controller implementation	5
3	Example figure. Try clicking or scanning the QR code to access the interactive version. [1ex]	1
1.1	Aerial view of the pilot plants at the Plataforma Solar de Almería (PSA), Spain. The developments presented in this thesis have been developed and validated around two test-rigs: a Combined Cooling System (CCS) and a Solar-driven Multi-Effect Distillation (SolarMED) pilot plants. In the picture, the CCS plant is located on the left side, and the...	8
2.1	ANN model configurations	10
2.2	Considered ANN architectures	11
7.1	Results for the analyzed case study in this part. The first bar plot compares the specific cost of the different cooling alternatives (lower is better). The second pie chart shows the breakdown of the costs, and the third and fourth pie charts show the cooling power distribution between Dry Cooler (DC) and Wet Cooling Tower (WCT) and the hydraulic distribution, respectively.	25
9.1	Control volume in the exchange area of a wet cooling tower arrangement.	31
9.2	Inputs-outputs block diagram of the main model components	35
9.3	Complete model diagram of the combined cooling system	36
10.1	Block diagram of the optimization scheme including environment components	37
10.2	Diagram of the dry cooler only cooling problem	39
10.3	Diagram of the wet cooler only cooling problem	40
10.4	Diagram of the combined cooler and condenser problem	41
10.5	Pareto front for a particular problem instance of the combined cooler optimization problem.	41
10.6	Visualization of a constrained search space for two decision variables	42
10.7	Proposed methodology. Decomposition-based multi-objective optimization with trajectory planning	44
11.1	PSA combined cooling system facility	47
11.2	Back view of the WCT	48
11.3	Layout of combined cooling systems pilot plant at PSA.	48
11.4	Example of one experiment at the pilot plant in July with two valid steady-state operating points.	50
12.1	Calibration, tuning, validation and comparison procedure	53
12.2	Experimental results for the Me number as a function of m_w/m_a	54
12.3	WCT samples distribution visualization	55
12.4	WCT Models performance regression	56
12.5	DC samples distribution visualization	57
12.6	DC Models performance regression	58
12.7	Heat transfer coefficient calibration results	59
12.8	Figure caption	61
12.9	Horizon optimization – path selection subproblem. Fitness evolution comparison for four different dates.	63
12.10	Detailed timeseries simulation results. Combined Cooler (CC)-horizon	64
12.11	Implementation of the optimization strategy in the real facility. Hierarchical control	65
13.1	Andasol I, II and III	67
13.2	Spanish electricity mix on July 12, 2024. The peak in photovoltaic generation is clearly visible at midday, while thermosolar generation is more evenly distributed throughout the day. Peak production is majorly from CSP plants with no storage. Data source: Figure elaborated using data extracted from https://www.ree.es/es/datos	68
13.3	A rotated figure	70
13.4	A rotated figure	71
13.5	Annual simulation results for the CC system optimized with static optimization. Results are resampled every 15 days using their mean values. The original frequency results can be found in the interactive version: [1ex]	73

15.1	SolarMED process diagram	81
15.2	MED plant at PSA with open effects for maintenance	82
15.3	83
16.1	Inputs and outputs variables in an MED process. The dash line delimits the control volume	88
16.2	Piping and Instrumentation Diagram (P&ID) with the required instrumentation, Key Process Variables (KPVs), and basic control loops (ANSI/ISA 5.1-2022) required in an MED plant	93
16.3	Sensitivity index results for different variables. Useful to assess the impact of the different measured variables uncertainty on the performance metrics.	94
16.4	Diagram of the steady-state identification procedure	96
16.5	97
16.6	Ryznar Stability Index (RSI) values as a function of temperature and concentration before (left) and after (right) pre-treatment using nanofiltration.	98
16.7	Flowchart of finite state machines for plant start-up (left) and shutdown (right)	99
16.8	Condenser outlet temperature controller implementation	100
16.9	101
16.10	Temperature and concentration evolution for operation points at each effect in the MED plant. Surface represents the RSI.	103
16.11	Per effect comparison between low and high Top Brine Temperature (TBT) operation points	103

List of Tables

1	MED plant at PSA specifications and nominal operating conditions	2
11.1	Characteristics of instrumentation (^a value of the temperature in °C, ^b of reading, ^c full scale, ^d mean value).	48
11.2	Design of experiments for model comparison.	51
12.1	Bounds and discretization of the model input variables.	54
12.2	Summary table of the prediction results obtained with the different modelling approaches studied.	56
12.3	Bounds and discretization of the model input variables.	57
12.4	Summary table of the prediction results obtained with the different modelling approaches studied.	58
12.5	Static optimization algorithm comparison results	63
12.6	Box-bounds for the decision variables.	65
13.1	ANDASOL-II plant main characteristics	67
15.1	MED plant at PSA specifications and nominal operating conditions	82
15.2	Characteristics of the instrumentation installed at MED-PSA unit (^a value of the measured temperature in °C, ^b of reading, ^c full scale).	83
16.1	RSI values and their interpretation in terms of scaling and corrosion risk [78].	97
16.2	Experimental campaign design specifications	98
16.3	Measured variables and performance metrics for some operation points of the experimental campaign. The values are expressed as mean ± standard deviation with a coverage factor of 2 (95% confidence interval). D is the duration of the steady state period.	102

List of Listings

How to read this thesis

TL;DR

This preliminary chapter explains how to read this thesis, mainly the different environment boxes used throughout the manuscript, why the large margins, what is placed in them, and how to use the interactive features of the manuscript. This is an example of a Too Long; Didn't Read (TL;DR) box. It contains an Abstract/Summary of the main point of the chapter and are placed at the beginning of every chapter.

This \LaTeX template is designed with large margins, on the one hand this allows to have shorter lines, which makes for an easier reading experience but most interestingly, it also allows to place additional information in the margins, such as side notes, side citations, figures, tables... your imagination is the limit! Or rather \LaTeX compilation errors and your patience are. Throughout this manuscript I will add side notes¹ to provide additional information and comments that would otherwise be too distracting and verbose to include in the main text, constantly interrupting the flow of the reading. The side notes are not essential to understand the content of the document, but mostly complementary.

1: Like this one! They are like footnotes, but placed in the margin of the page

Boxed environments

Both problem definition boxes (e.g. ref) and model definition boxes (e.g. Model 0.2) are countered environments and can (and will) be referenced in the text.

Problem: Problem definition box example

This is an example of a problem definition box. It is used to formally and concisely define an optimization problem.

$$\min_{\mathbf{x}, \mathbf{e}; \theta} J = f(\mathbf{x}, \mathbf{e}; \theta) = \text{XXXX}$$

with:

$$\begin{aligned} \text{out}_1, \text{out}_2 &= f(\text{in}_1, \text{in}_2, \dots, \text{in}_N) \\ \text{out}_1, \text{out}_2 &= f(\text{in}_1, \text{in}_2, \dots, \text{in}_N) \end{aligned}$$

- ▶ Decision variables

$$\mathbf{x} = [x_1, x_2]$$

- ▶ Environment variables

$$\mathbf{e} = [e_1, e_2, \dots, e_3]$$

- ▶ Fixed parameters

$$\theta = [\theta_1 = X, \theta_2 = Y]$$

subject to:

- ▶ Box-bounds

$$\begin{aligned} \cdot x_1 &\in [x_1, \bar{x}_1] \\ \cdot x_2 &\in [x_2, \bar{x}_2] \end{aligned}$$

- ▶ Constraints



Figure 3: Example figure. Try clicking or scanning the QR code to access the interactive version.



Table 1: MED plant at PSA specifications and nominal operating conditions

Parameter	Value
Capacity	72 m ³ /day
Number of effects	14
Feed type	Forward feed
Physical arrangement	Vertically stacked
Heat exchanger configuration	90/10 Cu-Ni HTE
Heat source type	Hot water
Top Brine Temperature (TBT)	70 °C
Condenser temperature	35 °C

2: I believe that this is a good way to make the document more accessible and to encourage readers to explore the content in more depth. However, the interactive features are optional and not necessary to understand the content of the document.



3:

¶: Like hoarding toilet paper

- $|out_X - out_Y| \leq \epsilon_1$
- $out_X \leq out_Z - \Delta Z$

Model 0.2: Model definition box example

$out_1, out_2 = \text{some cool model}(in_1, in_2, in_3)$

Other boxes

Other boxes are used to highlight important points, or to provide additional information that is not essential to the main text.

In order to make the book more interactive and link-friendly, I have enabled hyperlinks in the PDF. This means that you can click on the references, citations, and links to external resources, and they will take you to the corresponding location. This is standard latex, however to maintain a consistent experience in the physical version, QR codes are inserted in the margin next to the links. The reader is invited to scan them with a QR code reader to access the corresponding online resource². Some figures also include QR codes that link to an interactive (HTML) version of the figure, see Figure 3 as an example.

The additional material as well as the source code of this document are hosted in a [Zenodo repository](#)³. Alternatively, a mirror repository is also available at:

<https://github.com/juan11iguel/my-thesis>

It seems unlikely that both Zenodo and GitHub will go down at a time where this document is still relevant, and if they do, I think there will be more important things to worry about than losing access to the interactive content of this thesis. ¶

About the author

Un payaso

– Lidia Roca, probablemente

I am currently completing my PhD thesis, with the defense planned for October. My research interests lie primarily in automatic control, optimization, and robotics, especially as applied to solar thermal processes.

I think I am mostly a creative person, but in order to implement those ideas, throughout my work, I've gained experience with a variety of tools and technologies, including Linux, Python, Docker, LaTeX, and the Robot Operating System (ROS). I'm particularly passionate about open science and open source software, and I strive to contribute to communities that value transparency and collaboration.

For my bachelor's thesis, I created a mobile robotics lab in the University of Almería by deploying the [Duckietown project](#). This gave me the opportunity to interact and work with ROS, and since the whole project was deployed using Docker, to learn about containerization technologies. For my master's thesis, work was also software-related, but this time it was about the implementation of a SCADA-like system using Python. During my PhD, I have had four years to really delve into these technologies, so today they are an integral part of my workflow and I am confident to say they've helped me become effective at implementing those (sometimes too) many ideas.



Lidia esto solo lo he copiado
por tener algo, ya lo mejoraré

INTRODUCTION

asdad



Figure 1.1: Aerial view of the pilot plants at the PSA, Spain.

The developments presented in this thesis have been developed and validated around two test-rigs: a CCS and a SolarMED pilot plants. In the picture, the CCS plant is located on the left side, and the...

2.1 Performance metrics

To evaluate the quality of the models fit to the experimental data, four performance metrics were evaluated: coefficient of determination (R^2), Root Mean Squared Error (RMSE), Mean Absolute Error (MAE) and Mean Absolute Percentage Error (MAPE). These metrics are described below.

Coefficient of determination. R^2 measures the proportion of the variance in the predicted variable that can be attributed to the independent variable(s), in this case the considered system inputs. Values close to one indicate a better prediction accuracy. It is calculated as follows:

$$R^2 = 1 - \frac{\sum_{i=1}^n (y_i - \hat{y}_i)^2}{\sum_{i=1}^n (y_i - \bar{y})^2},$$

where y_i is the measured or observed value for the output variable, in the i -th observation, \hat{y}_i is the estimated value of the same variable and n is the total number of observations. Finally, \bar{y} is the mean value of the experimental values.

Root Mean Square Error. RMSE is a statistical measure of the difference between the values predicted by a model and the observed values. It is calculated as the square root of the mean of the squared differences between the predicted and observed values and it has its units.

$$\text{RMSE} = \sqrt{\frac{1}{n} \sum_{i=1}^n (y_i - \hat{y}_i)^2}$$

Mean Absolute Error. It represents the average absolute difference between predicted and actual values.

$$\text{MAE} = \frac{1}{n} \sum_{i=1}^n |y_i - \hat{y}_i|$$

Mean Absolute Percentage Error. As the MAE, it calculates the difference between the predicted and the actual values, but in this case it does so in relative terms:

$$\text{MAPE} = \frac{1}{n} \sum_{i=1}^n \left| \frac{y_i - \hat{y}_i}{y_i} \right| \times 100\%$$

2.2 First principle modelling

2.3 Data-driven modelling

Machine learning algorithms are unique in their ability to obtain models and extract patterns from data, without being explicitly programmed to do so. They

2.1 Performance metrics	9
2.2 First principle modelling	9
2.3 Data-driven modelling	9
2.3.1 Gaussian Process Regression	10
2.3.2 Artificial Neural networks . . .	10
2.3.3 Random Forest	12
2.3.4 Gradient Boosting	12
2.4 Hybrid modelling	12
2.5 DD from FP. Sample generation	12

are more effective with large volumes of data but can also be applied to build steady state regression models with less information of a process.

2.3.1 Gaussian Process Regression

2.3.2 Artificial Neural networks

Artificial Neural Networks (ANNs), as the name suggests, have a behavior similar to biological neurons. Their structure is formed by a succession of layers, each one composed by nodes (or neurons) and they receive as input the output of the previous layer. This process is subsequently repeated until the final layer which has a number of neurons equal to the number of outputs.

There are important aspects to be considered in the ANN model design, such as the model configuration, the network architecture and the network topology. They are discussed below.

Model configuration. If the model has more than one output, several configurations are available for the implementation of the model as shown in Figure 9.2. The first one is a Multiple Inputs Multiple Outputs (MIMO) configuration, where a single network receives all the inputs and directly produces all predicted outputs. The second one is a cascade structure. This cascading approach involves training a network (*network A* in Figure 9.2 (b)) to predict one output using the available inputs. Subsequently, these inputs, along with the output from the first-output-predicting network, are fed into a second network (*network B* in Figure 9.2 (b)) that is in charge of forecasting the second output. This procedure can be repeated as many times as desired. A potential advantage of this configuration is that it may reduce the experimental data requirements to obtain satisfactory results. A third option is the combination of both configurations, where some networks may predict several outputs, while others are fed some of these outputs as subsequently use them as inputs.

Network architectures. Three network architectures have been implemented and tested:

1. Feed Forward (FF) network - Figure 2.2 (a). This is the base network architecture, where different layers are added sequentially and the flow of information is unidirectional. The transfer function adopted in the hidden layers is the differentiable *Log-Sigmoid*¹, whereas the one employed in the output layer is a linear one with no saturations.
2. Cascade-forward (CF) network - Figure 2.2 (b). It is a variation on the feedforward network since it adds direct connections from the input and hidden layers to the output layer.
3. Radial Basis Function (RBF) network - Figure 2.2 (c). The transfer functions used in the first layer of the RBF network are different, they are local Gaussian like functions. Also, instead of multiplying by the weights, the distance between inputs and weights is computed and the bias is multiplied instead of added [1].

Network topology. Two-layer networks (one hidden and one output layer) can learn almost any input-output relationship, including non-linear ones. Adding more layers can improve the learning for more complex problems. However, increasing the number of layers or neurons per layer increases the training computational requirements, requires more data for a satisfactory model and can lead to overfitting. Therefore, the process is usually started with two layers and then the number of layers is increased if they do not perform satisfactorily [1]. In this study, for the feedforward and cascade-forward architectures, one and two hidden layers have been tested with the following configurations: 5, 10, 20, 5-5, 5-10, 10-5, 10-10. For the case of the RBF, it only has one hidden layer and

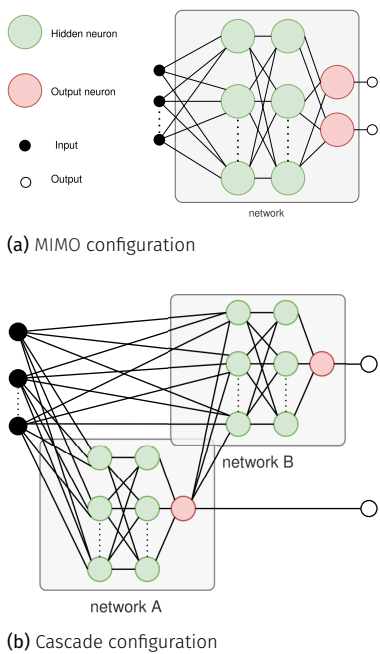


Figure 2.1: ANN model configurations

1: Defined as $\text{logsig}(x) = 1/(1 + e^{-x})$, mapping any real input to a value between 0 and 1.

[1]: Hagan et al. (2014), *Neural Network Design*

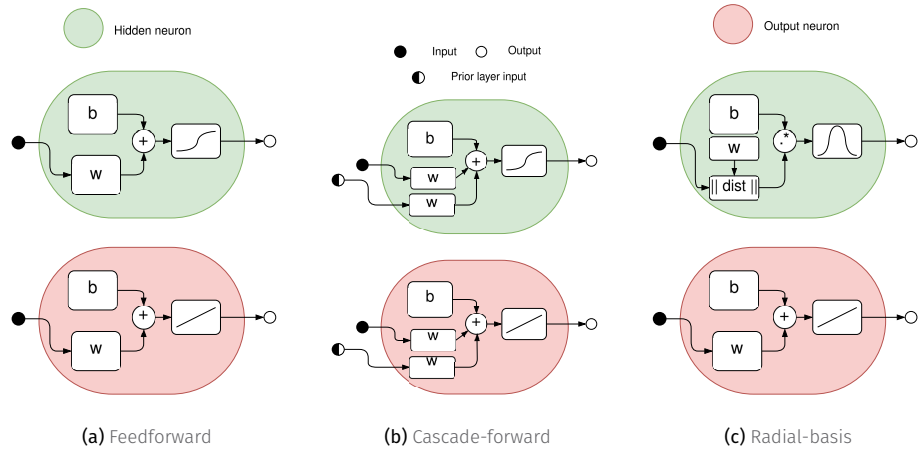


Figure 2.2: Considered ANN architectures

neurons are added sequentially during the training process up to a maximum which is set to 120 neurons.

Training process. The next important aspect to consider is the training process. For the FF and CF networks many Gradient- or Jacobian-based algorithms can be utilized. In this case, the Levenberg-Marquardt backpropagation algorithm [2] has been used. It is a fast algorithm, ideal for multilayer networks with up to a few hundred weights and biases enabling efficient training. The training in this case is done in batches since sequential training is slower and does not produce better results. All data have been normalized applying the z-score normalization method. The criteria established for deciding when to stop the training is the following one: when the performance on the validation set increases (worsens) or when the gradient is below a minimum (1×10^{-7}) for a number of iterations or epochs, or when a maximum number of 1000 epochs is reached. The number of iterations to wait, often referred as patience, is set to 6. Finally, the selected network parameters will be those of the best epoch.

[2]: Beale et al. (2010), "Neural Network Toolbox"

For each network architecture, the training process was repeated a total of ten times (this is the recommended practice if the computational requirements allow it, since it guarantees reaching a global optimum with a high degree of confidence [3]). The optimal architecture and training was selected according to a performance function, which in this case has been the Mean Squared Error (MSE) with the values normalized.

[3]: Hamm et al. (2007), "Comparison of Stochastic Global Optimization Methods to Estimate Neural Network Weights"

In the case of the RBF network, the chosen training method consists in two stages which treats the two layers of the RBF network separately. The first layer weights and biases are tuned based on the orthogonal least squares method [1], while for the second layer are computed in one step using a linear least-squares algorithm. During training, neurons are added to the first layer (in increments of 20) trying to minimize the MSE to some goal, which in this case is set depending on the case study: 10 for the MIMO configuration and 0 ($^{\circ}\text{C}^2$) and 20 (L^2/h^2) for temperature and water lost networks, respectively, for the cascade configuration. Finally, a parameter called spread is used to set the first layer biases. Larger values of this parameter promote a smoother approximation of the training data (more generalization), conversely, lower values provide a more exact fit to the training data. Values from 0.1 to 30 have been tested for this parameter.

[1]: Hagan et al. (2014), *Neural Network Design*

2.3.3 Random Forest

2.3.4 Gradient Boosting

2.4 Hybrid modelling

2.5 Data-driven from first-principles models. Sample generation

One important advantage that first-principles models have over data-driven is their scalability, that is, the ability to adapt a model developed and validated in a pilot-scale system, to a large scale one. This is true for many systems as long as the system configuration remains the same. This allows to study and analyze pilot scale plants and extrapolate the results to industrial sized plants. In addition, these type of model are also capable of predicting the behaviour of the modelled systems in conditions that have not been tested (*e.g.* different operating or environmental conditions), although the reliability of the model could be lower if these conditions move away from those experimentally used for some parameter calibration.

On the contrary, data-driven models are very specific to the system and operating ranges they are trained for. That is why training/calibrating a data-driven model with data from a first-principles model is a common practice to obtain a model that can be used in a larger range of operating conditions...

The process of generating samples from a first-principles model to train a data-driven model is called sample generation. It consists of running the first-principles model for a set of input parameters, which can be selected randomly or following a specific distribution, and then using the outputs of the first-principles model as the training data for the data-driven model.

The first step is to define the input parameters and their ranges. This can be done by selecting the most relevant parameters for the system and determining their ranges based on the system's operating conditions. The next step is to generate a set of input parameters, which can be done using different methods such as Latin Hypercube Sampling, Monte Carlo Sampling, Sobol Sampling, or simply grid sampling. These methods allow to generate a set of input parameters that cover the entire range of the input parameters and ensure that the generated samples are representative of the system's behaviour. Once the input parameters are defined, the first-principles model is run for each set of input parameters, and the outputs of the model are recorded. Finally, the recorded outputs are used to train the data-driven model.

3

Sensitivity analysis

It involves systematically assessing how variations in input parameters impact the model's outputs. In this case, the Sobol method [4], which is a variance-based approach, has been used. This method decomposes the total variance of the model output into contributions from individual input parameters and their interactions. By quantifying the relative importance of each parameter, Sobol analysis facilitates the identification of influential factors, enabling a more nuanced understanding of complex systems characterized by numerous interacting variables.

The analysis results are different sensitivities indices such as total sensitivity indices (total-order), first-order sensitivity indices (first-order), and interaction sensitivity indices (second-order). First-order measures the direct effect of an input variable on the output, excluding interaction effects with other variables, while the second-order measures specifically this interaction effects. Finally, total-order indices account for the total effect of an input variable, including both direct and interaction effects.

[4]: Nossent et al. (2011), "Sobol'sensitivity Analysis of a Complex Environmental Model"

4

Control overview

The PID control algorithm continuously calculates and adjusts the control inputs based on the error between the desired setpoint and the actual system output, ensuring precise and stable control over various parameters.

4.1 PID controllers 15

4.2 Hierarchical control 15

4.1 PID controllers

4.2 Hierarchical control

A general expression to define an optimization problem is:

$$\min_{\mathbf{x}, \mathbf{e}; \theta} J = f(\mathbf{x}, \mathbf{e}; \theta) \quad \text{s.t.} \quad g_i(\mathbf{x}) \leq 0, \quad i = 1, \dots, m \quad (5.1)$$

where \mathbf{x} is the vector of decision variables, $f(\mathbf{x})$ is the objective function to be minimized, and $g_i(\mathbf{x})$ are the constraints of the problem. The objective function is a scalar function that maps the decision variables to a real number, representing the cost or performance of the system. The constraints are functions that restrict the feasible region of the problem, defining the set of values that the decision variables can take. The optimization problem is to find the values of the decision variables that minimize the objective function while satisfying the constraints.

Regarding the constraints, they can be categorized in two types depending whether they can be evaluated before evaluating the objective function or not:

- ▶ **Bounds.** These are constraints that limit the range of the decision variables, such as

$$x_i \in [l_i, u_i], \quad i = 1, \dots, n$$

where l_i and u_i are the lower and upper bounds of the decision variable x_i , respectively¹.

- ▶ **Constraints.** These are constraints that restrict the feasible region of the problem, such as

$$g_i(\mathbf{x}) \leq 0, \quad i = 1, \dots, m$$

where $g_i(\mathbf{x})$ are the constraint functions that depend on the decision variables \mathbf{x} , and m is the number of constraints. They can only be known after evaluating the objective function.

5.1 NLP problems	17
5.2 MINLP problems	17
5.3 Multi-objective optimization	17
5.4 Optimization algorithms	17

¹: Also known as box-bounds

5.1 NLP problems

Non-Linear Programming (NLP)

5.2 MINLP problems

Mixed Integer Non-Linear Programming (MINLP)

5.3 Multi-objective optimization

5.4 Optimization algorithms

- ▶ **Improved Harmony Search algorithm (IHS)** [5, 6] is a metaheuristic optimization algorithm inspired by the improvisation process of musicians. In this analogy, each musician represents a decision variable, each note corresponds to a value, and the goal is to create the best possible harmony—analogous to finding the global optimum.

[5]: Geem et al. (2001), "A New Heuristic Optimization Algorithm"

In the algorithm, every member of the input population contributes to the search process. At each iteration, a new solution (individual) is generated.

[6]: Biscani et al. (2020), "A Parallel Global Multiobjective Framework for Optimization: Pagmo"

2: While HS has shown competitive performance, it has also faced criticism—not for its results, but for its metaphor. The musical analogy adds little explanatory value and arguably obscures the algorithm's mechanics. At its core, HS operates similarly to Evolutionary Strategies or Genetic Algorithms, employing concepts like mutation and crossover.

If this new solution outperforms the worst individual in the population, it replaces it. The total number of fitness function evaluations equals the number of iterations.

An enhanced version of HS introduces dynamic parameters: the probability of selecting values from the decision vector is adjusted linearly, while the mutation rate changes exponentially over time. These improvements aim to balance exploration and exploitation more effectively.²

► Another

asdad

6.1 Hypothesis 19

6.2 Objectives 19

6.1 Hypothesis

6.2 Objectives

asdad

OPTIMAL WATER AND ELECTRICITY MANAGEMENT IN A COMBINED COOLING SYSTEM

TL;DR

In the pursuit of extending the use and feasibility of solar thermal applications, a case study consisting of a commercial 50 MW-8 hours of storage Concentrated Solar Power (CSP) plant, Andasol-II, is analyzed in annual simulations where the cooling solution makes use of the novel proposed CCS. To obtain these results, a model of the CCS has been developed based on the same configuration as the PSA pilot plant. Different optimization strategies based on evolutionary algorithms have been implemented to adapt the system operation to the changing conditions. The strategy has been experimentally validated in the pilot plant and the simulated results show that the proposed scheme can yield ... compared to the DC only and ... with the WCT only alternatives.

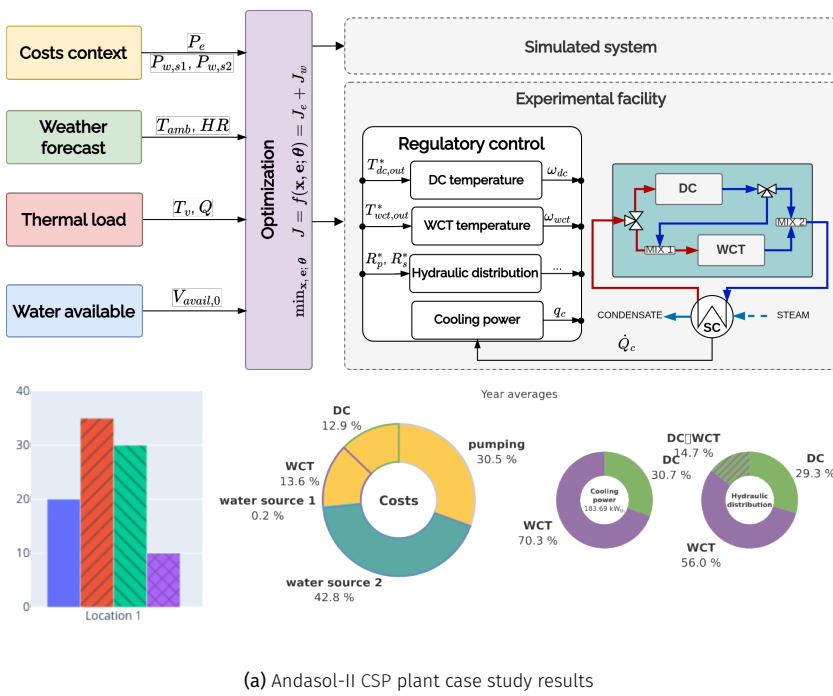


Figure 7.1: Results for the analyzed case study in this part. The first bar plot compares the specific cost of the different cooling alternatives (lower is better). The second pie chart shows the breakdown of the costs, and the third and fourth pie charts show the cooling power distribution between DC and WCT and

Derived scientific contributions

Structure

This part is structured as follows: in the first two chapters the methodology is described, specifically the modelling in (Chapter ?? (??)) is presented for the CCS, and the optimization framework in Chapter 10 (Optimization of a combined cooling system). The third chapter presents the experimental facility (Chapter 11 (Combined cooling pilot plant at Plataforma Solar de Almería)) that is used to experimentally validate the model and the optimization strategy integrated in a hierarchical control scheme in Chapter 12 (Validation in the combined cooling pilot plant). The final chapter, Chapter 13 (Annual analysis: ANDASOL-II CSP plant), describes and analyzes the results of the annual simulations performed for the Andasol-II CSP plant.

In the pursuit of eliminating reliance on fossil fuels sources for energy generation and replacing them by renewable sources, CSP has proven to be a reliable contributor. In particular, in providing much needed energy storage, dispatchability and ensuring grid stability.

CSP plants use mirrors to concentrate the sun's energy to finally drive a turbine that generates electricity. This technology currently represents a minor part of renewable energy generation in Europe. Only approximately 5 GW are installed globally (of which 2.3 GW in Europe are concentrated in Spain). However, the potential for growth is significant given the capability of CSP to provide renewable electricity when needed thanks to in-built energy storage continuing the production even in the absence of sunlight, unlike other renewable technologies that are dependent on the availability of the energy source. Of increasing importance is also their potential application in improving the manageability of the grid, replacing fossil fuel alternatives. Their dispatchability enables plants to respond to peaks in demand, and provide ancillary services to the grid. According to the International Energy Agency forecasts, CSP has a huge potential in the long term, ranging from the 986 TWh by 2030 up to 4186 TWh by 2050 [7], which means that CSP will account for 11% of the electricity generated worldwide and for 4% in the case of Europe.

[8]: IEA (2014), *Energy Technology Perspectives*

8.1 Cooling and water use

The cooling of the power block in this technology plays a crucial role in its feasibility. The cheapest and most efficiency cooling technology is evaporative cooling, and that is why most plants, specially in Spain where built using this alternative (XX % [8]), however, the high-radiation areas in which they are located are usually regions with rapidly-degrading water availability due to climate change, so water has become a scarce resource. Nowadays most likely those plants would have been built with dry cooling technologies, significantly increasing the cost (up to 8% during periods of high ambient temperatures when energy demand and prices peak [[empty citation](#)]).

[8]: Thonig et al. (2023), *CSP.Guru* 2023-07-01

CSP plants are, in general, located in arid areas, where sun irradiance is high but water is scarce. The efficiency of these plants is highly dependent on the temperature at which the steam is condensed. To date, the conventional systems used to remove excess heat from CSP plants are either wet (water-cooled) or dry (air-cooled). The lowest attainable condensing temperature is achieved in wet cooling systems that depend on the wet-bulb temperature, allowing CSP plants to achieve higher efficiencies. However, this efficiency increase is at the expense of a high cost: excessive water use. Dry cooling systems eliminate the water use but they lead to lower plant efficiencies when the ambient air temperature is high. Those hot periods are often the periods of peak system demand and higher electricity sale price. The combination of the advantages of each of them into an innovative cooling system is thus of great interest. There are different types of innovative cooling systems: those that integrate the dry and wet cooling systems into the same cooling device, which are called hybrid cooling systems [9–11] and those that combine separate dry and wet cooling systems, which are called combined cooling systems. In the case of hybrid cooling systems, the dry section are composed of compact heat exchangers included in a wet cooling tower [9]. This kind of cooling systems can be considered as an efficient cooling solution for CSP plants [12] due to the energy conservation and water

[empty citation](#)

[9]: Rezaei et al. (2010), "Reducing Water Consumption of an Industrial Plant Cooling Unit Using Hybrid Cooling Tower"

[10]: Asvapoositkul et al. (2014), "Comparative Evaluation of Hybrid (Dry/Wet) Cooling Tower Performance"

[11]: Hu et al. (2018), "Thermodynamic Characteristics of Thermal Power Plant with Hybrid (Dry/Wet) Cooling System"

[12]: El Marazgioui et al. (2022), "Impact of Cooling Tower Technology on Performance and Cost Effectiveness of CSP Plants"

[13]: Barigozzi et al. (2011), "Wet and Dry Cooling Systems Optimization Applied to a Modern Waste-to-Energy Cogeneration Heat and Power Plant"

[14]: Barigozzi et al. (2014), "Performance Prediction and Optimization of a Waste-to-Energy Cogeneration Plant with Combined Wet and Dry Cooling System"

[15]: Palenzuela et al. (2022), "Experimental Assessment of a Pilot Scale Hybrid Cooling System for Water Consumption Reduction in CSP Plants"

[16]: Asfand et al. (2020), "Thermodynamic Performance and Water Consumption of Hybrid Cooling System Configurations for Concentrated Solar Power Plants"

[17]: Wazirali et al. (2023), "State-of-the-Art Review on Energy and Load Forecasting in Microgrids Using Artificial Neural Networks, Machine Learning, and Deep Learning Techniques"

and greenhouse gas emissions savings. In the case of combined cooling systems, different configurations can be found. The most commonly proposed in the literature is the one that considers an Air-Cooled Condenser (ACC) in parallel with a WCT, as can be seen in [13, 14]. In this kind of configuration, the exhaust steam from the turbine is condensed either through the ACC or through a Surface Condenser (SC) coupled with the WCT. Another configuration, recently proposed in [15] is a wet cooling tower and a DC (type Air-Cooled Heat Exchanger (ACHE)) sharing a surface condenser. In this case, the exhaust steam from the turbine is condensed through the surface condenser and the heated cooling water is cooled either through the WCT or through the dry cooler. This kind of combined cooling systems are proposed as the most suitable option for a flexible operation as a function of the ambient conditions, since they allow to select the best operation strategies to achieve an optimum water and electricity consumption compromise [16]. In addition, if the optimization is combined with energy demand forecasting as described in [17], the expected results can be even better.

Modelling of a combined cooling system

TL;DR

This chapter describes the steady-state modelling of the different components of a combined cooling system, mainly a WCT and a DC. Different alternatives are presented: from physical models to data-driven approaches, including the generation of samples for data-driven models trained using data from a physical model. Models are also developed for the other components of the system and finally it is shown how they are integrated into a complete system model. The complete system model interface is defined at Model ?? and a block diagram is presented in Figure 9.3 including all relevant variables.

Introduction

In order to study the potential advantages of making use of a combined cooling system, it is first necessary to develop the modelling of its components. Since the objective is performance prediction, this chapter focuses on the steady state modelling of the combined cooler main components, *i.e.* the WCT and the DC. More specifically, the aim is to compare two modelling strategies: that based on physical equations (Section 2.2) and that based on black box models (Section 2.3) such as ANNs, in order to see which one is more suitable for its integration in the optimization of the complete process.

This chapter presents a comparison between the two modelling approaches, at steady state and with a focus on optimization applications, in terms of predictive capabilities, experimental and instrumentation requirements, execution time, implementation and scalability. A sensitivity analysis is performed to further analyze and compare each case study. It also presents and evaluates all relevant aspects of interest in the development of such models, specifically for ANNs, model configuration, architecture and topology are discussed. Other system components are also described in Section 9.3 (Other components) and finally their integration is discussed in Section 9.4 (Complete system).

9.1 Wet cooler

In the case of the models based on physical equations, the analysis of wet cooling towers has its origin in [18], in which the theory for their performance evaluation was developed. Merkel proposed a model based on several assumptions to simplify the heat and mass transfer equations to a simple hand calculation. However, these assumptions mean that Merkel's method does not reliably represent the physics of the heat and mass transfer process in a cooling tower. This was already stated by Bourillot [19] who concluded that the Merkel method is simple to use and can correctly predict cold water temperature when an appropriate value of the coefficient of evaporation is used. However, it is insufficient for the estimation of the characteristics of the warm air leaving the fill and for the calculation of changes in the water flow rate due to evaporation. Jaber and Webb [20] developed the equations necessary to apply the effectiveness-NTU¹ method directly to counterflow or crossflow cooling towers. This approach is particularly useful in the latter case and simpler compared to a more conventional numerical procedure. Notice that the effectiveness-NTU

9.1	Wet cooler	29
9.1.1	Poppe model	30
9.1.2	Samples generation for first-principles to data-driven models	32
9.1.3	Model interface	32
9.2	Dry cooler	33
9.2.1	Physical model	33
9.2.2	Samples generation for first-principles to data-driven models	33
9.2.3	Model interface	33
9.3	Other components	34
9.3.1	Electrical consumption	34
9.3.2	Surface condenser	34
9.3.3	Mixers	35
9.4	Complete system	35

Ahora mismo esta introducción es demasiado parecida al TL;DR, hay que distinguirla

[18]: Merkel (1925), "Verdunstungskühlung"

[19]: Bourillot (1983), "Hypotheses of Calculation of the Water Flow Rate Evaporated in a Wet Cooling Tower"

[20]: Jaber et al. (1989), "Design of Cooling Towers by the Effectiveness-NTU Method"

1: The effectiveness-NTU method estimates how well a heat exchanger transfers heat by comparing the actual heat transfer to the maximum possible, using a parameter, Number of Transfer Units (NTU), that reflects its size and flow characteristics.

[21]: Poppe et al. (1991), "Berechnung von Rückkühlwerken"

[22]: Kloppers et al. (2005), "A Critical Investigation into the Heat and Mass Transfer Analysis of Counterflow Wet-Cooling Towers"

[23]: Cutillas et al. (2021), "Energetic, Exergetic and Environmental (3E) Analyses of Different Cooling Technologies (Wet, Dry and Hybrid) in a CSP Thermal Power Plant"

[24]: Hosoz et al. (2007), "Performance Prediction of a Cooling Tower Using Artificial Neural Network"

2: The notation $n_1 \dots n_l$ represents the architecture of the ANN model, where l is the number of layers and n_i are the nodes in each one of the layers.

[25]: Gao et al. (2013), "Artificial Neural Network Model Research on Effects of Cross-Wind to Performance Parameters of Wet Cooling Tower Based on Level Froude Number"

[26]: Song et al. (2021), "A Novel Approach for Energy Efficiency Prediction of Various Natural Draft Wet Cooling Towers Using ANN"

3: ANN uses as input f_{fan} whereas Poppe's model uses \dot{m}_a .

[27]: Navarro et al. (2022), "Critical Evaluation of the Thermal Performance Analysis of a New Cooling Tower Prototype"

method is based on the same simplifying assumptions as the Merkel method. On the other hand, Poppe and Rögner [21] developed the Poppe method. They derived the governing equations for heat and mass transfer in a wet cooling tower and did not make any simplifying assumptions as in the Merkel theory, which makes it a very precise model. As a matter of fact, predictions from the Poppe formulation have resulted in values of evaporated water flow rate that are in good agreement with full scale cooling tower test results [22]. This model has already been used for the evaluation of the thermal performance of solar power plants using different condensation systems (wet, dry and hybrid system), as can be found in Cutillas et al. [23].

In the case of black box models, numerous authors in the literature have designed ANN models for WCT with different objectives, such as performance prediction, simulation and optimization. One of the first works in this area is the one described in [24] where an ANN model was developed to predict the performance of a forced-counter flow cooling tower at lab scale. In this case, the input variables were the dry bulb temperature, the relative humidity of the air stream entering the tower, the temperature of the water entering the tower, the air volume flow rate and the cooling water mass flow rate. The outputs of this model were the heat rejection rate at the tower, the mass flow rate of water evaporated, the temperature of the cooling water at the tower outlet, the dry bulb temperature and the relative humidity of the air at the outlet of the tower. The results obtained with a 5-5-5² ANN demonstrated that wet cooling towers at lab-scale can be modelled using ANNs with a high degree of accuracy. There are also ANN models for Natural Draft Counter-flow Wet Cooling Towers (NDWCT) at lab-scale, such as the one proposed by [25]. In this case, the authors used a 4-8-6 ANN structure and considered some additional variables, such as air gravity, wind velocity, heat transfer coefficients and efficiency as outputs. All these works can be useful to validate the model development methodology but may fail predicting the performance of WCT at larger scale. In this sense, special attention deserves the study carried out by [26] where an 8-14-2 ANN model was proposed to predict the performance (the cooling number and the evaporative loss proportion) of NDWCTs at commercial scale. The model is based on 638 sets of field experimental data collected from 36 diverse NDWCTs used in power plants. It is a very challenging work since it covers samples from a wide range of tower sizes and capacities being the Mean Relative Error (MRE) below 5 %.

From the literature review, it can be stated that there are works based on Poppe and ANN models that evaluate the main output variables of WCTs. Nevertheless, to the author knowledge, there are no studies focused on the comparison between both modelling strategies. Also lacking is a comprehensive analysis of the different aspects that affect the models development and performance.

The static models presented in this section have been developed to predict two main outputs, the water temperature at the outlet of the WCT, $T_{w,or}$ and the water consumed due to evaporation losses, $\dot{m}_{w,lost}$. The inputs variables required by both modelling approaches, Poppe model and ANN models, are: the cooling water flow rate (\dot{m}_w), the water temperature at the inlet of the WCT ($T_{w,i}$), the ambient temperature (T_∞), the ambient relative humidity (ϕ_∞) and the frequency percentage of the fan (f_{fan}) (or its equivalence in air mass flow rate³, \dot{m}_a).

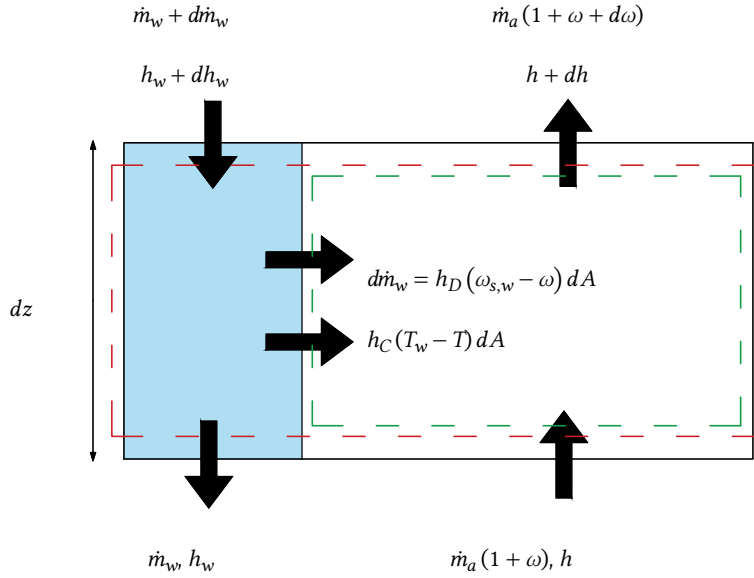
9.1.1 Poppe model

The well-known Merkel number is accepted as the performance coefficient of a wet cooling tower [27]. This dimensionless number is defined in Equation 9.1, and it measures the degree of difficulty of the mass transfer processes occurring in the exchange area of a wet cooling tower.

$$Me = \frac{h_D a_V V}{\dot{m}_w}, \quad (9.1)$$

where h_D is the mass transfer coefficient, a_V is the surface area of exchange per unit of volume and V is the volume of the transfer region.

The Merkel number can be calculated using the Merkel and Poppe theories for the performance evaluation of cooling towers. On the one hand, the Merkel theory [18] relies on several critical assumptions, such as the Lewis factor (Le) being equal to 1, the air exiting the tower being saturated with water vapour and it neglects the reduction of water flow rate by evaporation in the energy balance. On the other hand, the Poppe theory [21], which is the one used in this work, do not consider simplifying assumptions, thus being the one most usually preferred. In this theory, the authors derived the governing equations for heat and mass transfer in the transfer region of the wet cooling tower (control volume shown in Figure 9.1) assuming a one dimensional problem. In this figure, the red and green dashed lines indicate the fill and air-side control volumes, respectively.



[18]: Merkel (1925), "Verdunstungskühlung"

[21]: Poppe et al. (1991), "Berechnung von Rückkühlwerken"

Figure 9.1: Control volume in the exchange area of a wet cooling tower arrangement.

Following the detailed derivation process and simplification of the previously-mentioned governing equations described in [27], the major following equations for the heat and mass transfer obtained, according to the Poppe theory, are:

$$\frac{d\omega}{dT_w} = \frac{c_{p_w} \frac{\dot{m}_w}{\dot{m}_a} (\omega_{s,w} - \omega)}{(h_{s,w} - h) + (Le - 1) [(h_{s,w} - h) - (\omega_{s,w} - \omega) h_v] - (\omega_{s,w} - \omega) h_w} \quad (9.2)$$

$$\frac{dh}{dT_w} = c_{p_w} \frac{\dot{m}_w}{\dot{m}_a} \left[1 + \frac{(\omega_{s,w} - \omega) c_{p_w} T_w}{(h_{s,w} - h) + (Le - 1) [(h_{s,w} - h) - (\omega_{s,w} - \omega) h_v] - (\omega_{s,w} - \omega) h_w} \right] \quad (9.3)$$

$$\frac{dMe}{dT_w} = \frac{c_{p_w}}{(h_{s,w} - h) + (Le - 1) [(h_{s,w} - h) - (\omega_{s,w} - \omega) h_v] - (\omega_{s,w} - \omega) h_w}, \quad (9.4)$$

where the quantity referred to as Me in Eq. 9.4, is the Merkel number calculated according to the Poppe theory. The above described governing equations can be solved by the fourth order Runge-Kutta method to provide the evolution of

[27]: Navarro et al. (2022), "Critical Evaluation of the Thermal Performance Analysis of a New Cooling Tower Prototype"

the air humidity ratio, air enthalpy and Merkel number inside the transfer area of the cooling tower (fill). Once these profiles are known, the amount of water lost due evaporation can be calculated as per Eq. Equation 9.6. Refer to [27] for additional information concerning the calculation procedure.

$$Me = \frac{h_D a_v V}{\dot{m}_w}, \quad (9.5)$$

$$\dot{m}_{w,lost} = \dot{m}_a (\omega_{a,o} - \omega_{a,i}) \quad (9.6)$$

[28]: Ashrae (2004), "HVAC Systems and Equipment"

It is important to mention that the Merkel number varies with the operation conditions and its value can be obtained using a correlation with the water-to-air mass flow ratio as an independent variable. One of the proposed correlations in ASHRAE [28] is:

$$Me = c (\dot{m}_w / \dot{m}_a)^{-n} \quad (9.7)$$

4: See Section 12.1.1 (Wet cooler model alternatives comparison and validation)

where the constants c and n can be obtained from the fitting of experimental data⁴.

9.1.2 Samples generation for first-principles to data-driven models

The first pair of input variables for the WCT sample generation are the wet bulb temperature (T_{wb}) and the difference between this temperature and the system inlet temperature (ΔT_{wb-in}). The wet bulb temperature is used instead of the ambient temperature or the relative humidity, because as it can be derived from the physical model, it is the most relevant thermodynamic variable for the wet cooling tower performance. Using both the ambient temperature and the relative humidity would lead to a larger than necessary input space with many duplicate samples, as the wet bulb temperature is a function of both variables. The second pair of input variables are the cooling water flow rate (q_{wct}) and, following the reasoning from the physical model, the air to water mass flow ratio ($\dot{m}_a / \dot{m}_{wct}$), since it is a key parameter in defining the operating conditions of the tower. From the resulting 2D grid, valid combinations are obtained by calculating the air mass flow rate and finding if a valid fan speed can be obtained using an air mass flow rate to fan speed empirical correlation.

Finally, all valid thermodynamic and operational combinations are merged into a comprehensive sample set, enabling detailed system evaluations across a realistic and constrained input space.

9.1.3 Model interface

Model 9.1: Wet cooling tower

$$T_{wct,out}, C_{w,wct} = \text{wct model}(q_{wct}, \omega_{wct}, T_{amb}, HR, T_{wct,in})$$

Model 9.2: Wet cooling system model

$T_{wct,out}, C_e, C_w, T_{c,in}, T_{c,out} = \text{wcs model}(q_{wct}, \omega_{wct}, T_{amb}, HR, T_{wct,in})$
 $T_{c,in}, T_{c,out} = \text{condenser model}(q_c, \dot{m}_v, T_v)$
 $T_{wct,out}, C_{w,wct} = \text{wct model}(q_{wct}, \omega_{wct}, T_{amb}, HR, T_{c,out})$
 $C_{e,c} = \text{electrical consumption}(q_c)$
 $C_{e,wct} = \text{electrical consumption}(\omega_{wct})$
 $C_e = C_{e,wct} + C_{e,c}$
 $C_w = C_{w,wct}$

9.2 Dry cooler

9.2.1 Physical model

a

Pendiente de basarse en el artículo del modelo físico del DC con Elxe

9.2.2 Samples generation for first-principles to data-driven models

Similar to the wet cooling tower case, setting absolute values for both the inlet temperature and the environment temperature will lead to many unfeasible combinations ($T_{dc,in} \leq T_{db}$). So instead, values are generated for the temperature difference, therefore, a 2D grid is constructed using combinations of ambient/dry-bulb temperature (T_{amb}) and the difference between inlet and ambient temperature ((ΔT_{amb-in})). For each valid temperature pair ($T_{amb}, T_{dc,in}$), additional independent variables (q_{dc}, ω_{dc}) are combined via a Cartesian product, resulting in a full multidimensional grid of plausible operating points. This systematic procedure ensures a dense and uniform sampling across all relevant input dimensions. Finally, infeasible combinations are filtered based on physical constraints.

9.2.3 Model interface

Model 9.3: Dry cooler

$T_{dc,out} = \text{dc model}(q_{dc}, \omega_{dc}, T_{amb}, T_{dc,in})$

Model 9.4: Dry cooling system model

$$\begin{aligned}
 T_{dc,out}, C_e, T_{c,in}, T_{c,out} &= \text{dcs model}(q_{dc}, \omega_{dc}, T_{amb}, T_{dc,in}) \\
 T_{c,in}, T_{c,out} &= \text{condenser model}(q_c, \dot{m}_v, T_v) \\
 T_{dc,out} &= \text{dc model}(q_{dc}, \omega_{dc}, T_{amb}, T_{c,out}) \\
 C_{e,c} &= \text{electrical consumption}(q_c) \\
 C_{e,dc} &= \text{electrical consumption}(\omega_{dc}) \\
 C_e &= C_{e,dc} + C_{e,c}
 \end{aligned}$$

9.3 Other components

9.3.1 Electrical consumption

Electrical consumption is modelled with polynomial regressions of order 3 from experimental data:

Model 9.5: Electrical consumption

$$\begin{aligned}
 C_e &= \text{electrical consumption model}(x) \\
 C_e &= p_1 \cdot x^3 + p_2 \cdot x^2 + p_3 \cdot x + p_4
 \end{aligned}$$

where C_e represents the electrical consumption, and x is the input variable (e.g., the recirculated cooling water flow rate, particular cooler fan speed, etc.). The coefficients p_i correspond to a polynomial regression and must be calibrated individually for each component.

9.3.2 Surface condenser

The surface condenser is a heat exchanger that condenses steam into water, assuming that all the vapor that enters the condenser (at saturated conditions), leaves it as saturated liquid, it can be modelled by applying the first law of thermodynamics, which states that the heat lost by the steam (*released*) is equal to the heat gained by the cooling water (*absorbed*), and equal to the heat transferred by the condenser heat transfer surfaces (*transferred*).

Model 9.6: Surface condenser

$$T_{c,in}, T_{c,out} = \text{condenser model}(\dot{m}_c, T_v, \dot{m}_v)$$

$$LMTD = \frac{T_{c,out} - T_{c,in}}{\ln\left(\frac{T_v - T_{c,in}}{T_v - T_{c,out}}\right)}$$

$$\dot{Q}_{released} = \dot{m}_v \cdot (h_{sat,vap} - h_{sat,liq})$$

$$\dot{Q}_{absorbed} = \dot{m}_c \cdot c_p(T_{c,out} - T_{c,in})$$

$$\dot{Q}_{transferred} = U \cdot A \cdot LMTD$$

$$U = \dots$$

The condenser area (A) is a constant parameter

where $T_{c,in}$ and $T_{c,out}$ are the cooling water inlet and outlet temperatures, respectively, \dot{m}_c the cooling water mass flow rate, T_v vapour temperature and \dot{m}_v its mass flow rate and $h_{sat,vap}$ and $h_{sat,liq}$ are the specific enthalpies of the steam at the inlet and outlet of the condenser, respectively. \dot{Q} represents the heat transfer rate i.e. the thermal power.

9.3.3 Mixers

The mixers outlet flow ($q_{mix,out,i}$) and temperature ($T_{mix,out,i}$) can be determined with a simple mass and energy balances from its inlets streams ($q_{mix,in}$, $T_{mix,in}$):

Model 9.7: Mixer model

$$q_{mix,out}, T_{mix,out} = \text{mixer model}(q_{mix,in,1}, T_{mix,in,1}, q_{mix,in,2}, T_{mix,in,2}) \quad (9.8)$$

$$q_{mix,out} = q_{mix,in,1} + q_{mix,in,2} \quad (9.9)$$

$$T_{mix,out} = T_{mix,in,1} \cdot \frac{c_p(T_{mix,in,1})}{c_p(T_{out,i})} \frac{q_{mix,in,1}}{q_{mix,out,i}} + \\ T_{mix,in,2} \cdot \frac{c_p(T_{mix,in,2})}{c_p(T_{out,i})} \frac{q_{mix,in,2}}{q_{mix,out,i}} \quad (9.10)$$

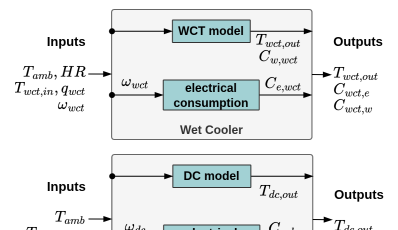
where $c_p(\cdot)$ is the specific heat, which can be assumed to be the same for the mixing temperature differences of this type of system.

9.4 Complete system

The complete model of the combined cooling system integrates the models of the WCT and DC, along with the surface condenser and the mixers, as defined in Model 9.8 (Complete system)⁵. The full diagram, including all variables, is shown in Figure 9.3.

To solve the system, the condenser model is evaluated first, providing the inlet temperature for the dry cooler. Once the dry cooler is solved, the resulting temperatures allow for solving the wet cooling tower. Finally, the mixers are evaluated to determine the final outlet temperature of the combined cooler, which should match the condenser's inlet temperature.

5: Although the electrical consumption for cooling water recirculation is attributed to the condenser in this model, other components—particularly the hydraulic circuit and the dry cooler—also contribute significantly to circulation resistance



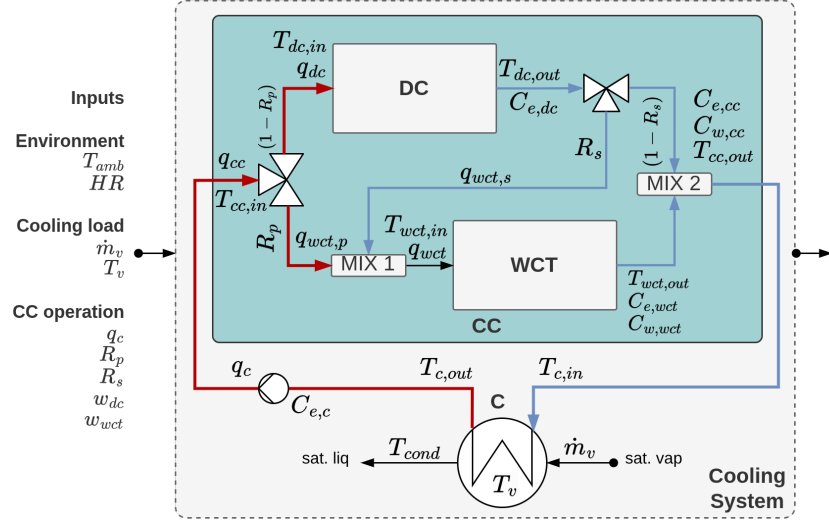


Figure 9.3: Complete model diagram of the combined cooling system

Model 9.8: Combined cooling system

$T_{cc,out}, C_e, C_w, T_{c,in}, T_{c,out} = \text{ccs_model}(q_c, R_p, R_s, \omega_{dc}, \omega_{wct}, T_{amb}, HR_i, T_v, \dot{m}_v)$
 $T_{cc,in} = T_{c,out}$
 $T_{dc,in} = T_{cc,in}$
 $q_{dc} = q_c \cdot (1 - R_p)$
 $q_{wct,p} = q_c \cdot R_p$
 $q_{wct,s} = q_{dc} \cdot R_s$
 $T_{dc,out}, C_{e,dc} = \text{dc_model}(q_{dc}, \omega_{dc}, T_{amb}, T_{dc,in})$
 $q_{wct}, T_{wct,in} = \text{mixer_model}(q_{wct,p}, T_{cc,in}, q_{wct,s}, T_{dc,out})$
 $T_{wct,out}, C_{e,wct}, C_{w,wct} = \text{wct_model}(q_{wct}, \omega_{wct}, T_{amb}, HR, T_{wct,in})$
 $T_{c,in}, T_{c,out} = \text{condenser_model}(q_c, \dot{m}_v, T_v)$
 $q_{cc}, T_{cc,out} = \text{mixer_model}(q_{wct}, T_{wct,out}, q_{dc}, T_{dc,out})$
 $C_{e,c} = \text{electrical consumption}(q_c)$
 $C_{e,dc} = \text{electrical consumption}(\omega_{dc})$
 $C_{e,wct} = \text{electrical consumption}(\omega_{wct})$
 $C_e = C_{e,dc} + C_{e,wct} + C_{e,c}$
 $C_w = C_{w,wct}$

Optimization of a combined cooling system

TL;DR

This chapter describes optimization problems for a combined cooling system, a DC and a WCT as well as different optimization strategies propositions to solve them. The objective is to minimize the daily cost of operation made up by the electricity and water costs, while ensuring the cooling demand is met. The key challenge is to manage the available water resource, since there is a limited amount of cheap rainwater available and any excess water required must be purchased at a significantly higher cost. From the alternatives, this can only be effectively achieved by the shrinking horizon optimization strategy applied to the combined cooler for which an implementation methodology is proposed.

10.1	Environment definition	37
10.2	Static optimization	38
10.2.1	Dry cooler	39
10.2.2	Wet cooler	39
10.2.3	Combined cooler	40
10.3	Horizon optimization	41
10.3.1	Problem discussion	42
10.3.2	Proposed solution	43

Introduction

From a literature review, works can be found that optimize the operation of the cooling system. Of special interest are the works of Marín [29, 30] where a strategy is proposed to optimize both the power block and the cooling system. In [29] a WCT is analyzed, while on [30] a DC is used instead. Annual analysis is performed (sampled monthly) and a techno-economic analysis is performed. The results show ... It can be concluded that there are not many works focusing on the operation optimization. From those that do, they study only one particular system, either a dry cooler or a wet cooler, and not the combined cooling system. From those do, they are focused on the design optimization side, not on the operation.

El estado del arte está por terminar L

[29]: Martín et al. (2013), “Optimal Year-Round Operation of a Concentrated Solar Energy Plant in the South of Europe”

[30]: Martín (2015), “Optimal Annual Operation of the Dry Cooling System of a Concentrated Solar Energy Plant in the South of Spain”

In this chapter, the optimization of the operation of different cooling alternatives is analyzed in terms of their two main consumptions: electricity and water. The optimization problems are formulated to minimize the cost of cooling a thermal load, where this cost is made up by the two mentioned consumptions. Even though in principle this methodology could be applied to any application where cooling a thermal load is required, special focus is put on modelling and considering the water resource availability, since it is a key factor especially in solar thermal applications.¹

The chapter is structured as follows: first, the environment definition is presented in Section 10.1 (Environment definition), which includes a description of the variables taking part in the costs context, weather forecast, thermal load, and water resource availability. Next the two optimization strategies are presented, first a static optimization in Section 10.2 (Static optimization) where the dry cooler, wet cooler and combined cooler static problems are defined; followed by a shrinking horizon optimization approach in Section 10.3 (Horizon optimization) where the combined cooler is optimized over a prediction horizon. This last section includes a discussion on the problem nature and then presents the proposed methodology to solve it.

10.1 Environment definition

The environment for the optimization problems described in this section includes the following components and is visualized in Figure 10.1:

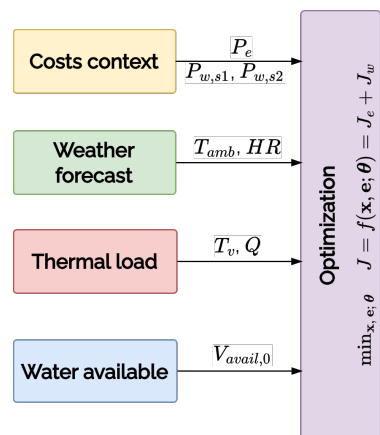


Figure 10.1: Block diagram of the optimization scheme including environment components

1: See Chapter ?? (??)

Costs context The cooling system has mainly two associated operational costs: electricity (J_e) and water use (J_w). For the electricity the sale price of electricity (P_e) is used since whatever is consumed by the cooling system, it is electricity that cannot be sold to the market in the case of a system that produces electricity like a CSP plant, and it is electricity that needs to be purchased at market price in the case of any other system.

As for the water, two sources are considered, water price from source 1 is referred as $P_{w,s1}$ and $P_{w,s2}$ for source 2. Source 1 is cheaper than source 2.

Weather forecast The only two weather variables that have an impact on the cooling system are the ambient temperature (T_{amb}) and the relative humidity (HR) since they set the dry and wet bulb temperatures.

Thermal load The thermal load is defined either by a vapor flow rate (\dot{m}_v) or a thermal power (\dot{Q}), which enters the condenser at a temperature T_v .²

Water resource availability Two sources of water are available, one of them, the cheaper one coming from a dam is limited in volume (V_{avail}). The cheaper source (s_1) is prioritized until it is depleted, then the alternative source (s_2) is used:

$$C_{w,s1,i} = \frac{\min(V_{avail,i}, C_{w,i} \cdot T_s)}{T_s} \quad (10.1)$$

$$C_{w,s2,i} = C_{w,i} - C_{w,s1,i} \quad (10.2)$$

$$V_{avail,i} = V_{avail,i-1} - C_{w,s1,i} \cdot T_s \quad (10.3)$$

where i represents the step, at every step the amount used from each source is estimated and the source 1 availability is updated accordingly. C_w represents the flow rate of water consumed and T_s is the sample time at which steps are computed.

10.2 Static optimization

Static optimization problems are defined in a particular time, given an environment, and decisions do not take into account prior states or decisions, neither consider the effect on future state.

From a process perspective this also characterizes the cooling process, except for the water resource availability, being the only variable that depends on the previous state, *i.e.* is not static. Each time a static problem is evaluated, it begins with a specific initial water volume ($V_{avail,0}$) for that step. After solving the problem, this volume must be updated before proceeding to the next step. As a result, evaluating multiple consecutive steps requires a sequential approach.

Reminder: Optimization problem definition

The general optimization function is defined as:^a

$$\min_{\mathbf{x}, \mathbf{e}; \theta} J = f(\mathbf{x}, \mathbf{e}; \theta) \quad \text{s.t.} \quad g_i(\mathbf{x}) \leq 0, \quad i = 1, \dots, m$$

where \mathbf{x} is the decision vector, \mathbf{e} represents the environment, and θ contains the fixed parameters.

^a See Section ?? (??)

In order to streamline the problem formulation, a general combined cooling system model is used for every scenario. This unified model incorporates both the dry and wet coolers, as well as the shared surface condenser. For cases where only one cooler is used, the other can be effectively disabled by setting

its associated variables to zero and configuring the hydraulic circuit to prevent water circulation through it.

10.2.1 Dry cooler

In the first case study, the optimization focuses exclusively on the dry cooler. Consequently, all variables and terms associated with the wet cooler, as well as water resource management, are omitted from the formulation, making the problem completely static³. This configuration is illustrated in Figure 10.2 and the problem is defined as follows:

3: Achieved by setting $R_p = 0$ and $R_s = 0$

Problem: DC - static

$$\min_{\mathbf{x}, \mathbf{e}; \theta} \quad J = f(\mathbf{x}, \mathbf{e}; \theta) = C_e \cdot P_e$$

with:

$$T_{dc,out}, C_e, T_{c,in}, T_{c,out} = \text{dcs model}(q_c, \omega_{dc}, T_{amb}, T_v, \dot{m}_v)$$

- #### ► Decision variables

$$x = [q_c, \omega_{dc}]$$

- ## ► Environment variables

$$e = [T_{\text{amb}}, P_e, T_v, \dot{m}_v]$$

- #### ► Fixed parameters

$$\theta = [R_p = 0, R_s = 0, \omega_{\text{Wct}} = 0]$$

subject to:

- #### ► Box-bounds

- $w_{dc} \in [\underline{w}_{dc}, \bar{w}_{dc}]$
- $q_c \in [q_c, \bar{q}_c]$

- ## ► Constraints

- $|T_{dc,out} - T_{c,in}| \leq \epsilon_1$
- $T_{c,out} \leq T_v - \Delta T_{c-v,min}$
- $|Q_{dc} - Q_{c\text{ released}}| \leq \epsilon_2$

See Section ?? (??) for a detailed description of the dry cooler and Section 9.3.2 (Surface condenser) for the condenser model.

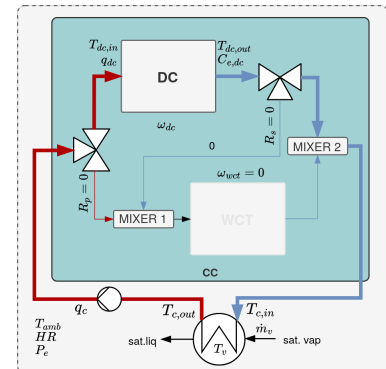


Figure 10.2: Diagram of the dry cooler only cooling problem

The cost of cooling (J) is equivalent to the cost of electricity (J_e), which in turn is the product of the electricity price (P_e) and the electricity consumption (C_e). Only two decision variables are defined, the cooling water recirculation flow rate (q_c) and the dry cooler fan speed (ω_{dc}). Any two pair of values for these variables that satisfy the bounds do not necessary yield a feasible solution, that is why three constrains are introduced, the first one ensures that the outlet cooler temperature matches the inlet condenser temperature (since they are directly connected, they must be the same), the second one ensures that the condenser outlet temperature respects the minimum temperature difference with the vapor temperature, and the last one ensures that the cooling duty of the dry cooler matches the one of the condenser.⁴.

4: In order to better comprehend why mismatches between cooler and condenser can exist, the reader is referred to Section 9.4 (Complete system)

10.2.2 Wet cooler

Conversely to the dry cooler, the wet cooler optimization problem is configured by setting $R_p = 1$, effectively disabling the dry cooler. In this case, water associated

5: See Section 9.1 (Wet cooler) for a detailed description of the wet cooler and condenser model.

variables are included in the problem formulation:⁵

Problem: WCT – static

$$\min_{\mathbf{x}, \mathbf{e}; \theta} J = f(\mathbf{x}, \mathbf{e}; \theta) = J_e + J_w$$

with:

$$J_e = C_e \cdot P_e$$

$$J_w = C_{w,s1} \cdot P_{w,s1} + C_{w,s2} \cdot P_{w,s2}$$

$$C_{w,s1} = \min((V_{avail}, C_w \cdot T_s)/T_s)$$

$$C_{w,s2} = C_w - C_{w,s1}$$

$$T_{wct,out}, C_e, C_w, T_{c,in}, T_{c,out} = \text{wcs model}(q_c, \omega_{wct}, T_{amb}, HR, T_v, \dot{m}_v)$$

- Decision variables

$$x = [q_c, \omega_{wct}]$$

- Environment variables

$$e = [T_{amb}, HR, P_e, P_{w,s1}, P_{w,s2}, V_{avail}, T_v, \dot{m}_v]$$

- Fixed parameters

$$\theta = [R_p = 1, R_s = 0, \omega_{dc} = 0]$$

subject to:

- Box-bounds

- $\omega_{wct} \in [\underline{\omega}_{wct}, \bar{\omega}_{wct}]$
- $q_c \in [\underline{q}_c, \bar{q}_c]$

- Constraints

- $|T_{wct,out} - T_{c,in}| \leq \epsilon_1$
- $T_{c,out} \leq T_v - \Delta T_{c-v, \min}$
- $|Q_{wct} - Q_{c, \text{released}}| \leq \epsilon_2$

Figure 10.3: Diagram of the wet cooler only cooling problem

6: See Section 9.4 (Complete system) for a detailed description of the combined cooler and condenser model.

In this version of the problem, the decision vector is composed by the recirculation flow rate, but now the fan speed of the wet cooler (ω_{wct}) is included. The cost of cooling now includes the cost of water (J_w) and its availability is updated using the water consumption (C_w) as described in Equations (10.1)–(10.3). The environment now includes the air relative humidity and water prices.

10.2.3 Combined cooler

The last static optimization problem is the combined cooler, which incorporates both the dry and wet coolers, as well as the condenser. Here the hydraulic distribution is not fixed but is part of the decision variables, allowing the optimization to determine the optimal distribution between the two coolers. The problem is defined as follows:⁶

Problem: CC - static

$$\min_{\mathbf{x}, \mathbf{e}; \theta} J = f(\mathbf{x}, \mathbf{e}; \theta) = J_e + J_w$$

with:

$$\begin{aligned}
 J_e &= C_e \cdot P_e \\
 J_w &= C_{w,s1} \cdot P_{w,s1} + C_{w,s2} \cdot P_{w,s2} \\
 C_{w,s1} &= \frac{\min(V_{\text{avail}}, C_w \cdot T_s)}{T_s} \\
 C_{w,s2} &= C_w - C_{w,s1} \\
 T_{cc,out}, C_e, C_w, T_{c,in}, T_{c,out} &= \text{ccs model}(q_c, R_p, R_s, \omega_{dc}, \omega_{wct}, T_{amb}, HR, T_v, \dot{m}_v)
 \end{aligned}$$

► Decision variables
 $x = [q_c, R_p, R_s, \omega_{dc}, \omega_{wct}]$

► Environment variables
 $e = [T_{amb}, HR, P_e, P_{w,s1}, P_{w,s2}, V_{\text{avail}}, T_v, \dot{m}_v]$

subject to:

- Box-bounds
 - $\omega_{dc} \in [\underline{\omega}_{dc}, \bar{\omega}_{dc}]$
 - $\omega_{wct} \in [\underline{\omega}_{wct}, \bar{\omega}_{wct}]$
 - $q_c \in [q_c^*, \bar{q}_c]$
 - $R_p \in [0, 1]$
 - $R_s \in [0, 1]$
- Constraints
 - $|T_{cc,out} - T_{c,in}| \leq \epsilon_1$
 - $T_{c,out} \leq T_v - \Delta T_{c-v,\min}$
 - $|Q_{cc} - Q_{c,\text{released}}| \leq \epsilon_2$

Figure 10.5 illustrates the various ways a combined cooler can meet a specific cooling load under identical environmental conditions. The optimal operating points—the Pareto front—are highlighted in the figure. The background color represents the distribution of cooling power: green indicates a greater contribution from the dry cooler, while purple indicates a greater contribution from the wet cooler. Notably, only the leftmost point relies exclusively on the dry cooler. Moving even slightly to the right results in a rapidly increasing contribution from the wet cooler.

10.3 Horizon optimization

The problem structure is very similar to the static alternative, the main difference is that now the decision and environment vectors are composed not from the expected value for the optimization step, but an array of values from the current optimization step (i) until the end of the prediction horizon (n_{steps})⁷:

Problem: CC - horizon

$$\min_{\mathbf{x}, \mathbf{e}; \theta} J = f(\mathbf{x}, \mathbf{e}; \theta) = \sum_{i=1}^{n_{\text{steps}}} (J_{e,i} + J_{w,i}) \cdot T_s$$

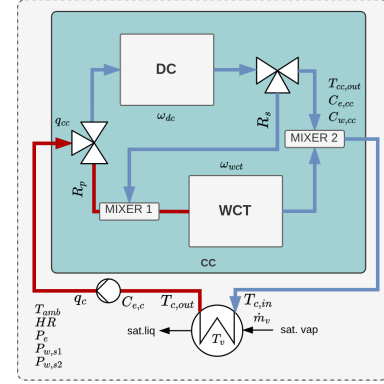
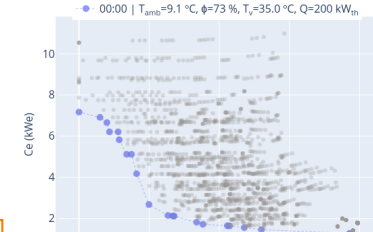


Figure 10.4: Diagram of the combined cooler



Add a background color antes del domingo

Reminder: Pareto front

When dealing with multiple objectives where no single solution is optimal, but improvements in one objective lead to trade-offs in others, a set of points is obtained that represents the best trade-offs between the objectives—known as a Pareto front⁸.

⁸ See Section 5.3 (Multi-objective optimization)

7: Bold notation is used to indicate that the variable is an array and not a single value, e.g. \mathbf{x}

$\forall i = 1 \dots n_{\text{steps}}$ is a notation to indicate that a condition must be held at every step i in the optimization horizon (n_{steps})

with:

for $i = 1 \dots n_{steps}$:

$$J_{e,i} = C_{e,i} \cdot P_{e,i}$$

$$J_{w,i} = C_{w,s1,i} \cdot P_{w,s1,i} + C_{w,s2,i} \cdot P_{w,s2,i}$$

$$C_{w,s1,i} = \frac{\min(V_{avail,i}, C_{w,i} \cdot T_s)}{T_s}$$

$$C_{w,s2,i} = C_{w,i} - C_{w,s1,i}$$

$$V_{avail,i} = V_{avail,i-1} - C_{w,s1,i} \cdot T_s$$

$$T_{cc,out,i}, C_{e,i}, C_{w,i}, T_{c,out,i} = f(q_{c,i}, R_{p,i}, R_{s,i}, \omega_{dc,i}, \omega_{wct,i}, T_{amb,i}, HR_i, T_{v,i}, \dot{m}_{v,i})$$

► Decision variables

$$\mathbf{x} = [\mathbf{q}_c, \mathbf{R}_p, \mathbf{R}_s, \omega_{dc}, \omega_{wct}]$$

$$\text{where } \mathbf{x} = [x_{1,1}, \dots, x_{1,n_{steps}}, \dots, x_{n_x,n_{steps}}]$$

► Environment variables

$$\mathbf{e} = [\mathbf{T}_{amb}, \mathbf{HR}, \mathbf{P}_e, \mathbf{P}_{w,s1}, \mathbf{P}_{w,s2}, \mathbf{V}_{avail,0}, \mathbf{T}_v, \mathbf{m}_v]$$

$$\text{where } \mathbf{e} = [e_{1,1}, \dots, e_{1,n_{steps}}, \dots, e_{n_e,n_{steps}}]$$

subject to:

► Box-bounds

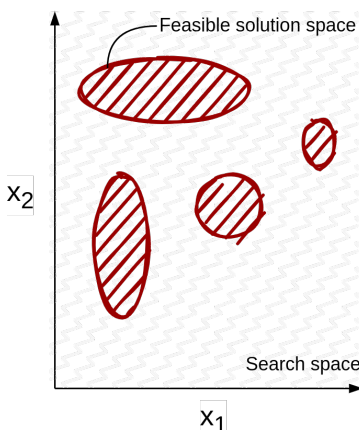
- $\mathbf{w}_{dc} \in [\underline{w}_{dc}, \bar{w}_{dc}]$
- $\mathbf{w}_{wct} \in [\underline{w}_{wct}, \bar{w}_{wct}]$
- $\mathbf{q}_c \in [q_c, \bar{q}_c]$
- $\mathbf{R}_p \in [0, 1]$
- $\mathbf{R}_s \in [0, 1]$

► Constraints, $\forall i = 1 \dots n_{steps}$:

- $|T_{cc,out,i} - T_{c,in,i}| \leq \epsilon_1$
- $T_{c,out,i} \leq T_{v,i} - \Delta T_{c-v,min}$
- $|Q_{cc,i} - Q_{c,released,i}| \leq \epsilon_2$

This formulation allows for an arbitrary long prediction horizon, however, since forecasts for each variable in the environment are needed, it will be limited to a number of steps where reliable predictions can be obtained. On this work water availability is allocated daily so the prediction horizon is established until the end of the operation day, and it starts from the current time when the optimization is launched.

10.3.1 A discussion on solving the optimization problem



As defined, the CCS problem decision vector is composed by five variables that are direct inputs on the process⁸. But as mentioned, not any five values for these variables will yield a feasible solution, in the real system this translates to the fact that a stable operation *i.e.* steady-state would never be reached for that set of inputs. To check for feasible operation the three mentioned constraints are introduced, however, this increases the complexity of the solution space significantly, since the solution space will not be continuous, but as seen in Figure 10.6, it will be formed by islands of feasible solution space regions separated by infeasible regions. This means that finding a feasible solution is not trivial, and the optimization algorithm will need to explore the solution space-a global search algorithm-in an attempt to find the global minimum.

Figure 10.6: Visualization of a constrained search space for two decision variables

For one single step, most global search algorithms with multiple runs⁹ were able to consistently find the global optima, this was not the case for local gradient-based algorithms, which were very sensible to the initial conditions and often converged to local minima, even when coupled with other techniques, such as Generalized Monotonic Basin Hopping [31], they struggled to consistently escape these local optima.

The problem becomes significantly more complex when the prediction horizon is extended, the decision vector grows five-fold for each additional step in the prediction horizon, and the optimization algorithm is tasked with finding a feasible solution for this much larger decision vector, in a very complex solution space, at once for all steps. The chances of finding a feasible solution decrease significantly, and this was reflected in the failure to find a single feasible solution. Even when providing an initial guess composed by the static problem solutions for each step in a 24 steps horizon, the returned solution was that same initial guess.

10.3.2 Proposed solution: Decomposition-based multi-objective optimization with trajectory planning

A two-level optimization strategy is proposed to solve a multi-step decision problem¹⁰. At each step of the prediction horizon, a multi-objective optimization problem is independently solved, yielding a Pareto front. A global optimization problem is then formulated to select a path through the sequence of Pareto fronts, minimizing a cumulative objective (*i.e.*, cost), akin to a pathfinding or Traveling Salesman Problem (TSP)-like over Pareto-optimal points.

The methodology is illustrated in Figure 10.7 and its components are described in the following sections.

Solving the multi-objective optimization problems

To limit the complexity of the problem, the decision space can be reduced by one by variable by analyzing how the complete model is solved and described in Section 9.4 (Complete system); firstly, the condenser can be solved just by using the recirculation flow rate (q_c), it follows the dry cooler by adding the first valve ratio (R_p) and dry cooler fan speed (ω_{dc}). The only remaining component to solve is the wet cooler. The wet cooler inlet conditions ($q_{wct}, T_{wet,in}$) can be determined by using the second valve ratio (R_s). As for the outlet conditions, from the condenser evaluation, its inlet temperature is known and it sets the value of the combined cooler outlet temperature ($T_{cc,out}$), which in turn is the result of the mixing from the DC and WCT outlet temperatures ($T_{dc,out}$ and $T_{wct,out}$, respectively).

The result of this analysis is that the wet cooler fan speed is not a decision variable anymore, but an output of the model, which can be computed by inverting the wet cooler model, where an outlet temperature is provided as input, and the fan speed is computed as an output. Summarizing, the decision vector can be reduced from five to four variables:¹¹

$$\mathbf{x} = [q_c, R_p, R_s, \omega_{dc}]$$

More importantly, now the optimization algorithm does not need to find a set of five inputs that produce a feasible solution in a complex solution space, but only four values from which a feasible wet cooling tower fan speed exists¹², thus greatly simplifying the problem.

9: Tried algorithms include: Algoritmos probados de pygmo y Poner Gaussian también

[31]: Wales et al. (1997), "Global Optimization by Basin-Hopping and the Lowest Energy Structures of Lennard-Jones Clusters Containing up to 110 Atoms"

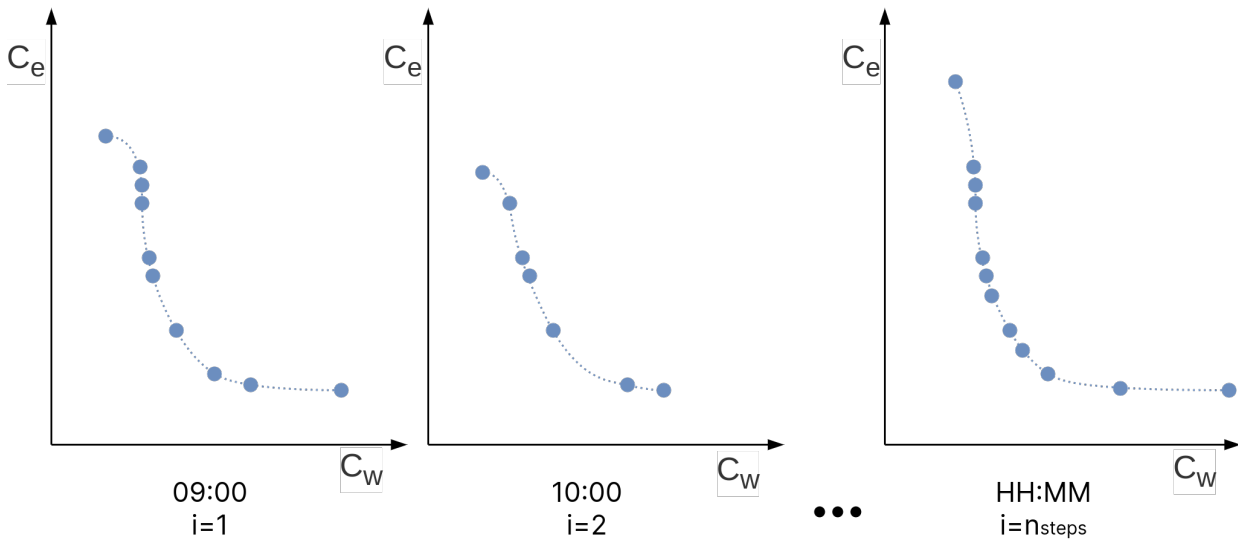
10: Alternative wording: Pareto front chaining, multi-step Pareto optimization, path planning on Pareto surfaces.

11: This reasoning works only for a system with this particular configuration, a different combined cooler layout would require a different analysis.

12: *i.e.* within its bounds $\omega_{wct} \in [\underline{\omega}_{wct}, \bar{\omega}_{wct}]$

0. Decompose the problem horizon into its n steps elements.

1. Solve a multi-objective optimization problem, independently for each step, to obtain a set of pareto fronts:



2. Select a path through these pareto fronts that minimizes a global objective: the cumulative operation cost of operation

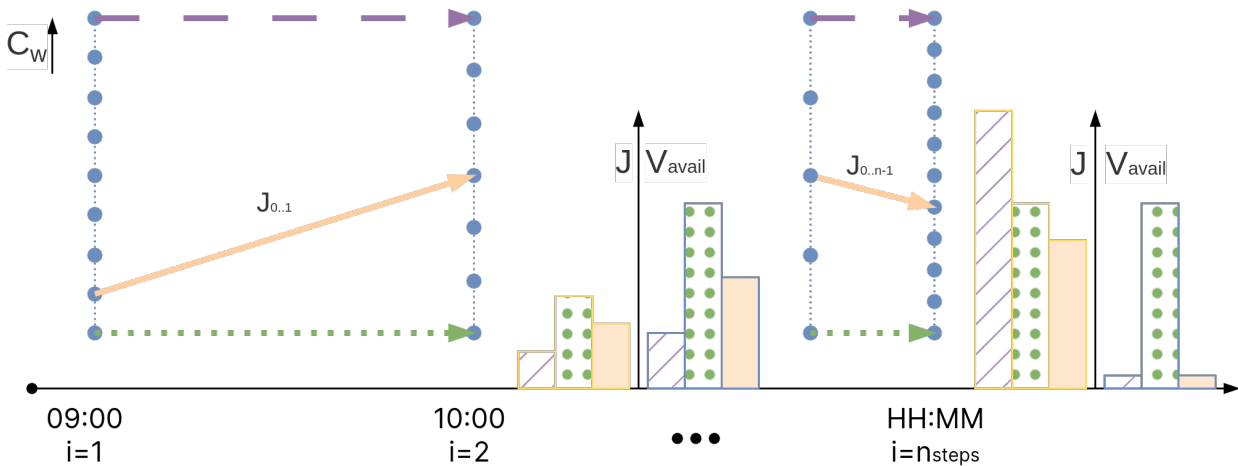


Figure 10.7: Proposed methodology. Decomposition-based multi-objective optimization with trajectory planning. In step 2, three paths are illustrated: a water-greedy dash-purple (-) path, a water-conservative green-dotted path (..) and a compromise-approach solid-orange path (-)

A straightforward approach to solve the multi-objective optimization is to do a grid-search over the decision space, evaluating the model for every combination of decision variables, and then storing only the points for which a feasible ω_{wct} exists. This approach is not recommended for large decision spaces, but for the four-dimensional decision space and with a model that can be evaluated in fractions of a second, it is feasible.

Next, the Pareto front is computed from the feasible points, which are evaluated in terms of the two consumptions: electricity (C_e) and water (C_w). By definition,

the Pareto front is the set of points that cannot be improved in one objective without worsening the other, and it is computed by checking for each point if there is another point that is better in both objectives, and if so, it is removed from the set of feasible points. The remaining points form the Pareto front. This process is repeated for each step in the prediction horizon, resulting in a set of Pareto fronts, one for each step, as visualized in Figure 10.7–1.

Path selection subproblem

The path selection subproblem is a combinatorial optimization problem over a layered weighted directed graph, where each layer corresponds to a time step in the prediction horizon, and each node in a layer represents a point on the corresponding Pareto front. The objective is to find a path $\mathbf{p} = (p_1, p_2, \dots, p_{n_{\text{steps}}})$, where p_i is the selected node at time step i , that minimizes the total cumulative cost along the path (J). The problem can be formulated as:

$$\min_{\mathbf{p}} \quad J = \sum_{i=1}^{n_{\text{steps}}-1} C_{\text{transition}}(p_i, p_{i+1})$$

Each transition cost $C_{\text{transition}}(p_i, p_{i+1})$ depends on both consumptions (i.e. electricity and water consumption) of the nodes p_i and p_{i+1} , as well as a dynamic price function that depends on the path history. Specifically, the transition cost is correlated to the current resource availability ($V_{\text{avail},i}$)¹³ and will depend on the current state of the system, which is a function of the previous decisions. This is a very simple calculation that can be computed almost instantly, and it is the only information needed to compute the transition costs between two points in the Pareto front:

$$C_{\text{transition}}(p_i, p_{i+1}) = P_e(i) \cdot C_e(p_{i+1}) + P_w(i) \cdot C_w(p_{i+1})$$

where:

- ▶ $C_e(p_{i+1}), C_w(p_{i+1})$: electricity and water consumption at node p_{i+1}
- ▶ $P_e(i), P_w(i)$: price coefficients for electricity and water at step i , which may be dependent on the previously selected nodes (i.e., the path so far)

Prices $P_e(i), P_w(i)$ depend on prior path decisions, this introduces path-dependency into the cost function, and makes the problem non-trivial to solve via simple shortest path algorithms. The problem could be handled via dynamic programming, graph search (like Dijkstra or A*), or metaheuristics such as genetic algorithms.

The subproblem is illustrated in Figure 10.7–2. Each node represents a point in the Pareto front of a step, and edges represent the transition costs between these points, that is, the cumulative cost so far ($J_{0..i}$). Three paths are illustrated in Figure 10.7–2. The dash-purple (- -) path is a path that chooses nodes with a high water use¹⁴, so in the first split it can be seen it achieves the lowest cost of operation, but also leaves the least water available for the next steps, resulting in a higher total cost of operation. On the other hand, the green-dotted path (..) chooses the nodes with the lowest water use, this translates in a consistently higher cost of operation and leaving some water available at the end of the horizon. Because of the formulation of the problem, this is sub-optimal since this unused water is considered lost. Finally, the solid-orange path (—) is a compromise between the two, it uses water more efficiently, leaving no water available at the end of the horizon and minimizing the overall cost of operation.

13: See Equations (10.1)–(10.3)

14: In Figure 10.7, nodes are ordered with increasing values of C_w from bottom to top.

TL;DR

In this chapter a detailed description of the combined cooling pilot plant at PSA is provided including a P&ID diagram and the methodology followed to perform the experimentation and data-processing. Three experimental campaigns for the WCT with XX, XX and XX different operating points and one for the DC with XX operating points are processed and made openly available in public repositories.

11.1	Plant description	48
11.2	Experimental campaigns . . .	49
11.3	Wet cooling tower	49
11.3.1	Exp 1	49
11.3.2	Exp 2	50
11.3.3	Exp 3	51
	11.3.4 Experimental campaigns for the dry cooler	51

Introduction

The combined cooling pilot plant at Plataforma Solar de Almería is a unique facility that integrates a wet cooling tower and a dry cooler in a flexible hydraulic configuration. It allows for the study and validation of different cooling strategies and the development of models.

...

This chapter describes the plant in Section 11.1 (Plant description) and the experimental campaigns carried out in Section 11.2 (Experimental campaigns).

completar esta sección antes del domingo

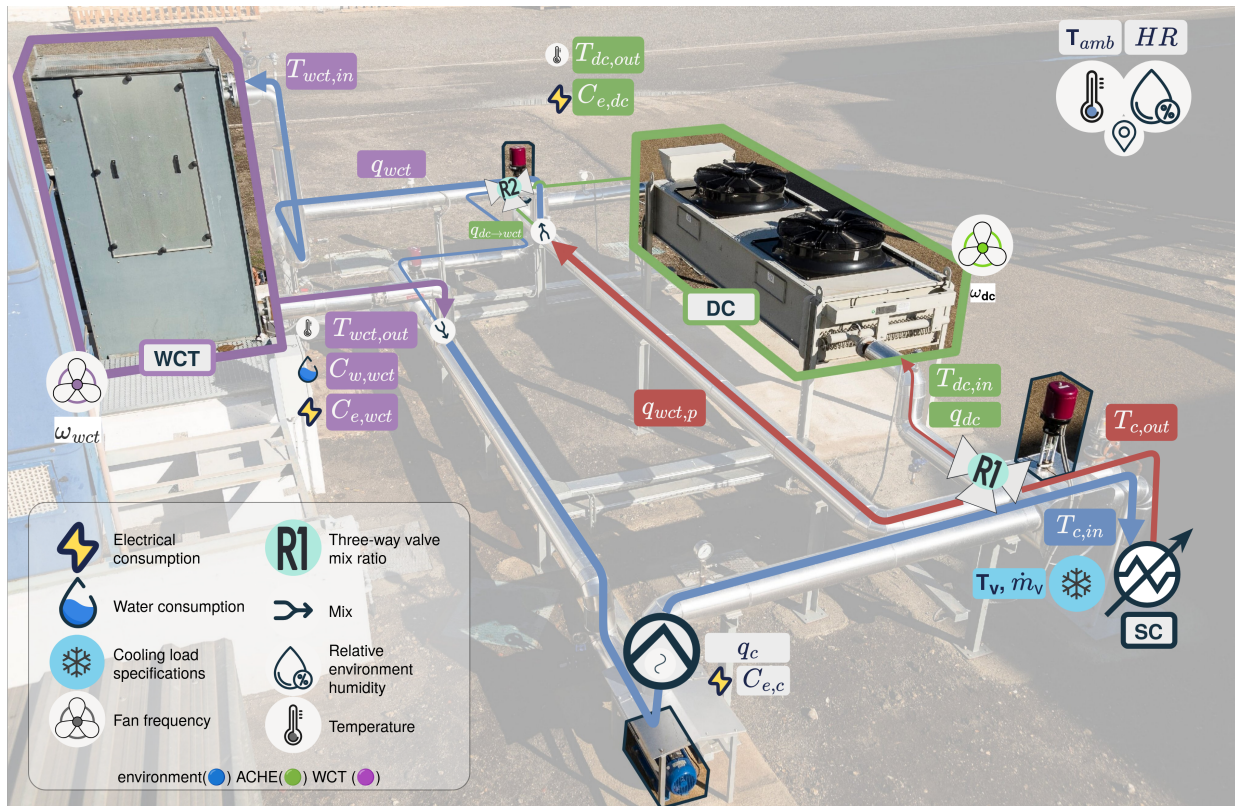


Figure 11.1: PSA combined cooling system facility

11.1 Plant description

The pilot plant of combined cooling systems located at PSA (see the layout in Figure 11.3) consists of three circuits: cooling, exchange and heating. In the cooling circuit (see a picture in Figure 11.2), water circulating inside the tube bundle of a Surface Condenser (SC) can be cooled through a Wet Cooling Tower and/or a Dry Cooling Tower (type Air Cooled Heat Exchanger, ACHE), both with a designed thermal power of 204 kW_{th}. In the exchange circuit, a saturated steam generator of 80 kW_{th} (on the design point), generates steam at different pressures (in the range between 82 mbar and 200 mbar), which is in turn condensed in the surface condenser. In this way, the steam transfers its latent heat of condensation to the refrigeration water, that is heated. Finally, in the heating circuit, a solar field with a thermal power of 300 kW_{th} at the design point, provides the energy required by the steam generator, in the form of hot water. It is a unique, very flexible, fully instrumented and versatile facility, able to operate in different operation modes: series and parallel mode, conventional dry-only mode (all water flow is cooled through the dry cooling tower) and wet-only mode (all water flow is cooled through the wet cooling tower). The instrumentation related to the WCT is described in Table 11.1. Note that the sensors measuring the air velocity and temperature and relative humidity at the outlet area of the wet cooling tower have not been installed in the plant. Portable sensors were used instead in some experiments, as described in Section ??.



Figure 11.2: Back view of the WCT.



In regards to operational aspects of the system, note that the cooling water and air flow rates at the experimental facility (\dot{m}_w and air, \dot{m}_a , respectively), are modified with the Pump 1 and the fan frequency percentage SC-001, respectively (see Figure 11.3).

Table 11.1: Characteristics of instrumentation (^a value of the temperature in °C, ^b of reading, ^c full scale, ^d mean value).

Measured variable	Instrument	Range	Measurement uncertainty
Water temperature (TT-001, TT-006)	Pt100	0 - 100 °C	0.03 + 0.005·T ^a
Cooling water flow rate (FT-001)	Vortex flow meter	9.8 - 25 m ³ /h	± 0.65 % o.r. ^b
Water flow rate (FT-004)	Paddle wheel flow meter	0.05 - 2 m ³ /h	± 0.5 % of FS ^c + 2.5 % o.r
Ambient temperature	Pt1000	-40 - 60 °C	± 0.4 @20 °C
Relative humidity	Capacitive sensor	0 - 98%	± 3 % o.r @20 °C
Air velocity	Impeller anemometer	0.1-15 m s ⁻¹	± 0.1 m s ⁻¹ + 1.5 % o.r
Outlet air temperature	Pt100	-20-70°C	±0.5°C
Outlet air humidity	Capacitive sensor	0-100%	± 2%

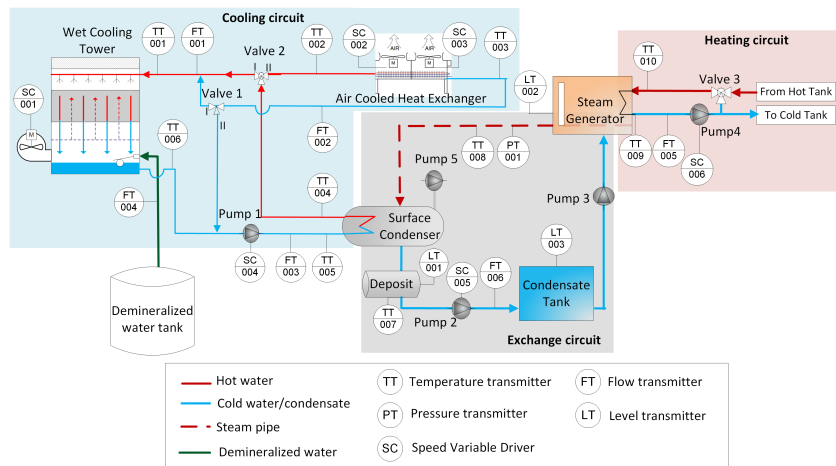


Figure 11.3: Layout of combined cooling systems pilot plant at PSA.

11.2 Experimental campaigns

With the aim of characterizing and developing models for this novel facility, over the years several experimental campaigns have been carried out. In particular, three different experimental campaigns have been performed to characterize the WCT specifically, while a campaign was also carried out to characterize the DC.

11.3 Experimental campaigns for the wet cooling tower

A total of 132 steady-state experimental points have been obtained. These data cover a large variety of ambient conditions (different seasons, days and nights) and thermal loads (from 27 kW to 207 kW). The objective of the experimental campaigns is to develop and validate two modelling strategies for the performance evaluation of the WCT¹.

The normative framework followed to carry out the experiments, in order to ensure stable conditions, has been the standards UNE 13741 [32] and the Spanish CTI [33]. These standards specify the test duration and the allowed variations of the most representative ambient and operating magnitudes (water flow rate, heat load, cooling tower range, wet-bulb and dry-bulb temperatures and wind velocity) during the tests. Although the duration of the test should not be less than one hour according to the standards, due to the low capacity of the WCT in the PSA pilot plant and the operational experience, the duration of the tests has been reduced to up to 30 minutes. Once stable conditions are maintained during the defined interval time, the average and deviations values of each measurement are calculated in order to check that they are within the allowable limits of the norm, which finally lead to a valid steady-state operating point.

Figure 11.4 shows the main variables involved in one of the experiments performed at the pilot plant at constant air flow rate ($f_{fan}=25\%$). As can be observed, there are two time intervals in this case, in which the process is at stationary conditions according to the normative framework mentioned. In order to process the results of the experimental tests and identify valid time intervals, such as the ones shown in this example, a function has been implemented in the MATLAB environment. This function identifies whether the standard criteria is met and calculates the mean values of the required variables.

The data from the different experimental campaigns is available at [\[palenzuela_steadystate_2024a\]](#), [\[34\]](#).

1: See Section 9.1 (Wet cooler)

[32]: UNE (2004), *Thermal Performance Acceptance Testing of Mechanical Draught Series Wet Cooling Towers*

[33]: CTI (2000), *Code Tower, Standard Specifications. Acceptance Test Code for Water Cooling Towers*

11.3.1 Experimental campaign 1 – Exp 1

This campaign was specifically designed for the calibration of the physical model. In total, 19 experimental tests were performed at the combined cooling pilot plant at PSA. The physical model focuses on the calculation of the Merkel number which, according to the literature ASHRAE [28], is not a constant value. Instead, it varies depending on the operating conditions (water-to-air mass flow ratio, \dot{m}_w/\dot{m}_a). Therefore, the experimental campaign has been designed to cover different water-to-air mass flow ratios. Both variables, the water and the air flow rates, were varied within the allowable range for plant operation. In the case of the water flow rate, it ranged from 8 m³/h to 22 m³/h, and in the case of the air mass flow rate, it was modified by changing the fan frequency from 12.5 Hz to 50 Hz (fan frequency percentage, f_{fan} , from 25 % to 100 %). The magnitudes required to experimentally determine the air mass flow rate (air velocity and air temperature and relative humidity) were measured at the outlet area of the

[\[palenzuela_steadystate_2024a\]](#), [\[34\]](#): Serrano et al. (2024), "Wet Cooling Tower Performance Prediction in CSP Plants"

[28]: Ashrae (2004), "HVAC Systems and Equipment"

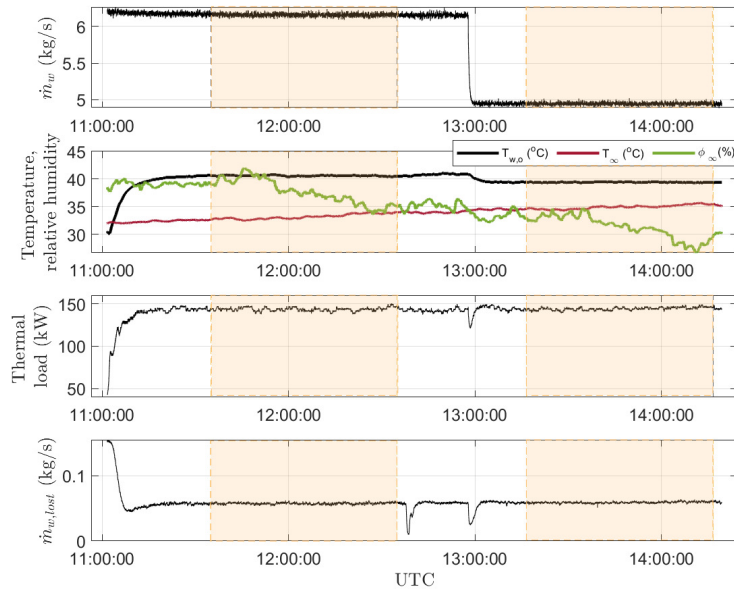


Figure 11.4: Example of one experiment at the pilot plant in July with two valid steady-state operating points.

2: Using the sensors listed in Table 11.1

3: This enables to obtain the air mass flow rate at the outlet of the cooling tower, $\dot{m}_{w,i}$, using the permanent sensors installed in the facility

cooling tower². The outlet area was divided into 9 quadrants and the above mentioned magnitudes were registered at the center of each quadrant. The obtained values were averaged to determine the mean velocity, temperature and relative humidity used in the air mass flow rate calculation.

Following the same experimental procedure, air velocity, temperature and humidity maps were measured for 8 different f_{fan} levels (ranging from 30 % to 100 % in 10 % intervals)³.

The range of air and water mass flow rates are 1.16–4.32 kg/s and 2.17–6.15 kg/s, respectively. Regarding the environmental conditions, these were quite similar for all tests in the campaign: high ambient temperatures (ranging between 32 °C and 41 °C), and low ambient relative humidities (between 13 % and 40 %) since the experiments were carried out during the summer season.

11.3.2 Experimental campaign 2 – Exp 2

The data required for data-driven models depends on several factors such as the complexity of the model and the error allowed or the diversity of the inputs. With the aim of obtaining a reliable model for the WCT, data collected over several years of operation of the combined cooling system have been used for tuning. They are a set of 115 stationary data covering the following operating ranges: ambient temperature, T_{∞} , [9-39] °C, ambient humidity, ϕ_{∞} , [10-87] %, inlet water temperature, $T_{w,i}$ [33-41] °C, cooling water flow rate, $q_{w,i}$ [6-23] m³/h and fan frequency percentage, f_{fan} [21-94] %. The thermal load in these tests varies in the range of [27-178] kW_{th}. The number of steady-state data obtained is a reasonable value when compared to other similar data-driven models of counter-flow cooling towers, as in the case of [24], where 81 experimental points were collected for training and testing⁴

4: Reminder, dataset is available at [palenzuela_steadystate_2024a]

11.3.3 Experimental campaign 3 – Exp 3

With the aim of validating and comparing different modelling approaches, a dataset of 17 tests (different from the ones taken for experimental campaigns 1 and 2) has been compiled. This experimental campaign was designed using a design of experiments based on full factorial design with 4 factors and 2 levels (low and high), whose values are shown in Table 11.2.

An additional test at design operating conditions of the WCT ($T_{b,\infty}=21\text{ }^{\circ}\text{C}$, $T_{w,i}=40\text{ }^{\circ}\text{C}$, $\dot{m}_w=6.9\text{ kg/s}$ and $T_{w,i} - T_{w,o}=7\text{ }^{\circ}\text{C}$) has been also included in this test campaign, where $T_{b,\infty}$ is the ambient wet bulb temperature and $T_{w,o}$ the temperature of the water at the outlet of the WCT.

11.3.4 Experimental campaigns for the dry cooler

Table 11.2: Design of experiments for model comparison.

Variable	Low level	High level
$T_b\text{ (}^{\circ}\text{C)}$	≤ 10	≥ 15
$T_{w,i}\text{ (}^{\circ}\text{C)}$	≤ 37	≥ 39
$\dot{m}_w\text{ (kg/s)}$	≤ 3.3	≥ 5
$T_{w,i} - T_{w,o}\text{ (}^{\circ}\text{C)}$	≤ 7	≥ 8

Validation in the combined cooling pilot plant

To Do

After the chapter is complete, find and replace all mentions to RBF, ANN, RMSE and all other acronyms with the acronym with \gls.

12.1 Modelling

The two main components of the system (WCT and DC) are modelled with different approaches and compared in detail. Afterward, the integration of the selected modelling approach with the rest of the system components (Section 9.3) is validated in Section 12.1.5 (Complete system model validation).

12.1.1 Wet cooler model alternatives comparison and validation

Physical model

As previously mentioned¹, three experimental campaigns have been performed, shown in Figure 12.1 as Exp 1, Exp 2, and Exp 3. Exp 1 corresponds to the Poppe model calibration campaign and it was designed for the calibration of the first principles model. The aims of such campaign was to fit a function (mapping) that relates the air mass flow rate at the outlet of the tower, \dot{m}_a , with the frequency of the fan, f_{fan} :

$$\dot{m}_a = -0.0014 f_{fan}^2 + 0.1743 f_{fan} - 0.7251. \quad (12.1)$$

and to calibrate a WCT performance coefficient: the Merkel number, Me. Figure 12.2 shows the variation of the Merkel number as a function of the water-to-air mass flow ratio (\dot{m}_w/\dot{m}_a) using data from Exp1. As can be seen, the Me decreases with \dot{m}_w/\dot{m}_a values following a linear trend on log-log scale.

12.1 Modelling	53
12.1.1 Wet cooler model alternatives comparison and validation .	53
12.1.2 Dry cooler model alternatives comparison and validation .	54
12.1.3 Main components modelling conclusions	57
12.1.4 Condenser model validation	59
12.1.5 Complete system model validation	60
12.2 Control and optimization results	62
12.2.1 Choosing an optimization algorithm	62
12.2.2 Comparing the static and horizon optimization strategies	63
12.2.3 Validation at pilot plant	64

1: See Section 11.3 (Experimental campaigns for the wet cooling tower)

Lidia, aquí la correlación no usa la temperatura ambiente

Make text in figure larger

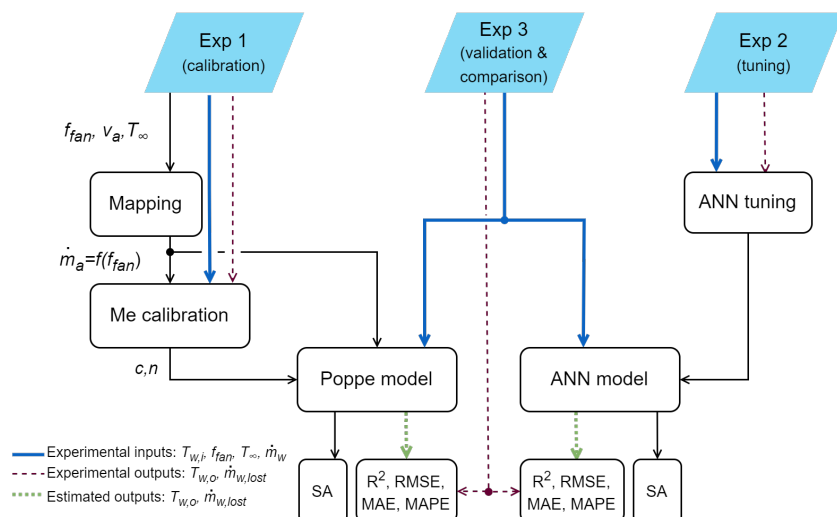


Figure 12.1: Calibration, tuning, validation and comparison procedure

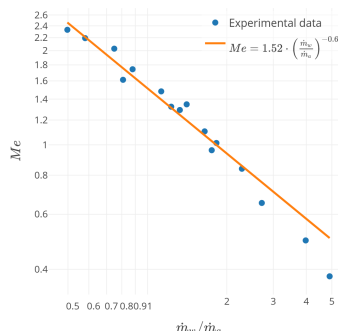


Figure 12.2: Experimental results for the Me number as a function of \dot{m}_w/\dot{m}_a .

Following the correlation for the Merkl number of a wet cooling tower described in Section 9.1.1, the parameters c and n obtained from the data fitting are 1.516 and 0.693, respectively.

Data-driven

In order to generate the data-driven from first-principles alternative, the most relevant input variables identified in Section ?? are discretized using a fixed number of resolution steps for each variable, within ranges based on expected operating conditions, as defined in Table 12.1.

Figure 12.3 shows the generated input space distribution. The upper plot shows the frequency distribution of the samples while the lower one the actual values per input, where the x-axis represents the samples and the y-axis the values for each of the input variables.

Prediction capabilities

Tabla tocha añadiendo casos (GPR, DD from FP, RF, GB)

The results of each modelling alternative and its comparison can be visualized in Figure ?? and Table 12.4. The results of each modelling alternative and its comparison can be visualized Figure ?? shows the results obtained with the models using Exp 3. It shows the perfect fit together with the results obtained with Poppe's model, MIMO FF, cascade CF, and MIMO RBF. In Table 12.4, the performance of the studied modelling approaches are included for the different performance metrics². T represents the performance metric value for the training / calibration dataset (Exp 1 or Exp 2 depending on the case), and V for the validation and comparison one (Exp 3). In all cases the model representing each alternative is in the best case scenario, *i.e.* maximum number of points available. On the other hand, s.u. indicates that the units of the column are the same as from the source variable.

Comparing both modelling approaches (see Figure ??), it can be outlined that both models provide a good prediction of the output variables, falling most of the discrepancies (errors) within the uncertainty range. Poppe's model provides a better prediction of the outlet temperature, obtaining an RMSE of 0.33 °C and an R^2 of 0.98. In comparison, the best ANN alternative (RBF MIMO) has a slight worse performance with an RMSE of 0.51 °C and $R^2 = 0.95$. In terms of water consumption, the physical model has a better prediction accuracy in terms of RMSE and R^2 (8.5 l/h and 0.97) compared to 11.24 l/h and 0.95 for the best ANN model (cascade CF). It can be stated that, although the results are better for the physical model (specially in the case of the outlet temperature prediction), both approaches produce valid results with high accuracy levels.

Incluir gráfica comparativa de evolución de RMSE (incluyendo GPR) para argumentar por qué GPR es mejor no solo en términos de error, si no también en requerimiento de datos.

12.1.2 Dry cooler model alternatives comparison and validation

Physical model

Data-driven

In order to generate the data-driven from first-principles alternative, the most relevant input variables identified in Section 9.2.2 are discretized using a fixed number of resolution steps for each variable, within ranges based on expected operating conditions, as defined in Table 12.3. and Section ?? (??) visualizes the

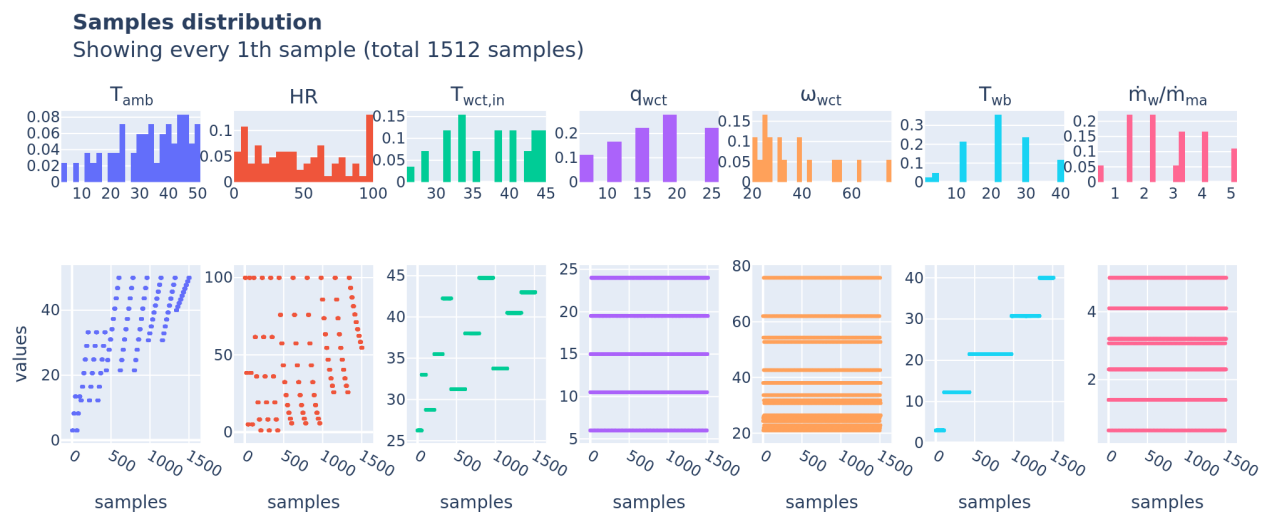


Figure 12.3: Data-driven from first-principles. Samples distribution visualization.



generated input space distribution where it can be appreciated that the samples are well distributed across the entire input space.

Figure 12.4: WCT models performance comparison between the different modelling approaches.

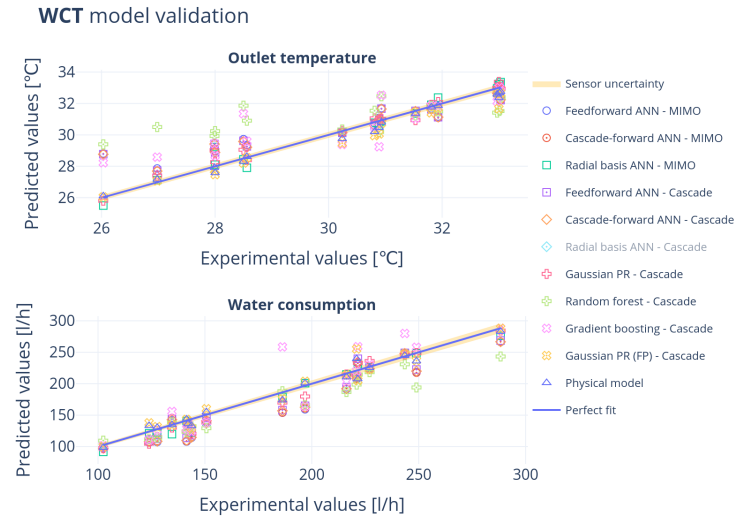


Table 12.2: Summary table of the prediction results obtained with the different modelling approaches studied.

Predicted variable	Modelling alternative	Model config	Topology	Performance metric								Evaluation time (s)	
				R ² (-)		RMSE (s.u.)		MAE (s.u.)		MAPE (%)			
				T	V	T	V	T	V	T	V		
$T_{wet,out}$ (°C)	Physical model	-	-	-	0.98	-	-	-	0.27	-	0.87	6.288	
	Feedforward ANN	MIMO	20-2	0.90	0.81	0.60	0.97	0.42	0.67	1.36	2.36	0.004	
	Cascade-forward ANN	MIMO	10-10-2	0.90	0.82	0.60	0.93	0.44	0.65	1.42	2.27	0.005	
	Radial basis ANN	MIMO	34-2	0.97	0.97	0.34	0.41	0.21	0.28	0.66	0.94	0.007	
	Feedforward ANN	Cascade	20-1	0.90	0.82	0.60	0.93	0.43	0.65	1.41	2.26	0.011	
	Cascade-forward ANN	Cascade	10-10-1	0.90	0.83	0.60	0.92	0.43	0.64	1.40	2.24	0.010	
	Radial basis ANN	Cascade	92-1	0.97	-1.44	0.33	3.45	0.10	2.12	0.32	7.43	0.009	
	Gaussian PR	Cascade	N/A	0.99	0.97	0.20	0.37	0.15	0.26	0.47	0.89	0.001	
	Random forest	Cascade	N/A	0.75	0.30	0.96	1.85	0.60	1.46	2.03	5.05	0.078	
	Gradient boosting	Cascade	N/A	1.00	0.68	0.00	1.24	0.00	0.95	0.01	3.29	0.015	
C_w (l/h)	Gaussian PR (FP)	Cascade	N/A	1.00	0.94	0.32	0.54	0.15	0.41	0.52	1.32	0.105	
	Physical model	-	-	-	0.97	-	8.47	-	6.74	-	3.74	6.288	
	Feedforward ANN	MIMO	20-2	0.92	0.83	14.77	21.58	11.98	18.64	9.91	10.75	0.004	
	Cascade-forward ANN	MIMO	10-10-2	0.92	0.84	15.47	20.90	12.51	17.84	10.48	10.22	0.005	
	Radial basis ANN	MIMO	34-2	0.99	0.97	5.58	9.34	3.81	7.47	3.23	4.68	0.007	
	Feedforward ANN	Cascade	20-1	0.92	0.88	15.00	18.45	11.97	15.77	10.20	8.92	0.011	
	Cascade-forward ANN	Cascade	10-10-1	0.92	0.85	15.01	20.34	12.11	17.66	10.00	10.18	0.010	
	Radial basis ANN	Cascade	33-1	0.99	0.93	4.99	14.28	3.45	10.14	2.68	6.22	0.009	
	Gaussian PR	Cascade	N/A	0.99	0.95	4.74	12.00	3.61	9.96	3.09	6.32	0.001	
	Random forest	Cascade	N/A	0.89	0.80	17.35	23.23	10.51	18.51	7.58	9.73	0.078	
	Gradient boosting	Cascade	N/A	1.00	0.77	0.24	25.07	0.07	17.21	0.05	9.55	0.015	
	Gaussian PR (FP)	Cascade	N/A	0.98	0.95	10.85	11.63	4.81	8.14	3.74	4.52	0.105	

Prediction capabilities

Tabla tocha añadiendo casos (GPR, DD from FP, RF, GB)

Experimental data requirements

12.1.3 Main components modelling conclusions

This section presents a comparison between two modelling alternatives: data-driven and first-principles. It applies to wet cooling towers and dry coolers, specifically to ACHE. The main conclusions obtained during the investigation and final recommendations can be summarized as follows:

Wet cooling tower

Regarding the prediction of the output variables, in the case of the outlet water temperature, both models reported good results, with low errors falling within the uncertainty range of the experimental equipment. Nonetheless, the physical model performs better than the best data-driven alternative (MIMO RBF): $R^2 = 0.98$ and RMSE= 0.33 °C compared to $R^2 = 0.95$ and RMSE= 0.51 °C, respectively.

For the predictions of water consumption, it was shown that the Poppe model accurately predicts this variable, with results of $R^2 = 0.97$ and RMSE= 8.47 l/h. The best ANN alternative (cascade CF) achieves close results with an $R^2 = 0.95$ and RMSE= 11.24 l/h.

However, the Poppe model reached such reliable prediction levels with a much lower number of tests, needing only 2. In comparison, the ANN alternatives need more data, at least 10 (with a good distribution over the operating range) for the FF and CF ANN models.

Table 12.3: Bounds and discretization of the model input variables.

x	Units	lb	ub	n
T_{amb}	°C	3	50	7
$\Delta T_{amb-dc,in}$	°C	3	30	7
q_{dc}	m³/h	6	24	7
$T_{dc,in}$	°C	25	45	-
ω_{dc}	%	11	99.18	6

completar esta sección antes del domingo

Samples distribution

Showing every 1th sample (total 798 samples)

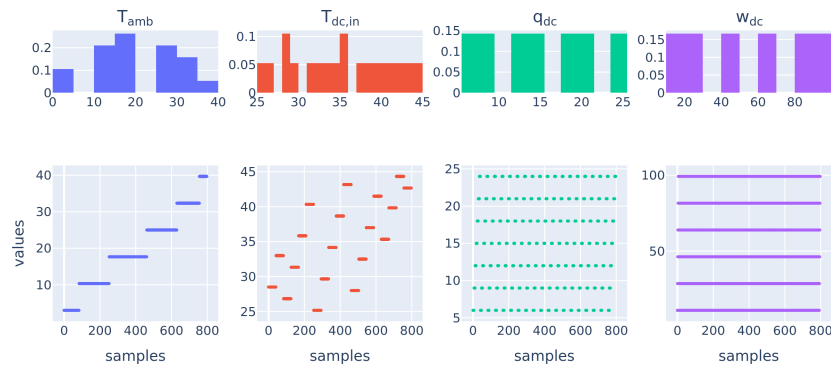


Figure 12.5: Data-driven from first-principles. Samples distribution visualization.



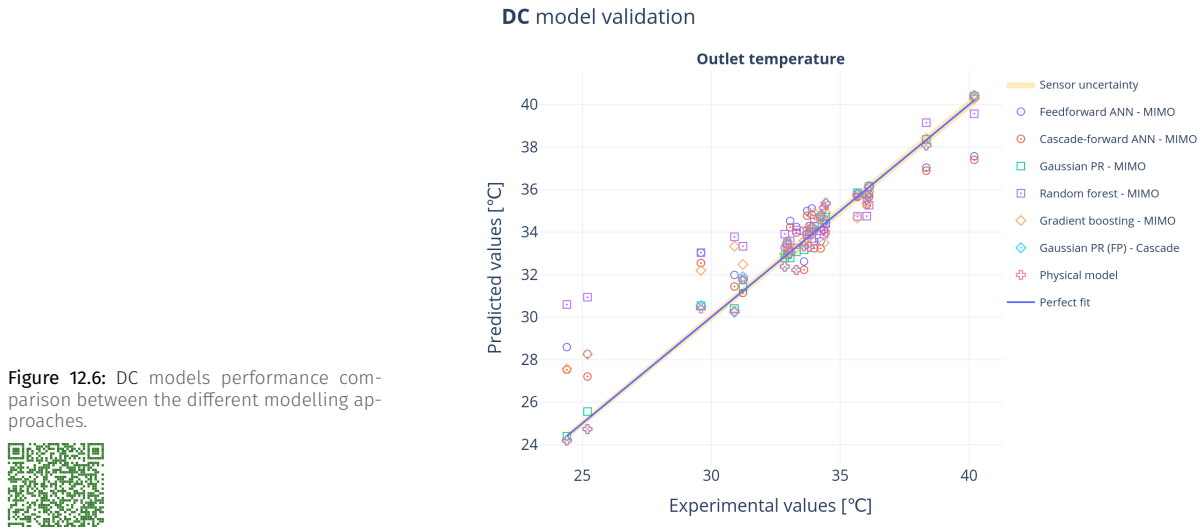


Figure 12.6: DC models performance comparison between the different modelling approaches.



Table 12.4: Summary table of the prediction results obtained with the different modelling approaches studied.

Predicted variable	Modelling alternative	Model config	Topology	Performance metric								Evaluation time (s)	
				R ² (-)		RMSE (s.u.)		MAE (s.u.)		MAPE (%)			
				T	V	T	V	T	V	T	V		
T _{dc,out} (°C)	Physical model	-	-	-	0.98	-	0.50	-	0.42	-	1.28	0.035	
	Feedforward ANN	-	20-1	0.77	0.78	1.42	1.62	1.13	1.18	3.29	3.85	0.005	
	Cascade-forward ANN	-	10-10-1	0.78	0.85	1.39	1.37	1.12	1.02	3.23	3.24	0.007	
	Gaussian PR	-	N/A	0.99	0.99	0.24	0.32	0.19	0.25	0.56	0.77	0.005	
	Random forest	-	N/A	0.84	0.61	1.19	2.17	0.72	1.36	2.05	4.69	0.022	
	Gradient boosting	-	N/A	1.00	0.86	0.00	1.31	0.00	0.86	0.00	2.92	0.035	
	Gaussian PR (FP)	-	N/A	1.00	0.98	0.03	0.53	0.02	0.44	0.07	1.35	0.002	

Air-cooled heat exchanger

Conclusions and recommendations

For the proposed optimization strategy in Section ?? (??), a fast, reliable model that can be scaled to different system sizes is required.

On the one hand, the first-principle models execution time is much higher than the data-driven alternatives, which is a significant drawback when it comes to the optimization strategy, where the model is evaluated many times in a short period of time. On the other hand, the data-driven counterparts are only applicable to the conditions and the particular system with which they are developed.

Conversely, one of the main strengths of both physical models presented in this chapter, is their ability to predict the operation of the coolers regardless of the conditions tested; while the data-driven execution time is faster by orders of magnitude, it can be vectorized and its execution time is more constant regardless of the input conditions.

Therefore, as combining a wet cooler and a dry cooler into a combined cooler offers potential advantages compared to the individual systems, combining both modelling approaches is the chosen solution to model the system. The best performing data-driven model, the Gaussian-Process Regression (GPR) is calibrated using data from the first-principle models, where physical models are adapted dynamically to the required scale and finally the data-driven model can be generated. This approach provides a way of having on-demand models that

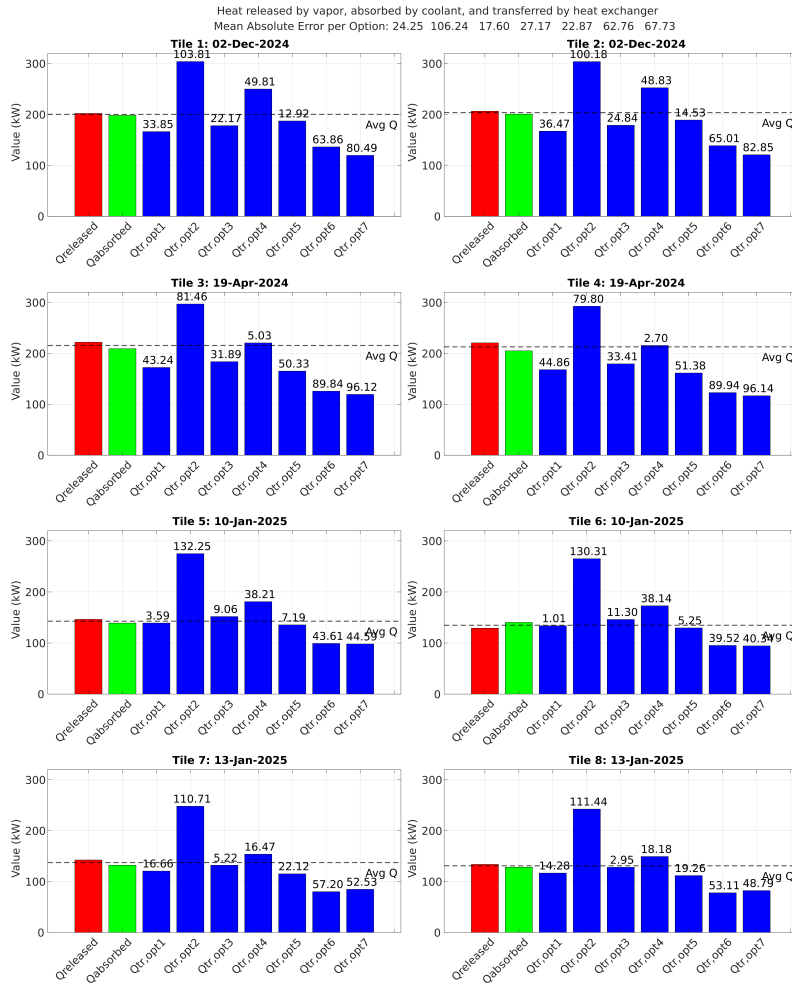


Figure 12.7: Heat transfer coefficient calibration results

can be adapted to the particular case study, while still being fast and efficient in terms of computational resources.

12.1.4 Condenser model validation

For the surface condenser³ a physical model is used, with the heat transfer coefficient as the only parameter to calibrate. Seven different alternative estimations of the heat transfer coefficient were calculated, using the data from the experimental campaign described in Section ?? (??). They are as follows:

1. Empirical correlation using the condenser flow rate (q_c) and the vapor temperature (T_v) as inputs.
2. Empirical correlation using the cooling water inlet temperature ($T_{c,in}$) and T_v as inputs.
3. Empirical correlation using the flow rate per condenser tube ($q_{c,tube} = q_c/n_{tubes} = q_c/24$) and the cooling water inlet temperature.
4. Nominal value from the manufacturer, which equals 1.838 W/m²°C
5. Calibra_Uexp_original
6. Calibra_Uexp_recortado

3: See Section ?? (??)

The results of the calibration are shown in Figure 12.7, where the y-axis shows the thermal power obtained and the x-axis holds different bars for the different heat transfer coefficient estimation methods, with bars also for the experimental

Estos qué son? Generar una nueva versión de la figura una vez se seleccionen los métodos finales

heat released by the vapor and absorbed by the coolant. As can be seen in the figure. The shown results are for steady-state conditions with the condenser in an equilibrium state ($Q_{\text{released}} \approx Q_{\text{absorbed}}$), and with a large variation in the condenser conditions (120 to 200 kW, the whole operating range of the condenser). The results show that the heat transfer coefficient obtained with the method 3 is the one that best fits the experimental data, with a MAE of 17.6 kW and a maximum error of 33.41 kW (15%).

12.1.5 Complete system model validation

a completar una vez se tengan resultados experimentales, hay que implementar la función para generar la visualización

Esto, o bien se hace comparando puntos en estático cuando todo el sistema está en estacionario, o en la gráfica de validación de la estrategia de optimización se muestra también una línea con las predicciones del modelo. Y después una tabla con cada una de las salidas del sistema, mostrando el error entre cada una de las predicciones del modelo (cada vez que se evalúa la optimización), en comparación al valor real obtenido en la planta.

Cuando haya un cambio en la planificación, las predicciones de predicciones antes a conocerse el cambio, cambiar su color a un gris para mostrar que esas predicciones ya no son válidas pues han cambiado las condiciones.

Figure 12.8 shows the model validation results for the complete system model. Different plots are shown for the main output variables⁴. Solid lines represent the measured variables in the real facility, while the different markers represent the predictions generated at different times. The plots also include a right-axis to display a metric error, specifically the MAPE of the predictions with respect to the measured values. The error is shown with a bar for each prediction.

The results show that the model is able to predict the main output variables of the system with a good accuracy. As expected the errors compound over time, specially after the change in the operation schedule at XX:XX. Nonetheless, the model is able to adapt after a new evaluation including the change and overall predictions below XX% of error are achieved.

4: C_w , $T_{dc,out}$, etc

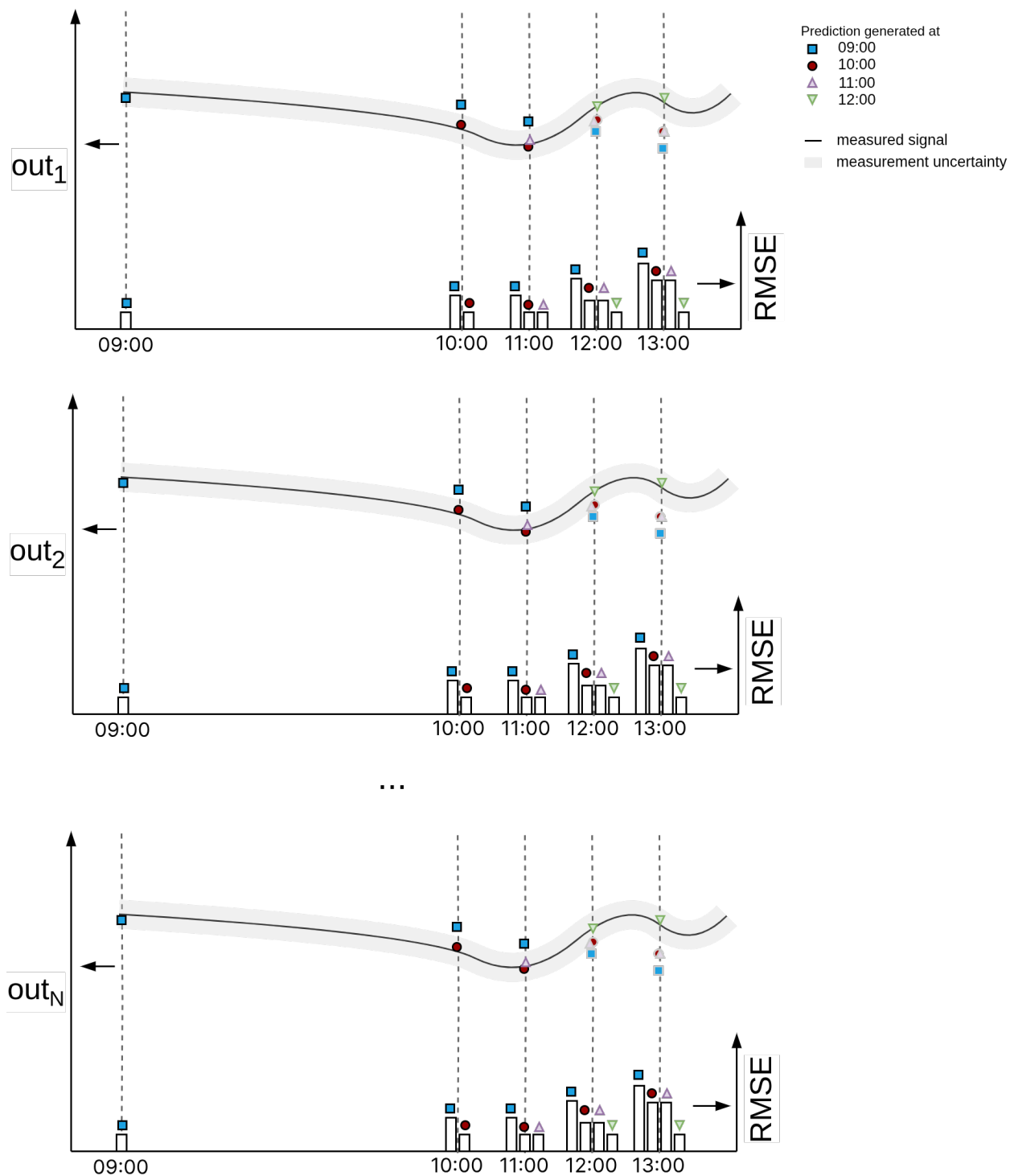


Figure 12.8: Figure caption.



12.2 Control and optimization results

Once the models of the main components of the system have been validated, the next step is to validate the optimization strategy proposed in Section ?? (??). First, an optimization algorithm is chosen by comparing different alternatives in Section 12.2.1 (Choosing an optimization algorithm). Then, the two proposed variants for the combined cooler are compared in simulation for one operation day in the simulated pilot plant in order to see which one performs better in Section 12.2.2 (Comparing the static and horizon optimization strategies). Finally, two validation scenarios are tested in the real facility, one where a regular operation schedule is followed throughout the operation, and a second one where planned changes are introduced in the operation schedule, in order to validate how the optimization strategy adapts to changing conditions.

12.2.1 Choosing an optimization algorithm

Static problems

For every static optimization problem (referencias a problemas) three different algorithms are tested: (N+1)-ES Simple Evolutionary algorithm with self-adaptive Constraint Handling (SEA-CSTR), IHS and Differential Evolution with self-adaptive Constraint Handling algorithm (DE-CSTR). For each alternative the same number of objective function evaluations are given (800) but they are distributed differently depending on the algorithm:

- ▶ SEA-CSTR and DE-CSTR make use of the Self-Adaptive Constraint handling algorithm (CSTR-SA) wrapper algorithm, which allows them to the constrained problems. 10 iterations are performed for this wrapper algorithm, leaving 80 iterations to spare for the inner algorithm.
- ▶ For all alternatives, three values are tested for the initial population size: 50, 100 and 400 individuals⁵.
- ▶ Depending on the algorithm only one individual is evolved (IHS and (N+1)-ES Simple Evolutionary algorithm (SEA)) or the whole population (Differential Evolution algorithm (DE)). This means that 800 generations are available for IHS, 80 generations for SEA-CSTR and for DE-CSTR, 1 generation is available for the population of 50 individuals, while only the initial generation is for the population of 100 and 400 individuals.

5: The initial population fitness evaluation is not counted for the budget of objective function evaluations

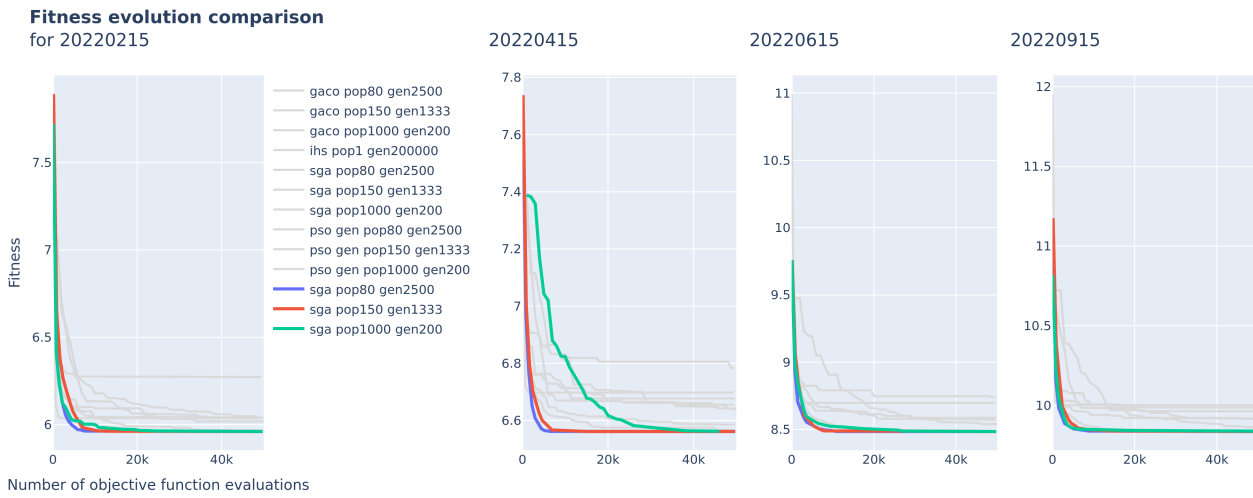
Table X shows the results obtained, in terms of fitness at different stages in the evolution. From the results it can be seen that for all alternatives the best performing and most consistent algorithm is ...

Horizon optimization. Path selection

A methodology similar to the static comparison is used. This time the algorithms evaluated are: Generalized Ant Colony Optimization algorithm (GACO), IHS, Simple Genetic Algorithm (SGA) and Particle Swarm Optimization algorithm (PSO). Three different population sizes are tested (80, 150 and 1000) if the particular algorithm evolves more than one individual; the number of generations is calculated accordingly so that all alternatives have the same budget of objective function evaluations, equal to 200k evaluations⁶. The results are visualized in Figure 12.9, where there are different plots for different dates, the y-axis represents the fitness and the x-axis shows the number of objective function evaluations. The results show that consistently the SGA outperforms the alternatives, and particularly, the smaller population size (80) configuration followed very closely by the 150 population size configuration.

6: Only up to 50k evaluations is shown in the figure for clarity

System	Algorithm	Parameters			Average fitness per obj. fun. evaluations			
		pop size	gen	wrapper algo iters	0	50	150	800
DC	ihs	50	800	N/A	1.28 ± 0.82	1.05 ± 0.29	0.80 ± 0.10	0.77 ± 0.09
		100	800	N/A	0.92 ± 0.18	0.87 ± 0.14	0.81 ± 0.11	0.77 ± 0.10
		400	800	N/A	0.81 ± 0.11	0.80 ± 0.11	0.79 ± 0.10	0.77 ± 0.10
	sea	50	80	10	1.19 ± 0.28	0.95 ± 0.11	0.79 ± 0.10	0.77 ± 0.09
		100	80	10	0.92 ± 0.13	0.86 ± 0.10	0.80 ± 0.10	0.77 ± 0.09
		400	80	10	0.82 ± 0.10	0.80 ± 0.10	0.78 ± 0.10	0.77 ± 0.09
	de	50	1	10	1.06 ± 0.40	0.97 ± 0.18	0.83 ± 0.10	1.04 ± 1.04
		100	0	10	0.95 ± 0.16	0.95 ± 0.16	0.95 ± 0.95	0.95 ± 0.95
		400	0	10	0.83 ± 0.10	0.83 ± 0.10	0.83 ± 0.10	0.83 ± 0.83
WCT	ihs	50	800	N/A	0.24 ± 0.08	0.18 ± 0.04	0.10 ± 0.00	0.07 ± 0.00
		100	800	N/A	0.12 ± 0.02	0.11 ± 0.01	0.08 ± 0.00	0.07 ± 0.00
		400	800	N/A	0.07 ± 0.00	0.07 ± 0.00	0.07 ± 0.00	0.07 ± 0.00
	sea	50	80	10	0.25 ± 0.04	0.16 ± 0.01	0.07 ± 0.00	0.06 ± 0.00
		100	80	10	0.17 ± 0.03	0.11 ± 0.00	0.07 ± 0.00	0.06 ± 0.00
		400	80	10	0.07 ± 0.00	0.07 ± 0.00	0.07 ± 0.00	0.06 ± 0.00
	de	50	1	10	0.29 ± 0.07	0.17 ± 0.02	0.09 ± 0.00	0.07 ± 0.07
		100	0	10	0.11 ± 0.00	0.11 ± 0.00	0.11 ± 0.11	0.11 ± 0.11
		400	0	10	0.07 ± 0.00	0.07 ± 0.00	0.07 ± 0.00	0.07 ± 0.07
CC	ihs	50	1000	N/A	0.77 ± 0.12	0.80 ± 0.11	0.77 ± 0.11	0.59 ± 0.11
		100	1000	N/A	0.70 ± 0.12	0.78 ± 0.10	0.82 ± 0.15	0.61 ± 0.13
		400	1000	N/A	0.79 ± 0.19	0.82 ± 0.21	0.80 ± 0.22	0.65 ± 0.16
	sea	50	100	10	0.92 ± 0.13	0.86 ± 0.14	0.74 ± 0.16	0.51 ± 0.10
		100	100	10	0.88 ± 0.16	0.82 ± 0.16	0.75 ± 0.21	0.62 ± 0.16
		400	100	10	0.84 ± 0.21	0.80 ± 0.18	0.74 ± 0.21	0.69 ± 0.19
	de	50	2	10	0.83 ± 0.16	0.79 ± 0.13	0.73 ± 0.14	0.56 ± 0.13
		100	1	10	0.82 ± 0.17	0.80 ± 0.13	0.77 ± 0.10	0.64 ± 0.13
		400	0	10	0.73 ± 0.16	0.73 ± 0.16	0.73 ± 0.16	0.73 ± 0.73

Table 12.5: Static optimization algorithm comparison results**Figure 12.9:** Horizon optimization – path selection subproblem. Fitness evolution comparison for different algorithms in four different dates.

12.2.2 Comparing the static and horizon optimization strategies

TODO

Poner la figura de resultados del horizonte para SOLO un día detallado aquí (más días hace que no se distingan bien las barras, tampoco se puede poner el pareto). Debe incluir la distribución hidráulica en barras comparando estático con horizonte, el frente de pareto del horizonte, y la comparativa de coste acumulado.

Comentar la figura, sobre el frente de pareto que se muestra, cómo la estática al principio abusa del agua y para el final del día aumenta muchos sus costes,

La figura es provisional. Actualizar la figura con cambios mencionados

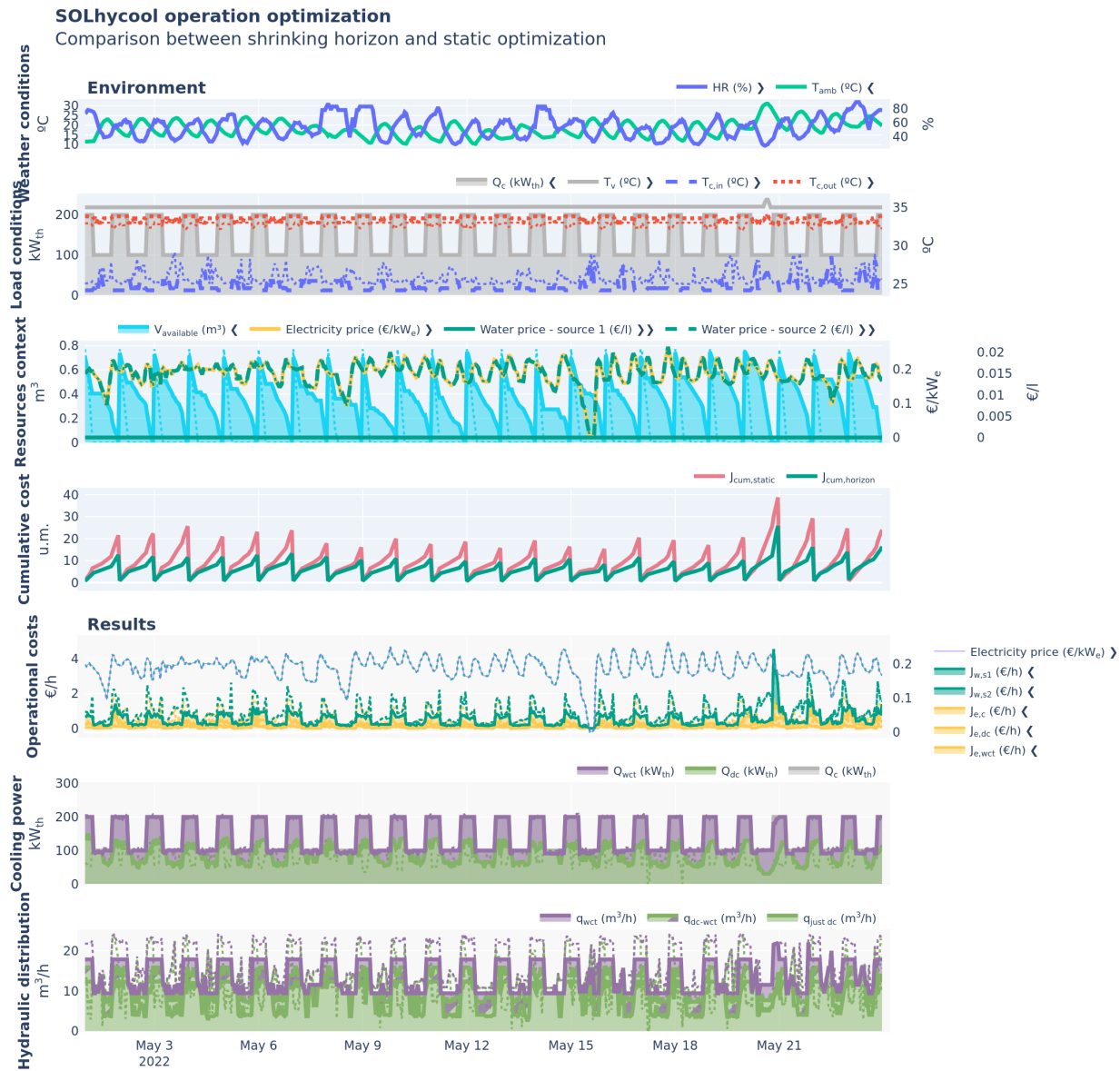


Figure 12.10: Detailed simulation results for the horizon optimization compared to the static alternative.



etc.

12.2.3 Validation at pilot plant

A hierarchical control strategy has been implemented in order to validate the optimization strategy in the real facility. Figure 12.11 shows a diagram of the methodology, where the left side represents the upper layer with the proposed

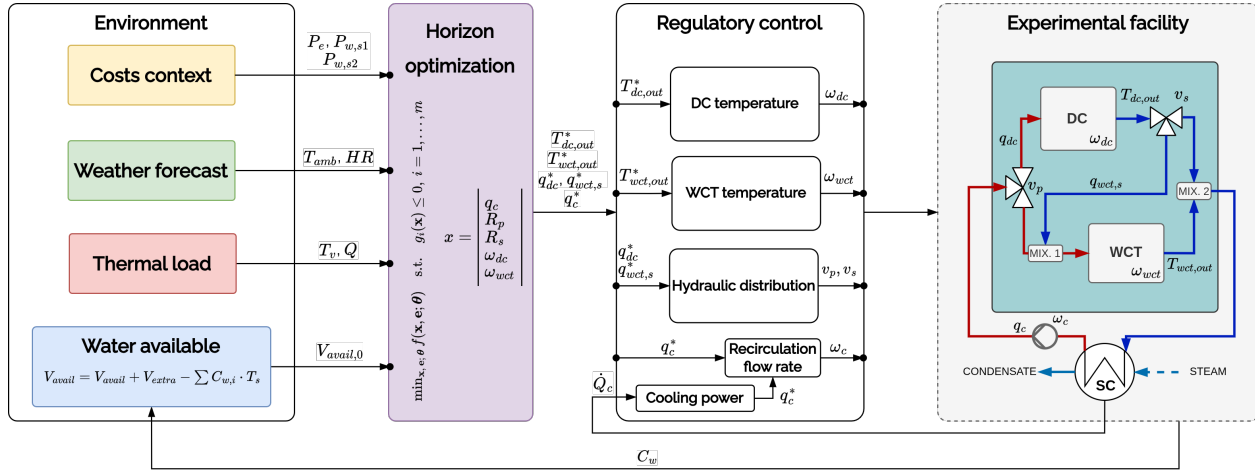


Figure 12.11: Implementation of the optimization strategy in the real facility. Hierarchical control

shrinking horizon optimization⁷ and the right side shows the low-level regulatory control layer, which directly interfaces with the actuators and sensors of the facility.

Environment. To generate the environment for the optimization, weather forecasts using the OpenWeather API were used[openweater_api], for the electricity costs data from the 2022 Spanish grid was used, updating the year to the one in which the experiment was performed, and the water cost was set to $C_{w,s1} = X$ and $C_{w,s2} = Y$. For the thermal load a profile was generated by setting a constant vapor temperature of $T_v = 45^\circ\text{C}$ while an arbitrary cooling power was generated considering the heat availability from the flat-plate collector field, which is the heat source of the system, for the particular day. Finally, an initial value for the water availability was set to $V_{avail,0} = 0.5 \text{ m}^3$, and from there it is updated by reading the actual system consumption online.

Optimization layer. The optimization algorithm is run every 30 minutes, and generates a new set of results for the remaining operation time. The results of the optimization are then passed to the regulatory control layer by setting them as setpoints for the low-level control. The box-bounds for the decision variables are shown in Table 12.6.

Control layer. Four controllers are implemented in this layer... aiuda Lidia!

Table 12.6: Box-bounds for the decision variables.

\mathbf{x} : See Section ??	Units	lb	ub
q_c	m^3/h	5.22	24.15
R_p	-	0.00	1.00
R_s	-	0.00	1.00
$\text{openweater_}?$		11.00	99.18
ω_{wct}	%	21.00	93.42

TL;DR

This chapter presents the annual simulation results for different cooling systems: a WCT, a DC and the presented CC optimized with static optimization and with horizon optimization. They provide cooling to the power block of the XX hours storage–CSP plant ANDASOL-II with an off-peak operation strategy. Results for the case study report a specific cooling cost of XX, XX and XX for the WCT, DC and CC, respectively, compared to the 5 L/kWh figure provided by the developer.

13.1	Limitations	67
13.2	Environment definition . . .	68
13.2.1	Water context	68
13.2.2	Thermal load	68
13.2.3	Costs context	69
13.3	Comparison	69
13.4	Alternatives comparison . .	72

Introduction

A modeling framework has been developed to simulate and optimize the operation of various cooling systems, with a particular focus on the proposed combined cooling system. This methodology has been validated using data from a pilot plant. In this chapter, the objective is to apply the framework to a specific case study: a CSP plant.

As previously mentioned, CSP plants are among the most water-intensive power generation technologies [35], a concern that is especially relevant in the arid regions where they are typically located. To assess the performance-water use and operational costs- of different cooling systems, the proposed methodology is applied to a real-world case study through an annual simulation. The case study examined is the Andasol-II CSP plant.

In the south-east of Spain, near Guadix and next to the Sierra Nevada mountain range (see Figure 13.1), thanks to the region high altitude (1100 m) and the semi-arid climate, the site has exceptionally high annual direct insolation (2260 W/m²) and thus is ideal for solar projects. This is why the first parabolic trough power plant in Europe, Andasol-I, was built there in 2008. One year later Andasol-II followed, located in the immediate neighbourhood and with almost identical construction. It has a rated output of 50 MW with 7.5 hours¹ of thermal storage, providing electricity for up to 200,000 people. More specifications are available in Table 13.1.

According to the developer, Andasol-II vaporizes 870 000 m³/year, or in specific units 5 l/kWh.

13.1 Limitations

1. The combined cooler analyzed has a 50% split in nominal cooling power of the WCT and DC components compared to the standalone cooling systems. Different ratios could be analyzed and one would probably be a better fit for the particular case study. This in itself is a design optimization problem that is not addressed in this thesis.
2. An ACHE is used for the DC, but other options could be considered, such as an ACC.



Figure 13.1: Andasol (I and II) aerial view.
Andasol is the “one of a kind”
Source: https://en.wikipedia.org/wiki/File:Andasol_5.jpg

1: This means that if fully charged, it can produce the nominal rated power of the turbine for that duration

Table 13.1: ANDASOL-II plant main characteristics

Technology	Parabolic Trough
Solar Resource	2260 W/m ²
Nominal Capacity	50 MW
Status	Operational
Start Year	2009
Considerar mover esto al apartado de trabajos futuros	
TF Inlet Temperature	293°C
TF Outlet Temperature	393°C
Power Cycle	Steam Rankine
Turbine Efficiency	38.1%
Cooling Type	Wet
Storage Type	Molten salts
Storage Capacity	7.5 Hours – 1 GWh

Source: Institute for Advanced Sustainability Studies (IASS) and others, 2022; data by Lilliestam@IASS, Thonig@IASS, Zang@CAS, Gilmanova@CAS and others. Licensed under a Creative Commons Attribution 4.0 International License.

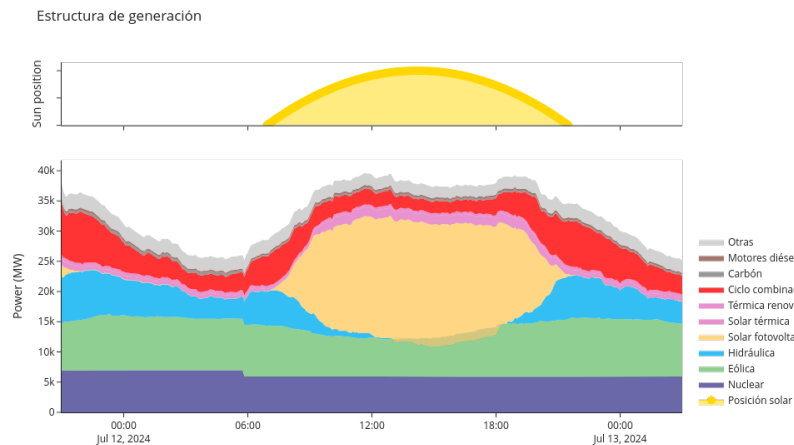


Figure 13.2: Spanish electricity mix on July 12, 2024. The peak in photovoltaic generation is clearly visible at midday, while thermosolar generation is more evenly distributed throughout the day. Peak production is majorly from CSP plants with no storage.

Data source: Figure elaborated using data extracted from <https://www.ree.es/es/datos>

13.2 Environment definition

13.2.1 Water context

Obtaining accurate water availability data is challenging. Unlike resources such as electricity—where demand, supply, and prices are readily available—water availability data is often lacking. Water prices are not standardized; they vary from region to region, and even within the same region, depending on the source and the specific agreements in place.

For the simulation scenario, two sources of water are considered². The first source is rainwater or water from a dam, which is assumed to be available at a constant price of XX [**<empty citation>**]. To create a representative dataset, water availability is modeled as a function of precipitation data, which can be obtained from hourly Typical Meteorological Year (TPY) data [**meteonorm_**]. A linear model is fitted to relate maximum precipitation to maximum available water, and when there is no precipitation, water availability is set to zero. The data is then resampled every 15 days, and the daily volume of available water is calculated by dividing the resampled fortnightly volume by 15. This approach accounts for the presence of water reservoirs and some degree of management capacity.

The alternative source is regenerated water³ is not limited in volume.

13.2.2 Thermal load

Traditionally, thermal power plants were designed and operated to generate electricity only when solar energy was available. This approach remained common until the rapid rise in competitiveness of Photovoltaic (PV) plants, which offer significantly lower generation costs. In response, concentrated solar power plants began integrating thermal energy storage systems to enable dispatchable power generation. Today, 21 out of 51 CSP plants in Spain—approximately 42%—have thermal storage capacities exceeding two hours [8, 36, 37]. This enables them to produce electricity even when solar input is unavailable.

However, many of these plants still follow traditional operating patterns, generating most of their electricity during peak solar hours⁴. This strategy is increasingly seen as suboptimal and is likely to be phased out as the electric grid becomes saturated with PV generation⁵.

2: See Section ?? (??)

<empty citation>

meteonorm_

In this work, a different operational strategy is adopted: the plant is configured to generate electricity during off-peak solar hours, typically in the evening when electricity demand is at its highest. This is achieved by shifting the plant's production to align with these peak demand periods.

A model of the Andasol-II plant, developed by Bartolomé et al. [[empty citation](#)], was configured to follow this production strategy and simulated over an entire year. The resulting thermal load profile represents the demand to be met by the cooling system. The simulation used the same weather dataset as that employed for modeling the cooling system.

[empty citation](#)

13.2.3 Costs context

Electricity. The spanish grid operator Red Eléctrica de España (REE) provides an API⁶ to access the electricity market prices. A python script was developed to systematically download monthly data⁷ for each month in the desired year. The data is fetched in hourly intervals and saved in JSON format, then every file is read and joined into a single dataset resulting in prices for the whole year.



6:

<https://api.esios.ree.es>

7: Longer periods would result in silent errors in the API

Water. Rainwater has a constant lower price of XX. This price was obtained considering that the plan has access to the same water than the irrigation community of the area [[empty citation](#)]. The alternative source, *i.e.* regenerated water, is considerably more expensive, and its price is linked to the electricity price, specifically by a factor of XX⁸.

[empty citation](#)

8: This value includes a scaling factor to normalize the values

Simulation data and parameters information

Weather data Hourly weather data from TPY of Guadix (Spain) for the year. Data was obtained from ...

Thermal load Hourly thermal load data from the power block of ANDASOL-II CSP plant from a simulation model.

Electricity price Spanish electricity market from 2022.

maximum available water The maximum available water for ...
active water source factor ...

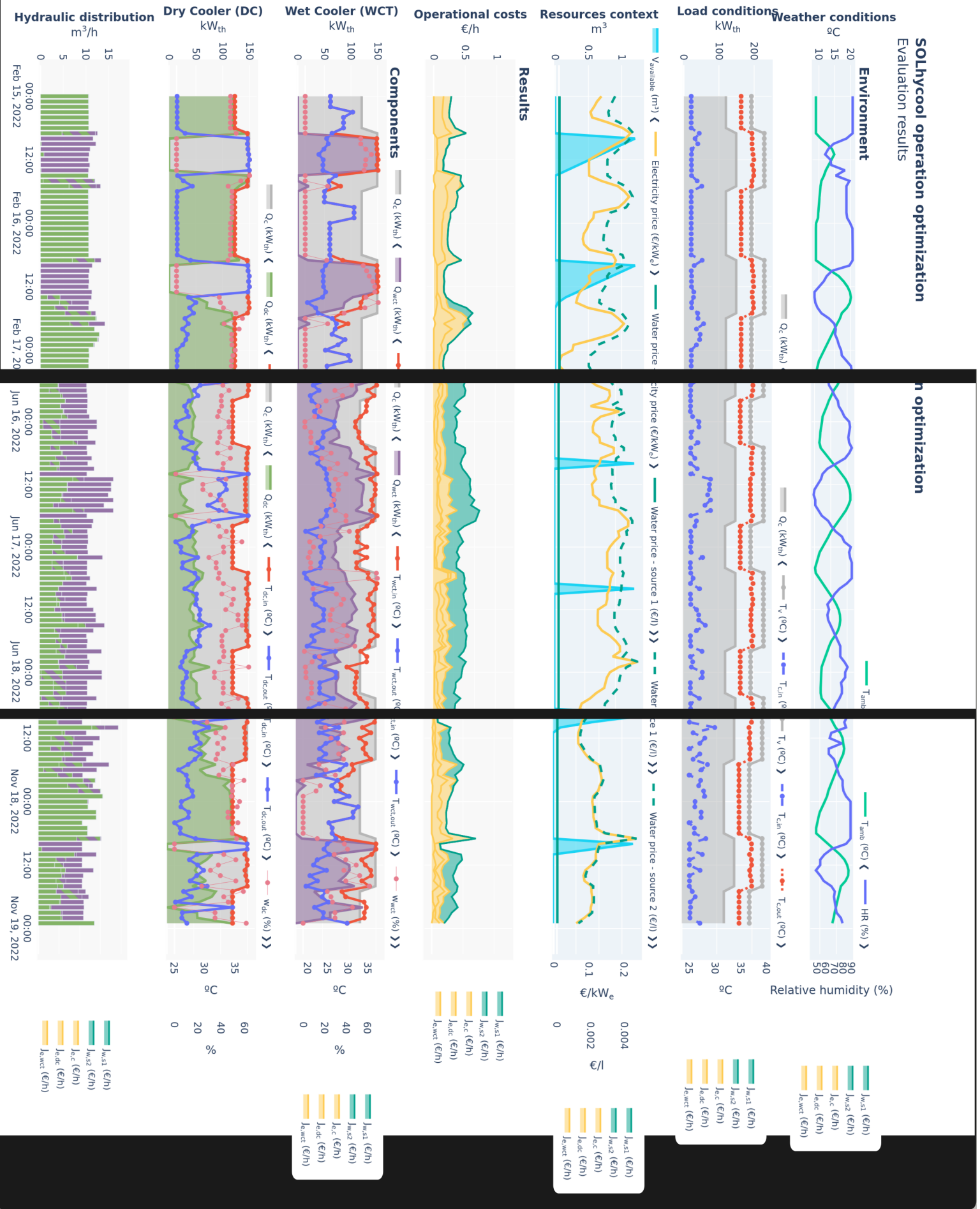
The full environment dataset is available at



13.3 Optimization strategies comparison

SOLhycool operation optimization

Evaluation results



SOLhycool operation optimization

Evaluation results

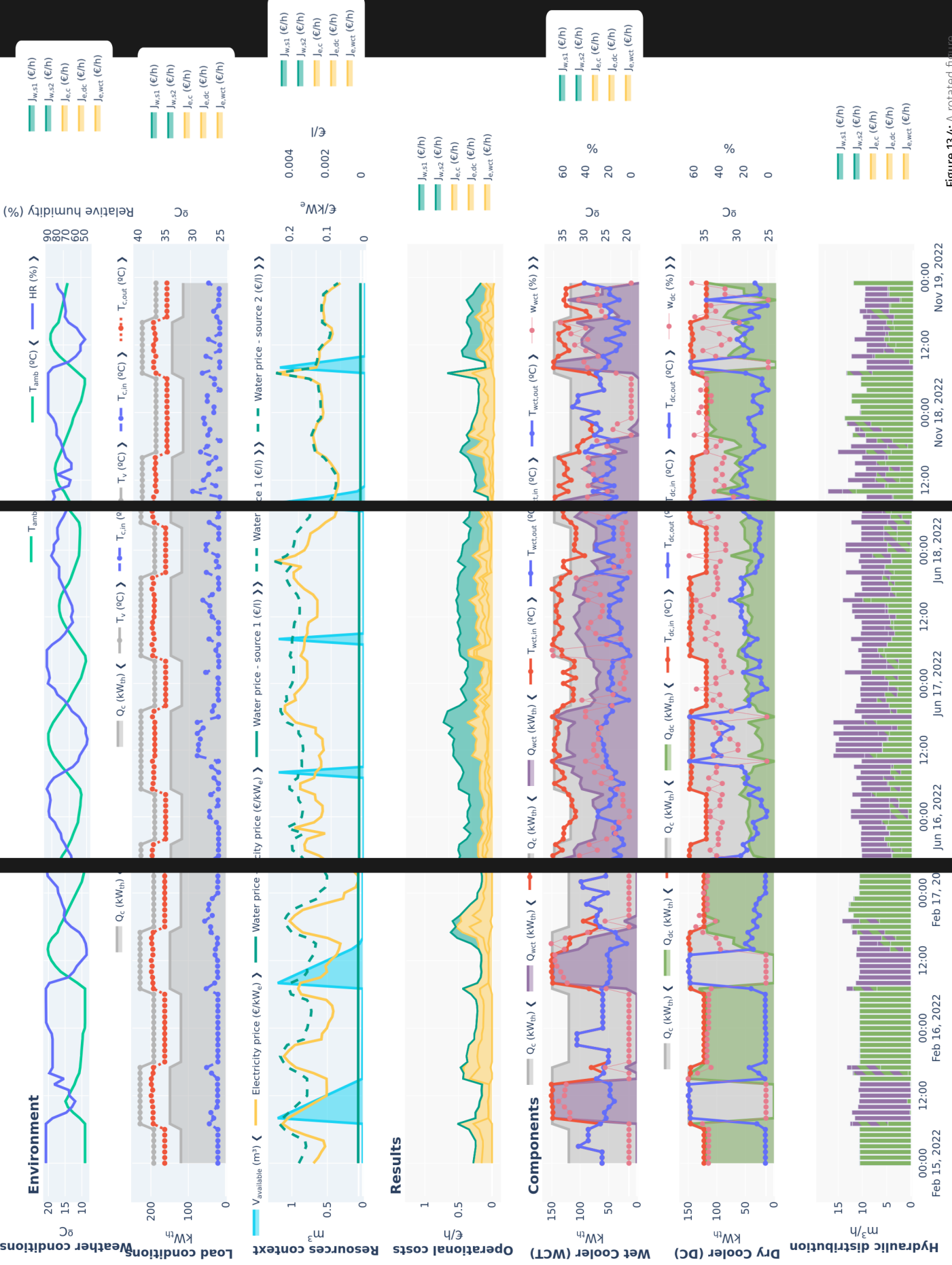


Figure 13.4: A rotated figure

13.4 Alternatives comparison

Fusionar las gráficas de resultados anuales remuestreados para que incluyan todas las alternativas. Cambiar fondo para cada sistema

ca de barras comparador kWh refrigerado

ca de barras comparación de potencia térmica por componente y distribución por componente cc y cc-horizon

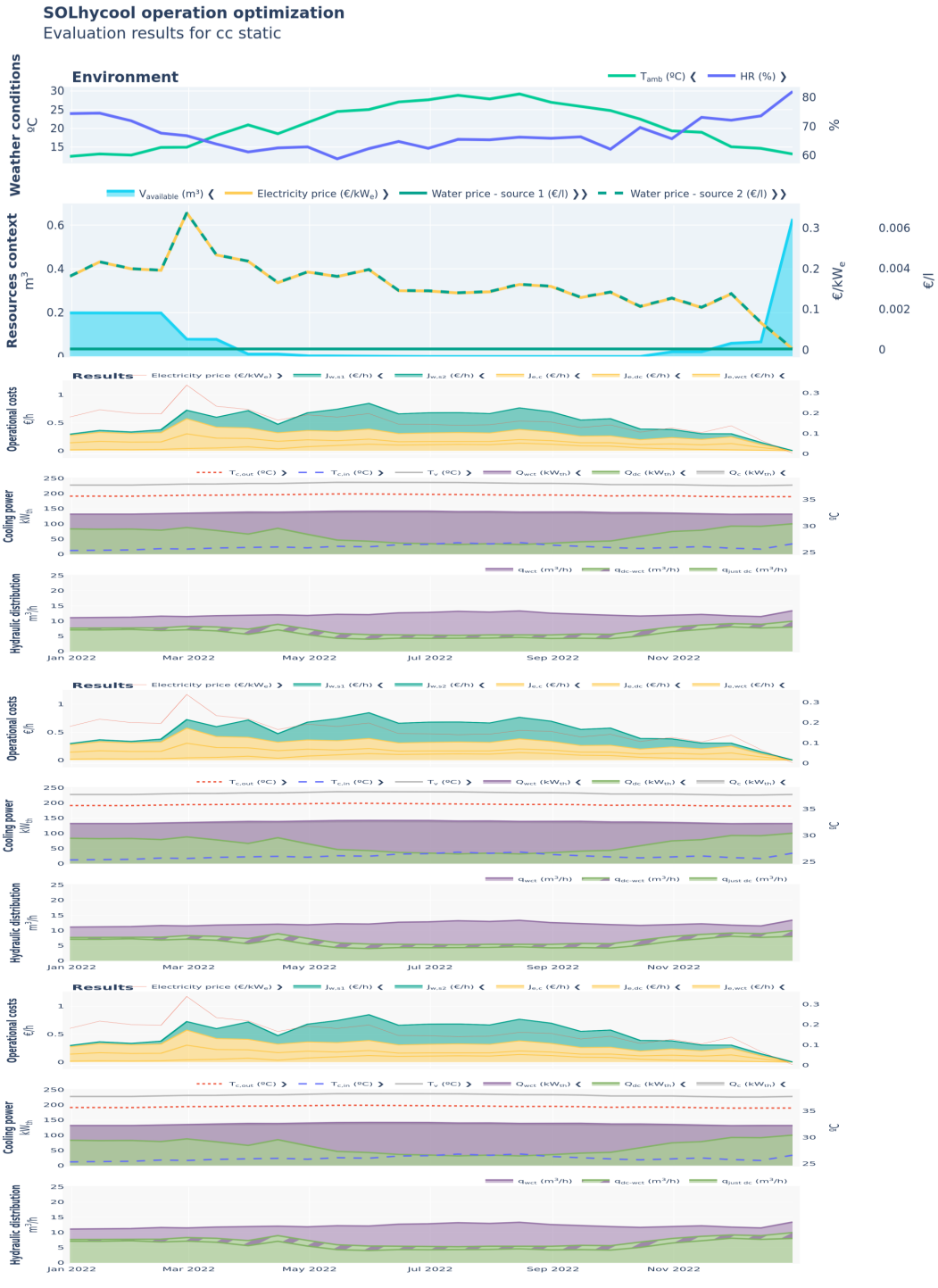


Figure 13.5: Annual simulation results for the system optimized with static cooling curves. The results are resampled every 15 minutes to mean values. The original frequency can be found in the interactive version of the figure.



ENERGY MANAGEMENT IN MED PROCESSES DRIVEN BY VARIABLE ENERGY SOURCES



Esta sección no está terminada. Siquieres puedes echarle un ojo para ver la estructura y cómo encaja con el resto pero no merece la pena revisarla en detalle en el estado actual.

TL;DR

...

a

Add visual abstract

Derived scientific contributions

Structure



Esta sección no está terminada. Siquieres puedes echarle un ojo para ver la estructura y cómo encaja con el resto pero no merece la pena revisarla en detalle en el estado actual.

Desalination is increasingly recognized as a key strategy to address global freshwater scarcity, driven by the combined pressures of climate change and population growth. Regions already facing drought and water stress, such as parts of Spain, are expected to see growing dependence on desalinated water to meet rising demand. While desalination technologies—particularly membrane-based systems like Reverse Osmosis (RO)—have seen rapid expansion, the energy intensity of the process remains a major challenge. To mitigate this, efforts have focused on improving energy efficiency and integrating renewable energy sources such as solar or geothermal heat. In particular, thermal desalination technologies like MED are gaining renewed interest due to their compatibility with low-exergy heat sources (e.g. waste heat) and the ability to treat high-salinity brines. These thermal processes also align better with circular economy approaches, allowing the concentration of brine and the recovery of valuable minerals such as lithium or magnesium, an emerging field known as brine mining.

WORK IN PROGRESS

Esta sección no está terminada. Si puedes echarle un ojo para ver la estructura y cómo encaja con el resto pero no merece la pena revisarla en detalle en el estado actual.

15.1 Heat generation and storage subsystem	81
15.2 Separation subsystem	81

The SolarMED system is an MED plant that receives its thermal energy from a solar field connected to a two-tank thermal storage system. It is one of the experimental facilities located in PSA as can be seen in Figure 1.1.

The different components are interconnected as depicted in Figure 15.1: a flat plate collector solar field which is the heat source, a pressurized hot water two-tank thermal storage system, and an MED plant which uses this heat to separate seawater into fresh water and brine. The solar field and thermal storage circuits are separated by a heat exchanger. Two subsystems are differentiated: the Solar Field and Thermal Storage (SFTS) subsystem and the thermal load that makes use of this heat for some useful application, in this case, to produce separation by means of the MED: the separation subsystem.

A esta figura quitar colores de decision variable and environ-

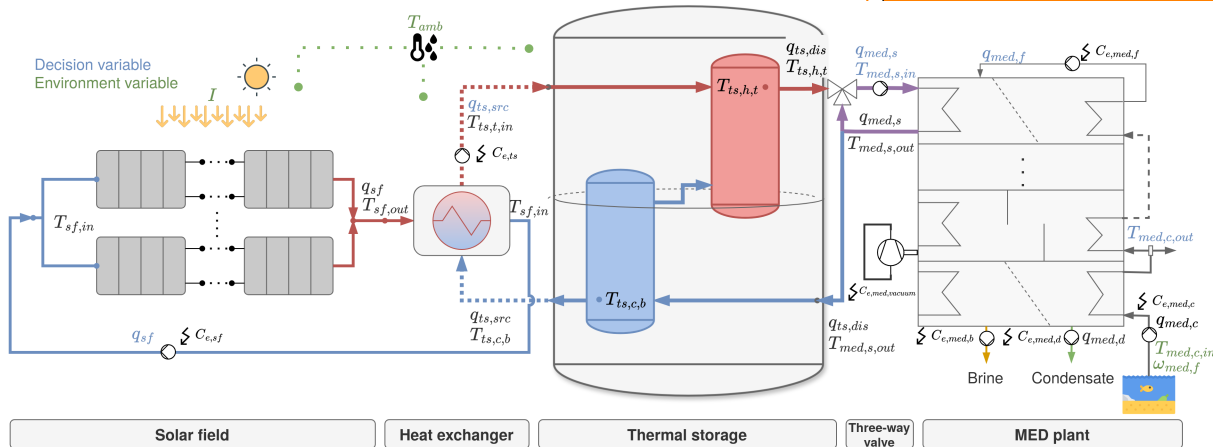


Figure 15.1: SolarMED process diagram

15.1 Heat generation and storage subsystem

Two pressurized water tanks with a total capacity of 40 m^3 coupled to a static solar field flat plate collectors with an aperture area of 606 m^2 and a total thermal power of 323 kW_{th} under nominal conditions.

15.2 Separation subsystem

The MED pilot plant was built in 1988 within the Solar Thermal Desalination project [REF]. It is a 14 effect, vertically stacked, forward-feed plant initially built to use low-pressure saturated steam as heat source for the first effect and

patricia

later replaced to use hot water within the XXX project in 2005. An image of the facility in its current state can be seen in Figure 15.2 It has been operated in different experimental campaigns and configurations robustly for more than two decades, as can be seen in Figure 15.3, which shows the operation history of the plant (starting from 2009). The campaign from 2009 to 2012 focused on ... [patricia] while the campaign from 2015 to 2016.... Finally, within the research work presented in this thesis, a new campaign was performed to validate a standardization methodology proposal and experimentally characterize the behaviour of the system at higher temperatures. This is explained in detail in the following chapter (Chapter 16 (Performance evaluation in MED processes: standard methodology proposal)).

Some particularities of this system are explained hereinafter:

- ▶ VFDs are used to control all flow rates in the system: heat source, cooling, feed, brine and distillate.
- ▶ As mentioned, the external heat source driving the process, is hot water from a thermal storage system. Water is drawn from one of the tanks and mixed with the water at the outlet of the first effect through a three-way valve, allowing independent regulation of flow and temperature.
- ▶ The inland location of this experimental plant is another particularity of the system. A fixed amount of seawater (30 m^3), stored in a reservoir, is available to be used in the process and replenished as needed. The effluents from the plant are mixed in a different reservoir (5 m^3), and returned to the feed in a close loop operation. Because water exits the process at a higher temperature than when it enters, this type of operation implies an ever-increasing heat sink temperature. A wet cooling tower, installed between the two reservoirs, is used to mitigate this effect.
- ▶ The previous particularity leads to a significant variation in the inlet water temperature from day to day and also within the same day depending on the operation conditions. To ensure the stability of the condenser (i.e. a constant vapor pressure and outlet cooling water temperature), the cooling flow rate is regulated. This allows to have a stable system representative of a real plant operating under normal conditions. However, this can lead to variable electrical consumption of the cooling pump.
- ▶ The vacuum system of the plant is based on two hydro-ejectors and a pump. The pump is operated always at fixed speed and its electrical consumption has been characterized with measurements under various conditions as being near-constant and independent of the operation conditions. Its associated nominal power is 5 kW_e .
- ▶ The salinity of the feedwater is checked before every test measuring its conductivity with a conductivity meter (see Table ??).



Figure 15.2: MED plant at PSA with open effects for maintenance

Table 15.1: MED plant at PSA specifications and nominal operating conditions

Parameter	Value
Capacity	$72 \text{ m}^3/\text{day}$
Number of effects	14
Feed type	Forward feed
Physical arrangement	Vertically stacked
Heat exchanger configuration	90/10 Cu-Ni HTE
Heat source type	Hot water
Vacuum system	Hydro-ejectors
Heat source flow rate	12 L/s
Feed water flow rate	8 m ³ /h
Brine rejection	5 m ³ /h
Distillate production	3 m ³ /h
Cooling flow rate at condenser	8-20 m ³ /h (10-25 °C)
Thermal power consumption	190 kW
Top Brine Temperature (TBT)	70 °C
Condenser temperature	35 °C

A summary of its main specifications is shown at Table Table 16.1.

The facility's instrumentation is shown in Table 15.2. As can be seen, Platinum temperature transducer, 100 ohms at 0 °C (PT100) sensors are used to measure all liquid temperatures (TT01..TT05), while a PT1000 sensor is used to measure the ambient temperature (TT06). The pressure inside the first effect and condenser (PT01 and PT02, respectively) is measured by two different pressure transducers which fundamentally differ in their measurement range. To monitor the power consumption of the system, various subsystems have been individually instrumented using a power meter (JT01..JT04). Conductivity is measured using a portable conductivity meter (CT01, CT02), to which a calibration is periodically performed to convert conductivity to salinity. Flow rates (FT01..FT04) are measured using different types of flowmeters depending on the characteristics of the fluid being evaluated. Electromagnetic flowmeters are used for conductive fluids, while vortex flowmeters are used for non-conductive fluids. All sensors transmit a 4-20 mA analog signal that is converted to digital by Analog-to-Digital Converter (ADC) converters.

Measured variable	Instrument	Model	Range	Measurement uncertainty
Water temperature, TT01...TT0N	PT100 Class A	SEDEM OF12871	0 - 100 °C	$\pm 0.15 + 0.002T^a$
Distillate flow rate, FT03	Vortex flow meter	ABB TRIO-WIRL VT4	1.6 - 18 m³/h	$\pm 0.75\% \text{ o.r.}^b$
Hot water flow rate, FT01	Electromagnetic	Endress+Hauser Proline Promag 50P	2.42 - 78.33 L/s	$\pm 0.5\% \text{ o.r.}$
Feedwater flow rate, FT02	Electromagnetic	Endress+Hauser Proline Promag P 300	2.1 - 66 m³/h	$\pm 0.5\% \text{ o.r.}$
Ambient temperature, TT05	PT1000	-	-40 - 60 °C	$\pm 0.15 + 0.002T$
Pressure, PT01	Pressure capacitive	Endress+Hauser Cerabar T-PMCI31	0 - 1 bar	$\pm 0.5\% \text{ FS}^c$
Pressure, PT02	Piezoresistive sensor	WIKA S-10	0 - 0.6 bar	$\pm 0.5\% \text{ FS}$
Level, LT01, LT02	Magnetic level gauge	IGEMA NA7-50	0-750 mm	$\pm 5 \text{ mm}$
Power, JT01...JT04	Power meter Class 1 IEC 62053-21	Circutor CM31	0-7 kW	$\pm 1\% \text{ o.r.}$
Conductivity, CT01...CT02	Conductivity meter	Prominent Portamess 911	0.1 μS/cm - 1000 mS/cm	$\pm 0.5\% \text{ o.r.} < 500 \text{ mS/cm}$ $\pm 1\% \text{ o.r.} \geq 500 \text{ mS/cm}$

Table 15.2: Characteristics of the instrumentation installed at MED-PSA unit (^a value of the measured temperature in °C, ^b of reading, ^c full scale).

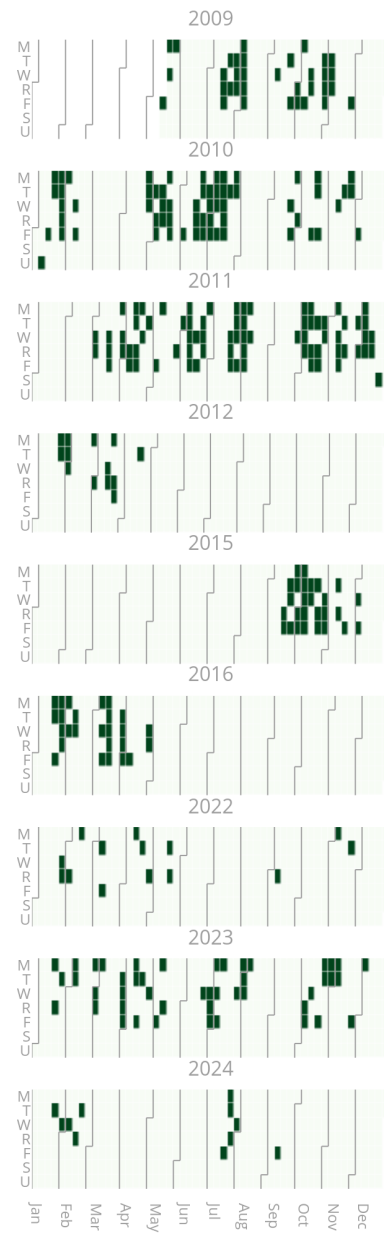


Figure 15.3: Operation history of the pilot plant.



TL;DR

This chapter presents a standardized method for evaluating the performance of MED processes, which can also be extended to other thermal separation technologies. The method addresses key aspects such as instrumentation requirements, process control, and the suitability of performance metrics, including the uncertainties associated with their determination. Additionally, an algorithm has been developed for the automatic detection of steady-state operation, enhancing the reliability and robustness of evaluations under variable conditions. Experimental results confirm that the proposed method is both robust and reliable, enabling fair comparisons of MED processes across different operating scenarios.

The experimentation includes the evaluation of the process at high TBTs. The results are analyzed using different performance metrics and the scale formation risk is estimated by the RSI. The results show that the MED process can be operated at high TBTs without significant scale formation and achieve higher concentrations, but without significant improvements in thermal performance and limited reconcentration capacity if no changes to its design are made.

16.1	Process analysis	87
16.2	Performance metrics	88
16.2.1	Separation metrics	88
16.2.2	Energetic metrics	89
16.2.3	Exergetic metrics	90
16.3	Instrumentation	92
16.3.1	Key process variables	92
16.3.2	Instrumentation requirements	93
16.3.3	Uncertainty determination .	94
16.4	Monitoring and process control	95
16.4.1	Monitoring: steady-state identification	95
16.4.2	Control system	95
16.5	Methodology application and results	97
16.5.1	Implementation results	98
16.5.2	Results analysis	102

Introduction

The future of MED in desalination and brine concentration applications depends on the technical development of the process and its integration with other technologies [38, 39]. The performance of this technology and how it is evaluated plays an important role in this development.

Although efforts have been made to propose performance metrics to evaluate the multi-effect evaporation process, there is neither consensus in which metrics are the most suitable [40] nor standards on how to evaluate the experimental process. The only standard existing in MED is not related to performance evaluation, but to cost structures and determinants [41].

For the performance evaluation of MED processes, originally, the index Gain Output Ratio (GOR) was used for plants operating with steam as external energy source. In order not to be limited to steam-driven systems and to take into account sensible heat sources, a new performance index was defined: the Performance Ratio (PR) [42, 43], which is currently the most widely adopted for MED performance evaluation although it is constrained by using a reference enthalpy of 2326 kJ equivalent to 1000 BTU. In [44], a variation of this metric called the Waste Heat Performance Ratio (PR_{WH}) was suggested to account for the potential of low-grade waste heat sources. Another widespread thermal performance metric that has been used in MED is the Specific Thermal Energy Consumption (STEC) and its electrical equivalent, the Specific Electrical Energy Consumption (SEEC). However, there are certain limitations in the aforementioned metrics that challenge making a fair comparison between desalination systems that use different energy sources *i.e.* electrical and thermal¹. Furthermore, the ability of thermal energy to perform work changes with its temperature, so it is essential to consider the quality of the thermal energy used in desalination processes. This limitation of traditional energetic metrics was showcased in Bouma et al. [46] where they compared four different configurations of MED plants: a low temperature MED configuration (LT-MED), a MED unit incorporating Thermal

[38]: Ghenai et al. (2021), "Performance Analysis and Optimization of Hybrid Multi-Effect Distillation Adsorption Desalination System Powered with Solar Thermal Energy for High Salinity Sea Water"

[39]: Son et al. (2020), "Pilot Studies on Synergistic Impacts of Energy Utilization in Hybrid Desalination System"

[40]: Burgess et al. (2000), "Solar Thermal Powered Desalination: Membrane versus Distillation Technologies"

[41]: Pinto et al. (2017), "Desalination Projects Economic Feasibility"

[42]: Mistry et al. (2011), "Entropy Generation Analysis of Desalination Technologies"

[43]: El-Dessouky et al. (2002), *Fundamentals of Salt Water Desalination*

[44]: Christ et al. (2014), "Thermodynamic Optimisation of Multi Effect Distillation Driven by Sensible Heat Sources"

1: the value of 1 kWh electric differs from that of 1 kWh thermal in terms of their ability to produce work, as the latter is constrained by the Carnot efficiency [45]

[46]: Bouma et al. (2020), "Metrics Matter"

Vapor Compression (MED-TVC), a MED unit using nanofiltration (NF-LT-MED) for feedwater pretreatment, and a combination of TVC and nanofiltration. Although the STEC values favored the use of TVC, a more rigorous analysis revealed that the most efficient systems were those that used lower temperature heat sources (LT-MED and NF-LT-MED).

[47]: Darwish et al. (2006), "Multi-Effect Boiling Systems from an Energy Viewpoint"

[48]: Shahzad et al. (2019), "A Standard Primary Energy Approach for Comparing Desalination Processes"

[45]: Lienhard et al. (2017), "Thermodynamics, Exergy, and Energy Efficiency in Desalination Systems"

[49]: Brogioli et al. (2018), "Thermodynamic Analysis and Energy Efficiency of Thermal Desalination Processes"

[50]: Spiegler et al. (2001), "El-Sayed, Y.M."

[51]: Sharqawy et al. (2011), "On Exergy Calculations of Seawater with Applications in Desalination Systems"

[52]: Sharqawy et al. (2010), "Formulation of Seawater Flow Exergy Using Accurate Thermodynamic Data"

[53]: Mistry et al. (2012), "Effect of Nonideal Solution Behavior on Desalination of a Sodium Chloride (NaCl) Solution and Comparison to Seawater"

[54]: Mistry et al. (2013), "Generalized Least Energy of Separation for Desalination and Other Chemical Separation Processes"

[55]: Thiel et al. (2015), "Energy Consumption in Desalinating Produced Water from Shale Oil and Gas Extraction"

[56]: Valenzuela et al. (2014), "Optical and Thermal Performance of Large-Size Parabolic-Trough Solar Collectors from Outdoor Experiments"

[57]: Prahil et al. (2018), "Protocol for Characterization of Complete Solar Concentrators Using Photogrammetry or Deflectometry"

[58]: Bayón et al. (2019), "Development of a New Methodology for Validating Thermal Storage Media"

Some authors have carried out exergy analyzes to overcome the limitations aforementioned of energy performance metrics. Darwish et al. [47] proposed two new metrics: Specific Fuel Energy and Equivalent Specific Work. The first compares the energy used for the desalination process that could otherwise be used for energy generation in a turbine for which it was assumed a value for the efficiency of the power plant. The second sets the work potential of the extracted steam as a baseline, considering the desalination plant separation efficiency and adding the energy consumption for pumping. The problem of this study is that it is limited to cogeneration schemes (joint electricity and water production) and would not be useful in the case of desalination with low-temperature sources. Shahzad et al. [48] developed an approach based on the second law of thermodynamics, which is also useful only for cogeneration schemes. They proposed a common metric called the Standard Universal Performance Ratio to compare desalination processes using different kinds of energy, which is based on conversion of different types and grades of energies to standard primary energy. In this case, conversion factors were proposed to convert the derived energy input to the standard primary energy. Other authors have performed exergy analyses for stand-alone desalination processes, as is the case of Lienhard et al. [45] and Brogioli et al. [49], who considered desalination processes as a black box and the ideal work or the thermodynamic limit for the separation of dissolved salts in seawater as the Carnot work.

The problem with the exergy analyses is that they are more complex [50] due to the need to consider several aspects not present in simple energetic metrics: definition of dead state and control volume [51], chemical exergy modeling of seawater [52, 53] and minimum energy reference (least and minimum work of separation) [54, 55]. Probably because of their complexity, they have not been widespread in the performance evaluation of practical setups. Also, none of the works published so far in the scientific literature addresses specifically the exergetic evaluation when using non-conventional energy sources such as waste heat.

Two important requirements for an accurate and reliable performance assessment, yet to be dealt with in thermal desalination, are the steady state identification and the uncertainty of both the direct measurement and that associated with the performance metric determination. With respect to the former, it is highly recommended to use automatic procedures that increase the reliability of the measurements. The steady state evaluation carried out manually so far by qualified operators [56–58], leads to high time consumption and full dependence on the operators' attention, leading to potential unreliable identifications. With respect to the latter, it allows for a more comprehensive and nuanced approach to performance evaluation, since it increases the robustness of the evaluation while providing information on the reliability of the results. Therefore, there is a gap in the establishment of standard methodologies that include all the necessary requirements for the reliable assessment of the performance of thermal desalination processes. This chapter aims to address this gap by proposing a method with potential for a broader application in other thermal desalination processes. The method is applied and validated in an experimental MED plant as part of a high TBT experimental campaign.

This chapter is structured as follows: first in the Section 16.1 (Process analysis) a process analysis focused on performance evaluation is done to clearly define the scope of the evaluation and the inputs and outputs of the process. Then in Section 16.2 (Performance metrics), the performance metrics are defined, including separation, energetic, and exergetic. Section 16.3 (Instrumentation)

is related to the instrumentation of the system: KPVs, instrumentation requirements and uncertainty determination for both direct measurement and derived metrics. Section 16.4 (Monitoring and process control) presents the proposed steady state identification algorithm for stable operation monitoring and the controllers to be implemented. Finally, in Section 16.5 (Methodology application in an experimental campaign) the proposed methodology is applied to a case study: a pilot MED plant evaluated in a TBT experimental campaign. The results from the campaign are also analyzed in this section.

16.1 Process analysis

Metrics are defined based on some criteria, and this criteria is of paramount importance because resources and efforts are invested in optimizing the process in its direction. In order to adequately define these criteria, it is important to have an overall perspective of the process: defining its inputs and useful outputs, from a qualitative point of view, as well as a clear delineation of the scope of the evaluation.

Metrics can be related either to the operation – isolated MED operation or considering primary energy [46] – or to the design of the system². This chapter focuses on the operation of an isolated MED system.³

Application. Two applications are distinguished:

- ▶ **Seawater desalination.** The objective is to obtain fresh water. The level of separation achieved is a secondary (not useful) output.
- ▶ **Brine concentration.** The objective is to extract resources from the brine in order to valorize it. Here, the level of separation is a crucial factor to consider.

External heat source type. Two types of external heat sources are distinguished:⁴

- ▶ **Process heat.** Process heat is the heat utilized by a system and its associated costs are related to the amount of energy consumed.
- ▶ **Waste heat.** Waste heat is the heat utilized by a system that would otherwise be lost to the environment. It has no associated costs to the amount of heat used, though there are other costs associated with its use [59, 60]⁵. Here the paradigm is different as described by Christ et al [44, 61, 62], the goal is to maximize the amount of product by maximizing the utilization of the waste source.

Process vs waste heat take on efficiency

In a process heat driven system, between two plants that produce the same amount of useful product, the most efficient one is the one that uses the least external heat to do so, whereas in a waste heat driven system, the two plants would be considered as efficient since the unused heat would be wasted to the environment. A more intuitive definition would be:

Given two plants that consume the same waste heat, the most efficient one is the one that produces more product with the available heat.

Based on the above considerations, Figure 16.1 shows the control volume of the MED process with the inputs and outputs used for the definition of the performance metrics. From left to right, seawater (including cooling water, c , and feed, f) enters the control volume at the seawater intake conditions ($T_{c,in}$). The cooling water is rejected at $T_{c,out}$. On the right side, the distillate and the brine are discharged from the MED system at temperatures $T_{d,out}$ and $T_{b,out}$ and mass fractions w_d and w_b , respectively. The temperatures of all these outlet streams,

2: e.g. specific area [43]

[46]: Bouma et al. (2020), "Metrics Matter"

3: It is as if an already built system is provided, so decision over its design parameters and energy source conditions is not an available degree of freedom, only optimization in its operational variables.

4: The use of electrical work will always be desired to be minimized, so the distinction is not needed.

[59]: Mistry et al. (2013), "An Economics-Based Second Law Efficiency"

[60]: Christ et al. (2017), "Techno-Economic Analysis of Geothermal Desalination Using Hot Sedimentary Aquifers"

5: e.g. a less efficient system will require a larger heat exchanger area to extract more energy from the waste source, directly increasing the cost of the system

[44]: Christ et al. (2014), "Thermodynamic Optimisation of Multi Effect Distillation Driven by Sensible Heat Sources"

[61]: Christ et al. (2015), "Application of the Boosted MED Process for Low-Grade Heat Sources — A Pilot Plant"

[62]: Christ et al. (2015), "Boosted Multi-Effect Distillation for Sensible Low-Grade Heat Sources"

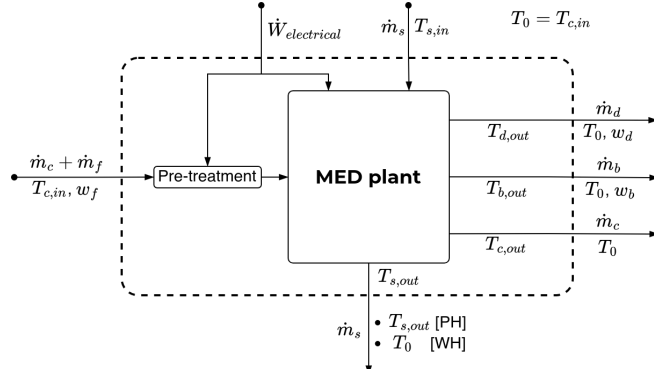


Figure 16.1: Inputs and outputs variables in an MED process. The dash line delimits the control volume

6: It is heat that is lost to the environment, no additional work can be feasibly extracted from these streams

from a qualitative (*i.e.* exergetic) point of view, are useless and thus considered to be at T_0 when leaving the control volume⁶.

From top to bottom, the energy sources for the system are depicted. Electrical work is depicted as $\dot{W}_{electrical}$ and it may include pumping, vacuum system, and feed water pretreatment, among others. The heat source is represented by the subscript (s) and as shown in the figure, it enters the MED plant at $T_{s,in}$ and leaves it at $T_{s,out}$ after releasing part of its energy. When leaving the control volume, $T_{s,out}$ value depends on the type of heat source:

- ▶ Process heat (PH). The value of $T_{s,out}$ does not change. In case steam is used, the primary energy driver is the latent heat of phase change and $T_{s,out}$ is usually similar to or equal to $T_{s,in}$. In case a sensible heat source is used, the driving force is the temperature difference and $T_{s,out}$ is between $T_{s,in}$ and T_0 .
- ▶ Waste heat source (WH). In this case, $T_{s,out}$ is considered to be at the sink conditions, T_0 , since this heat is not reused but lost to the environment.

16.2 Performance metrics

A performance metric is a quantitative measure used to evaluate the effectiveness or efficiency of a system. It provides objective information that can be used to monitor progress, identify areas for improvement, and inform decision making. A metrics division in three categories is proposed: separation, energetic, and exergetic metrics. A detailed description of each of them within each category is presented below.

16.2.1 Separation metrics

[63]: Jones et al. (2019), "The State of Desalination and Brine Production"

[64]: Palenzuela et al. (2015), *Concentrating Solar Power and Desalination Plants*

The Recovery Ratio (RR) represents the flow ratio of unit of distillate produced per unit of feed and is very useful in seawater brine concentration applications [63]. It is related to electricity consumption, since the lower the RR the higher the feed pumping needs are for the same distillate production [64]. It is determined as follows:

$$RR = \frac{\dot{m}_d}{\dot{m}_f} \times 100 [\%], \quad (16.1)$$

where \dot{m}_d is the mass flow rate of distillate and \dot{m}_f is the feedwater mass flow rate, both in kg/s.

An equivalent metric is the concentration factor, which accounts for how many times the brine is concentrated with respect to the feed concentration:

$$CF = \frac{w_b}{w_f} = \frac{\dot{m}_f}{\dot{m}_f - \dot{m}_d} [-], \quad (16.2)$$

where w_b is the brine concentration and w_f is the feedwater concentration, both in g/kg.

Apart from the already known previous metrics, a new one is proposed in this work that can be useful for seawater brine concentration applications. This metric is called Reconcentration Index (RI), and it allows to determine how close the separation achieved (RR) is to the theoretical maximum recovery ratio (RR_{max}). It is defined as:

$$RI = RR/RR_{max} [-], \quad (16.3)$$

where RR_{max} is calculated as follows [55]:

$$RR_{max} = w_{w,f} \left(1 - \frac{b_{NaCl,f}}{b_{NaCl,sat}} \right) \times 100 [\%], \quad (16.4)$$

[55]: Thiel et al. (2015), "Energy Consumption in Desalinating Produced Water from Shale Oil and Gas Extraction"

where $w_{w,f}$ is the water mass fraction in the feed (which is $1 - w_{sol,f}$, where $w_{sol,f}$ is the mass fraction of the solutes in the feed) and $b_{NaCl,f}$ is the molality of sodium chloride in the feed, in mol_{NaCl}/kg_w (both can be obtained from a feedwater chemical analysis). On the other hand, $b_{NaCl,sat}$ is the molality of sodium chloride at saturation conditions (see Section ?? for more details of its estimation)⁷.

⁷: sodium chloride is the only solute considered, as it sets the concentration limit being the solute in seawater with the highest concentration and the greatest solubility [55]

16.2.2 Energetic metrics

The energetic metrics are metrics that consider only the first law of thermodynamics (*i.e.* quantity). They are: GOR, STEC, and SEEC and are described in the following.

Regarding the GOR, a universal definition of this metric that avoids the limitations of some of the commonly used definitions mentioned⁸ is the ratio between the energy in the form of latent heat required to vaporize all the distillate produced and the external thermal energy contributed to the system (Eq. 16.5) [65].

$$GOR = \frac{\dot{m}_d \cdot \Delta h_{avg}}{\dot{Q}_{in}} \quad (16.5)$$

⁸: Limited to steam or 1000 BTU as arbitrary conversion factor

[65]: Lienhard V et al. (2012), "SOLAR DESALINATION"

where Δh_{avg} is the latent heat of vaporization at the average vapor temperature between the first effect and the last effect, in kJ/kg, and \dot{Q}_{in} is the external thermal energy consumption required to drive the process, in kW. It is determined by \dot{m}_s (mass flow rate of the external energy source supplied in the first effect, in kg/s) and Δh_s , which can be calculated as $h_{s,in} - h_{s,out}$ (in case of sensible heat) or as $h_{s,sat,vap} - h_{s,sat,liq}$ (in case of latent heat of phase change at saturation conditions from vapor to liquid at temperature $T_{s,in}$).

In case waste heat is used as external thermal energy source for the MED system, \dot{Q}_{in} is determined with \dot{m}_s and Δh but referred to the lowest temperature of the system ($T_{c,in}$).

Another performance index widely used in thermal desalination is the STEC. For desalination applications, it is defined as the input heat to the system per unit

of product (distillate). This index has units of energy per fraction of volume and its expression is shown in Eq. 16.6.

$$STEC = \frac{\dot{m}_s \cdot (h_{s,in} - h_{s,out})}{\dot{m}_d} \cdot \rho_d \cdot \frac{1 \text{ kWh}}{3600 \text{ kJ}} \left[\frac{\text{kWh}_{\text{th}}}{\text{m}^3} \right]. \quad (16.6)$$

For brine concentration applications, it is named as $STEC_{bc}$ and it is determined as the energy required (in kJ) per unit of feed (in kg) (i.e. \dot{m}_f in the denominator) [66].

Both STEC and GOR are equivalent and are related via Eq. 16.7.

$$STEC = \frac{2326 \text{ kJ/kg}}{GOR} \cdot \rho_d \cdot \frac{1 \text{ kWh}}{3600 \text{ kJ}}, \quad (16.7)$$

where ρ_d is the density of the distillate in kg/m^3 .

For the cases in which waste heat source is used as energy source, a variation of the STEC is proposed: the waste heat STEC. For desalination applications, it is determined as follows:

$$STEC_{wh} = \frac{\dot{m}_s \cdot (h_{s,in} - h_{c,in})}{\dot{m}_d} \cdot \rho_d \cdot \frac{1 \text{ kWh}}{3600 \text{ kJ}} \left[\frac{\text{kWh}_{\text{th}}}{\text{m}^3} \right]. \quad (16.8)$$

As before, for brine concentration applications, \dot{m}_d would be replaced by \dot{m}_f in the denominator.

Another important index in desalination is the SEEC, which represents the total electrical consumption of the plant and its auxiliary systems per unit of distillate water produced. These are the subsystems that should be considered:

- ▶ J_s . External energy source
- ▶ J_f . Feed pumping
- ▶ J_c . Cooling
- ▶ J_d, J_b . Discharge extractions
- ▶ J_{vacuum} . Vacuum system
- ▶ J_{aux} . Auxiliary consumptions. Represents any additional power that the system may require to function (e.g., electrical consumption for the feedwater pretreatment such as nanofiltration)

For desalination applications, the following equation is used for the calculation of this metric:

$$SEEC = \frac{\sum_{i=1}^N (J_i)}{\dot{m}_d} \left[\frac{\text{kWh}_e}{\text{m}^3} \right], \quad (16.9)$$

where J_i is the electrical consumption of the i_{th} subsystem. In the case of brine concentration applications, the index is called $SEEC_{bc}$ and the denominator would be replaced by \dot{m}_f .

16.2.3 Exergetic metrics

Exergy is the maximum amount of work achievable when a system is brought into equilibrium from its initial state to a reference state (known as the dead state and represented by the subscript "0") [51, 67]. This reference state is usually established for desalination applications as the seawater intake temperature

[66]: Chen et al. (2021), "A Zero Liquid Discharge System Integrating Multi-Effect Distillation and Evaporative Crystallization for Desalination Brine Treatment"

$(T_{c,in})$. In contrast to the energetic metrics, it considers not only the first law of thermodynamics (quantity), but also the second law (quality).

The most widespread exergetic metric is the second law efficiency (η_{II}) [45], which accounts for irreversible losses within a system. It is calculated as the ratio of the useful exergy output of a system ($\dot{E}x_{out,useful}$) to the exergy input given to the system ($\dot{E}x_{in}$) (a further explanation of how to determine the different exergy flows can be found in Section ?? (??)):

$$\eta_{II} = \frac{\dot{E}x_{out,useful}}{\dot{E}x_{in}} \times 100 [\%]. \quad (16.10)$$

[45]: Lienhard et al. (2017), "Thermodynamics, Exergy, and Energy Efficiency in Desalination Systems"

Considering exergy losses, which are the sum of exergy destroyed in each individual component ($\dot{E}x_{destroyed}$) and exergy losses due to discharge streams in disequilibrium to the environment ($\dot{E}x_{streams}$), the previous equation can be written as follows:

$$\eta_{II} = 1 - \frac{\dot{E}x_{destroyed} + \dot{E}x_{streams}}{\dot{E}x_{in}} \times 100 [\%]. \quad (16.11)$$

For brine concentration applications and in case waste heat is used, the metric is called $\eta_{II,wh}$ and $\eta_{II,bc}$, respectively, to distinguish between the type of application and external energy source.

Another useful metric is the Specific Exergy Consumption (SEXC), which was firstly referenced as specific consumed available energy in [47]. Similarly to SEEC and STEC, it accounts for the exergy input to the system per unit of distillate produced (Eq. 16.12) and it is determined as follows [46]:

$$SEXC = \frac{\dot{E}x_{in}}{\dot{m}_d} \left[\frac{\text{kWh}_{\text{ex}}}{\text{m}^3} \right]. \quad (16.12)$$

[47]: Darwish et al. (2006), "Multi-Effect Boiling Systems from an Energy Viewpoint"

[46]: Bouma et al. (2020), "Metrics Matter"

It is important to note that the terms $\dot{E}x_{out,useful}$ and $\dot{E}x_{in}$ from the previous exergetic metrics are determined depending on what is considered as useful exergy leaving the process and what is deemed as exergy input to the system.⁹

Useful exergy output . The useful exergy output of the system ($\dot{E}x_{out,useful}$) depends on what is considered the valuable product generated by the process. In a separator in which the objective is to separate water and brine, the useful exergy is the chemical exergy of separation. As discussed in [45], for seawater desalination applications, where the valuable product is fresh / pure water, the chemical exergy of separation corresponds to that of a reference ideal separator that achieves the *minimum separation work* ($\dot{W}_{least}^{min} = \dot{W}_{least}|_{RR \rightarrow 0}$). The objective is to minimize the required energy consumption to produce fresh / pure water, regardless of how much separation takes place ($RR \rightarrow 0$), so $\dot{E}x_{out,useful} = \dot{W}_{least}^{min}$.

On the other hand, in brine concentration applications, since the objective is to maximize the separation achieved, the separator takes into account the amount of separation achieved ($\dot{W}_{least}|_{RR}$), and $\dot{E}x_{out,useful} = \dot{W}_{least}$ [55]. The definition and determination of the least and minimum least work of separation can be found in Section ??.

Exergy input . The exergy input ($\dot{E}x_{in}$) is determined according to the type of external heat source. In case process heat is used, the exergy input is determined as:

$$\dot{E}x_{in} = \dot{E}x_{s,in} - \dot{E}x_{s,out} + \sum_i \dot{E}_i, \quad (16.13)$$

9: It mirrors the qualitative analysis presented in Section 16.1

[45]: Lienhard et al. (2017), "Thermodynamics, Exergy, and Energy Efficiency in Desalination Systems"

[55]: Thiel et al. (2015), "Energy Consumption in Desalinating Produced Water from Shale Oil and Gas Extraction"

where $\dot{E}x_{s,in}$ and $\dot{E}x_{s,out}$ are the exergy flows associated with the thermal energy source at the inlet and outlet, respectively.

When using waste heat sources, the exergy input is determined as:

$$\dot{E}x_{in} = \dot{E}x_{s,in} - \dot{E}x_{s,out}^{wh} + \sum_i \dot{E}_i, \quad (16.14)$$

where $\dot{E}x_{s,out}^{wh}$ is the outlet heat source exergy flow, which is evaluated at temperature T_0 (dead state).

16.3 Instrumentation

16.3.1 Key process variables

The KPV are those variables that uniquely define an operating point, which is obtained by averaging all monitored variables when stable operation is achieved. In other words, any change in the key variables is associated with a different operating point, since the plant outputs are affected accordingly. The following selected variables apply to any MED plant with any configuration in terms of seawater flow direction, tube arrangement in tube bundles, or effect layout [64]. They are represented in Figure 16.2 and described hereinafter:

- ▶ Heat source flow rate (\dot{m}_s - FT01), inlet temperature and pressure ($T_{s,in}$ and $P_{s,in}$ - TT01 and PT03) for sensible heat sources, and just FT01 and TT01 if saturated steam is used (otherwise steam quality needs to be estimated). They determine the hot side conditions, which usually take place in the first effect that is at the highest temperature and pressure. If multiple effects receive external heat sources, each one has to be monitored.
- ▶ Feed water flow rate (\dot{m}_f - FT02), which affect the overall plant operation conditions. A precise and stable input feed flow rate ensures consistent heat transfer rates, residence times, and separation efficiencies.
- ▶ Distillate flow rate (\dot{m}_d - FT03). It is a basic variable that gives information about the production of the system. As long as this output variable is stable, it can be assumed that the sum of it plus the brine flow rate is equal to the feed flow rate.
- ▶ Condenser pressure / temperature ($P_{v,c}$ - PT02 / $T_{v,c}$) or condenser outlet temperature ($T_{c,out}$ - TT02). The stability of any of these variables, together with that of the distillate production, establish a stable heat sink.
- ▶ Effect pressure / temperature ($P_{v,1}$ - PT01 / $T_{v,1}$) or heat source outlet temperature ($T_{s,out}$ - TT05), which is always required in case that sensible heat source is considered as the external energy source. The stability of this output variable determines a stable hot side. In case other effects, apart from the first one, receive external heat sources, each one has to be monitored.
- ▶ Feed water salinity (w_f - CT01). It affects the overall plant operation conditions since any stream with different salinity would have different thermodynamic properties (i.e. boiling point elevation) and therefore, different energy requirements to perform the separation.
- ▶ Condensate salinity (w_d - CT02). This variable together with the distillate flow rate gives information on the levels of salt separation from water achieved.
- ▶ Ambient temperature (T_{amb} - TT06). The ambient conditions determine the losses to the environment which can change the results for the, otherwise, same operating conditions.
- ▶ Seawater temperature or condenser inlet temperature ($T_{c,in}$ - TT04). It is another environment variable that sets the minimum achievable temperature in the system.

[64]: Palenzuela et al. (2015), *Concentrating Solar Power and Desalination Plants*

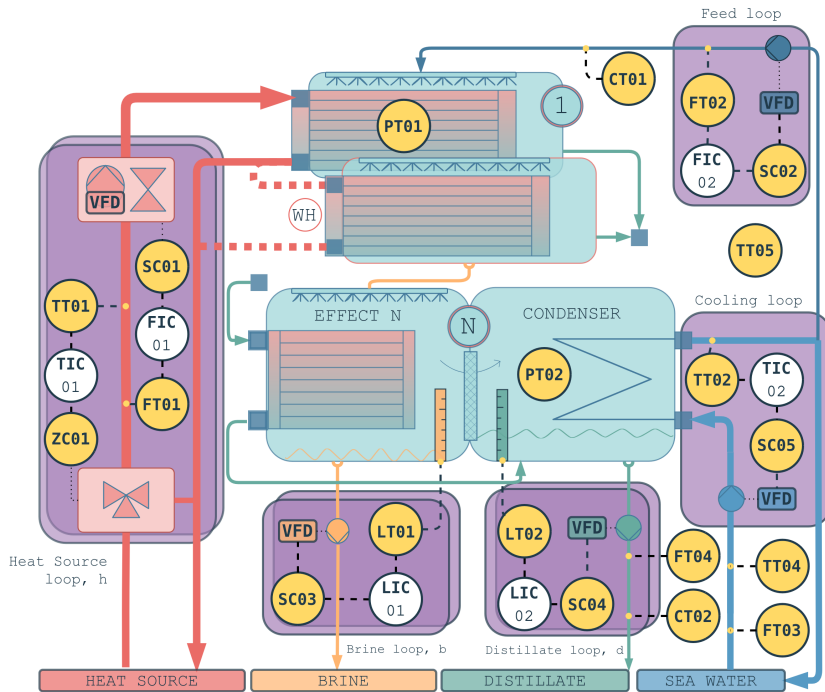


Figure 16.2: P&ID with the required instrumentation, KPVs, and basic control loops (ANSI/ISA 5.1-2022) required in an MED plant

- Last effect (L_b - LT01) and condenser (L_d - LT02) levels. In the case of the final condenser, it is a vessel in which the vapor coming from the final effect condenses, producing distillate that is continuously extracted from the system. The stability in this vessel is achieved when the extraction rate is equal to the condensate production rate. A higher extraction rate would eventually lead to unstable production, while a lower extraction rate would cause an increase in the vapor pressure, which would lead to induced lower production caused by misoperation. A stable level throughout the operation can ensure that the extraction and production rates (\dot{m}_d) are in balance. In the case of the last effect, it is important to keep the level as low as possible in order to avoid brine contamination in the final condenser.

16.3.2 Instrumentation requirements

The installed instrumentation must measure magnitudes such as flow rate (mass or volumetric), temperature, pressure, water conductivity, level, and power. First, it is important to account for the influence of the quality of each measured variable on the reliability of the performance metrics, which is determined by a sensitivity analysis.

Reminder: How to interpret Sensitivity Analysis (SA) results

The results are different sensitivity indices such as total sensitivity indices (total-order), first-order sensitivity indices (first-order), and interaction sensitivity indices (second-order). First-order measures the direct effect of an input variable on the output, excluding interaction effects with other variables, while the second-order measures specifically these interaction effects. Finally, total-order indices account for the total effect of an input variable, including both direct and interaction effects.^a

^a More in Chapter 3 (Sensitivity analysis)

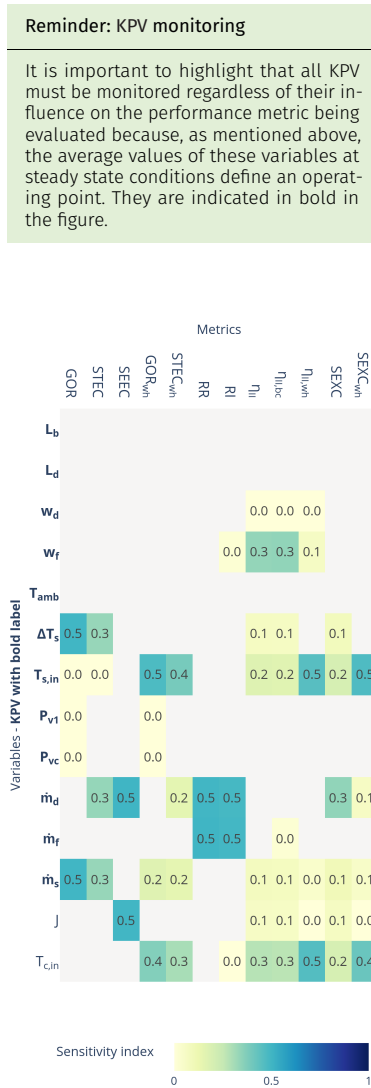


Figure 16.3: Sensitivity index results for different variables. Useful to assess the impact of the different measured variables uncertainty on the performance metrics.

[69]: Smith (2013), *Uncertainty Quantification*

Figure 16.3 shows the results obtained from the sensitivity analysis in terms of total-order Sensitivity Index (SI). The closer the SI is to 1, the greater the influence of the variable (shown on the left axis) on the reliability of the performance metric (shown on the top). In other words, the quality of the variable measurement should be higher for variables with a higher SI. The cases where no sensitivity index is obtained indicate that the variable has no effect on the metric.

In general, monitoring of these variables must be performed online for each operating point evaluated. However, some of the variables rarely change and can be measured periodically or offline. This is the case of environment variables such as w_f , w_d , T_{amb} .

Another aspect that deserves careful consideration is the measurement of the temperature of the heat source. To determine the thermal efficiency of the system when a sensible heat source is utilized, it is crucial to accurately measure the temperature difference between the inlet and outlet of this energy source (ΔT_s). Using temperature transmitters with high accuracy rates (i.e. PT100), uncertainties of about 0.5 °C or below 1 % for the absolute temperature can be expected at temperatures exceeding 60 °C. However, when considering the small temperature differences between the inlet and outlet, which can be as low as 2 °C, the resulting relative uncertainty could be up to 25 %. To address this problem, it is recommended that both temperature transmitters are identical and calibrated simultaneously, using the same calibration pattern, which translates into observed values for the uncertainty of the temperature difference in the range of 0.1 °C or 5 %.

On the other hand, the total electrical energy consumption (represented as JT01 in Figure 16.2 can be monitored as global system consumption, or independently per subsystem (J_s , J_c , J_f , J_d , J_b , J_{vacuum} , J_{aux}).

16.3.3 Uncertainty determination

Uncertainty determination is particularly valuable in assessing the reliability and validity of predictions, forecasts, or results evaluation. The framework on which the uncertainty assessment of this paper is based is JCGM 100:2008 [68].

In an uncertainty analysis, the uncertainties of direct measurements must first be determined. The uncertainty of each direct measure (ΔX_i) consists of the sum of two components, as indicated below:

$$\Delta X_i = \Delta X_{sensor} + \Delta X_{control}$$

where:

- ▶ ΔX_{sensor} is the contribution of the sensor, which depends on its accuracy, calibration and conversion errors, and should be available from the instrument datasheet.
- ▶ $\Delta X_{control}$ is the uncertainty attributed to the quality of the control and is estimated using the standard deviation of the measurement throughout the period considered as stable.

On the other hand, when working with derived variables, *i.e.* quantities that are calculated based on other measured or known quantities, the uncertainty is determined through uncertainty propagation. There are several analytical and numerical methods to propagate uncertainty [69]. One simple approach is the use of first-order Taylor series approximation, obtained calculating the partial derivative of the different direct measurements ($X_i = 1..N$) that take part in the calculation of an output (y):

$$Y = f(X_1, \dots, X_N),$$

$$\Delta Y = \left(\sum_{i=1}^N \left(\left| \frac{\delta Y}{\delta X_i} \right| \Delta X_i \right) \right)^{1/2},$$

where ΔY_i can be expressed in terms of absolute uncertainty, relative, or standard uncertainty [70]. This alternative provides a simple mathematical expression to directly estimate uncertainty. Expressions for the uncertainty estimation of energetic and separation metrics of MED processes with this approach are available in Section ???. However, first-order Taylor series approximation has certain limitations, being the main one that it is not adequate for highly non-linear models, where a higher order Taylor expansion is required, or when uncertainties are far from the mean. Also, when working with complex models, as in the case of exergetic metrics, its expression can not be practically obtainable. For these cases, the recommended approach are numerical methods, specifically the Monte Carlo method [71], which despite its higher computational requirements does not have the aforementioned limitations [72].

[70]: nist (), “NIST Guidelines for Evaluating and Expressing the Uncertainty of NIST Measurement Results Cover”

[71]: (2008), JCGM101:2008. *Evaluation of Measurement Data — Supplement 1 to the “Guide to the Expression of Uncertainty in Measurement” — Propagation of Distributions Using a Monte Carlo Method*

[72]: Wolff (2007), “Monte Carlo Errors with Less Errors”

16.4 Monitoring and process control

16.4.1 Monitoring: steady-state identification

The evaluation of the system performance must be carried out when the plant is at steady state conditions, that is, when the mass and energy balances are in equilibrium and thus do not change with time; otherwise, erroneous results can be obtained. Steady-state conditions can be identified by observation by qualified and experienced plant operators. However, the use of automatic detection algorithms is recommended for experimental facilities where a wide range of operating conditions are involved. In this work, an automatic detection algorithm has been purposely developed and implemented to identify the steady state of the process. The methodology is based on the idea presented by M. Korbel [73] et al. and consists of combining an algorithm to detect anomalies, such as the wavelet transform [74, 75] (which allows detecting abrupt signal changes and distinguishing between high-frequency noise, transient states and steady states), with a trend detection method to identify smooth ramps as non-steady states. Whereas M. Korbel [73] et al propose a statistical trend detection approach, in this paper the derivative of the signal is used due to its simplicity (only one parameter, the threshold, must be established). A diagram of the steady-state detection procedure is shown in Figure 16.4, where three parameters are mainly required: wavelet transform threshold (y_a), derivative threshold (y_d) and time window duration (T_{ss}). At each k -sample time, a new value is read, and the *Anomaly detection* algorithm is applied (in this case the wavelet transform). If the output is positive (true, no anomaly), the second step is to analyse the *Trend detection*. Only if all elements in the result vector are positive along T_{ss} , is the value considered to be at steady state (ss) conditions. As a final step, the *Global steady state evaluation* identifies a steady-state period if all the values of the N variables involved have been previously classified as ss.

[73]: Korbel et al. (2014), “Steady State Identification for On-Line Data Reconciliation Based on Wavelet Transform and Filtering”

[74]: Jiang et al. (2003), “Application of Steady-State Detection Method Based on Wavelet Transform”

[75]: Jiang et al. (2000), “Industrial Application of Wavelet Transform to the On-Line Prediction of Side Draw Qualities of Crude Unit”

[73]: Korbel et al. (2014), “Steady State Identification for On-Line Data Reconciliation Based on Wavelet Transform and Filtering”

16.4.2 Control system

Figure 16.2 shows the control loops to be implemented in an MED unit, whose subsystems and their control are described below:

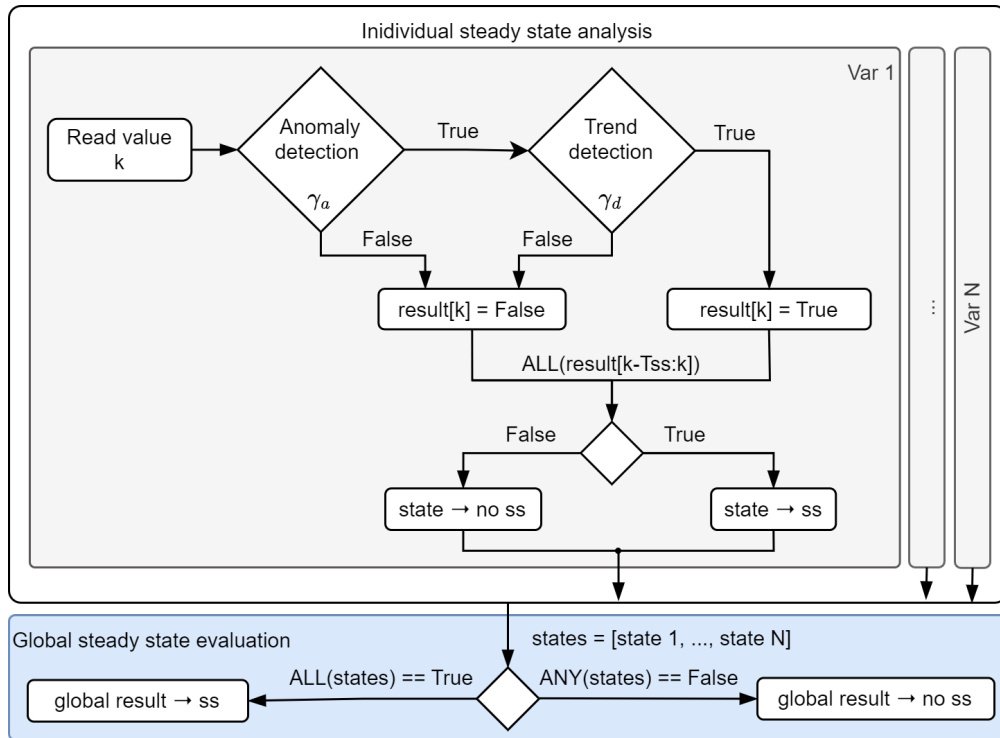


Figure 16.4: Diagram of the steady-state identification procedure

► **Heat source** (*Heat Source loop* in Figure 16.2). Both the inlet temperature (TT01) / pressure (PT03) and the flow rate of the heat source (FT01) must be controlled. It can be done either by direct control over the heat source obtaining heat under the required operating conditions or by performing a transformation. Depending on the heat source characteristics, this transformation involves:

For sensible heat sources, independent variation of temperature and flow rate can be achieved by means of: 1) a mixing three-way valve that mixes part of the return fluid, at temperature TT05, with the inlet fluid, at TT01 by acting over ZC01, the control signal for temperature regulation and; 2) flow (FT01) regulation by acting over the control signal SC01, which can be a Variable Frequency Drive (VFD) or valve. This decoupled regulation is shown in Figure 16.2, where ZC01 represents the control signal for temperature regulation. The flow rate regulation (FT01) is achieved by acting on the selected actuator (SC01), which can be a VFD or a valve¹⁰. For latent heat sources (steam), the pressure-flow-independent regulation is not possible since they are intrinsically coupled variables. In this case, a pressure regulator valve (ZC01) can be used to control either the flow rate (FT01) or the pressure (PT03).

► **Cooling** (*Cooling Loop* in Figure 16.2). The pressure inside the condenser (PT02) or the condenser outlet temperature (TT02) can be controlled by regulating the cooling flow rate (FT03), being the cooling water inlet temperature (TT04) a disturbance. This control loop (TIC02) consists in turn in two control loops (cascade control [76]), where an outer loop sets a reference flow rate value to achieve the desired condenser outlet temperature (or pressure), and an inner loop (not shown in Figure 16.2) acts on SC05 (VFD's frequency) to achieve the desired flow rate. Direct regulation of condenser outlet temperature using the VFD is also valid in case the measurement of the cooling flow rate is not available.

► **Brine extraction** (*Brine loop* in Figure 16.2). The brine level in the last

10: It should be noted that this decoupling is at the expense of energy losses in the mixing process

[76]: Åström et al. (1995), *PID Controllers: Theory, Design, and Tuning*

16.5 Methodology application in a pilot plant

effect (**LT01**), or in all effects if a parallel feed configuration is used, is controlled by the brine flow rate (see control loop **LIC01** in Figure 16.2). In this case, the controller can act directly on the VFD frequency (**SC03**) to avoid the need for an additional flow meter.

- ▶ **Distillate extraction** (*Distillate loop* in Figure 16.2). As in the previous case, the distillate level (**LT02**) is controlled by acting on the control variable (**SC04**).
- ▶ **Feedwater** (*Feed loop* in Figure 16.2). The feed water flow rate is regulated by the **FIC02** control loop, using a VFD (**SC02**) and a flow meter (**FT02**).

A standard method for performance evaluation of thermal separation processes

1. Define the KPVs (Section 16.3.1)
2. Select the required performance metrics to be evaluated according to the application and type of energy source(s) (Section 16.1).
3. Define the required instrumentation of the KPVs and of any additional variables needed for the target performance metrics (Section 16.3.2).
4. Define the uncertainty associated with the measurement and that associated with the performance metric determination (Section 16.3.3)
5. Implement the required actuators and integrate them into a control system to ensure the stability of the plant operation (Section 16.4.2).
6. Identify a time window where stable operation is achieved (Section 16.4.1).

16.5 Case study: methodology application in a high TBT experimental campaign at the pilot plant

Reminder: Performance of a thermal separator

The performance of a thermal process, such as MED, is dictated by the Carnot cycle [49], which sets the theoretical maximum efficiency for any heat engine. The efficiency of the Carnot cycle is limited by the temperature difference between the hot and cold sinks, which determine the amount of thermal energy that can be converted into useful (separation) work.

An approach to bring the MED closer to its thermodynamic limit can be achieved by raising the TBT, which allows to increase the number of effects [77] while maintaining an optimal temperature drop across them¹¹. This leads to an improvement in the thermal performance of traditional desalination or an increase of the concentration factors that can be achieved, potentially enabling applications such as brine mining, introduced in Chapter 14 (Thermal desalination).

In practice, the TBT in the MED system is limited to 70°C. As shown in Figure 16.6, higher TBTs increase the risk of precipitation of divalent ions, which tend to form incrustations on the heat exchange surfaces. These deposits reduce heat transfer efficiency, as noted in [43]. For un-treated feedwater (Figure 16.6 - left) this risk of precipitation is present at almost any temperature due to its composition¹². A nanofiltration pre-treatment¹³ is used to selectively remove the divalent ions while leaving relatively unaffected the components to be separated in the MED process, *i.e.* NaCl. This allows the operation of MED processes at higher TBTs or higher feed concentration, with only severe scaling above 80°C and ≈ 100 g/kg as shown in Figure 16.6 - right.

To showcase the application and usefulness of the proposed methodology, a case study consisting on the application of the methodology to an experimental campaign at the SolarMED pilot plant is presented. The campaign was designed

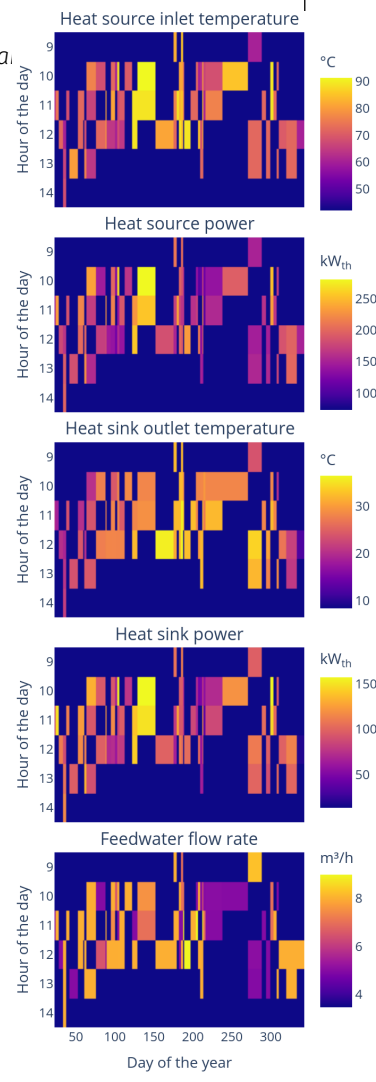


Figure 16.5: Visualization of the different process inputs values during the experimental campaign.



11: With limitations, on each effect a considerable exergy is destroyed. It has been shown that around XX effects is the limit ...

Table 16.1: RSI values and their interpretation in terms of scaling and corrosion risk [78].

RSI > 9	Severe corrosion
7.5 < RSI < 9	Heavy corrosion
7 < RSI < 7.5	Significant corrosion
6 < RSI < 7	Stable water
5 < RSI < 6	Moderate to light scaling
4 < RSI < 5	Severe scaling

12: Figure 16.6 - seawater in center bar plot

13: Figure 16.6 - pretreated water in center bar plot

to evaluate the performance of the MED process under different operating conditions (see Table 16.2 and Figure 16.5), with the aim of improving its thermal performance and assessing the feasibility of using higher TBTs.

16.5.1 Implementation results

Table 16.2: Experimental campaign design specifications

Variable	Unit	Range
$T_{s,in}$	°C	60-89
q_s	l/s	7-14
$T_{c,out}$	°C	20-40
q_f	m ³ /h	5-9
w_f	g/kg	40

The experimental facility at PSA is a complex system of considerable size for a pilot plant. It includes over 100 variables, between inputs and monitored outputs. Additionally, due to the large number of target operating points, each experimental campaign requires a significant number of test days. Achieving a valid steady state takes approximately 20–30 minutes, not including the transition time between operating points. On a good day, 3–4 stable operating points can be reached; on a bad day, due to for example unfavorable environmental conditions, none may be achieved. This makes the duration of experimental campaigns complex and extensive as illustrated in Figure 15.3, making it highly suitable for extensive subsystem automation. The following sections describe the implementation of the methodology, which is showcased in Figure 16.9 for one particular test and further discussed in the following.

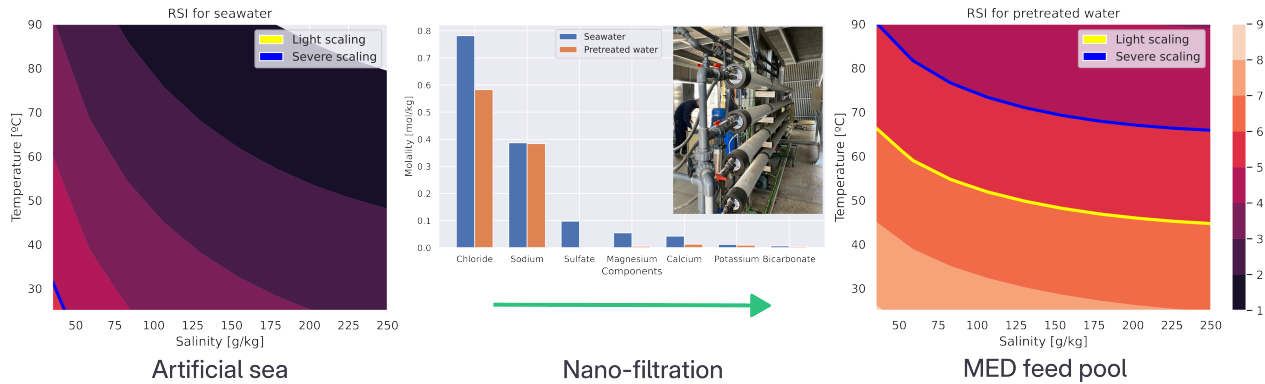


Figure 16.6: RSI values as a function of temperature and concentration before (left) and after (right) pre-treatment using nanofiltration.

Monitoring and control system

Finite state machines. Each day of operation requires starting up and shutting down the system, making it a repetitive and sufficiently complex process that requires an experienced operator. Manual management of the process leads to errors that cause setbacks or, in the worst cases, premature failures in the facility: contamination of the condenser with brine due to erratic draining of the last effect, accumulation of scale on the surfaces of heat exchangers due to rapid cooling after shutdown, pumps cavitating because they are not stopped when the water flow at the intake ceases, etc. For this reason, two finite state machines have been implemented to manage the startup and shutdown of the facility. These have been designed to perform a sequence of operations that take the plant from an initial state to a final state following proper operating practices. A diagram of the process is shown in Figure 16.7.

The machines are responsible for managing the activation and deactivation of devices as well as controllers. Additionally, they set reference values for these based on a previously established configuration and evaluate whether the reference has been reached before proceeding to the next step. They also adjust certain parameters of the control system (level control) and restore the initial values once the task is completed.

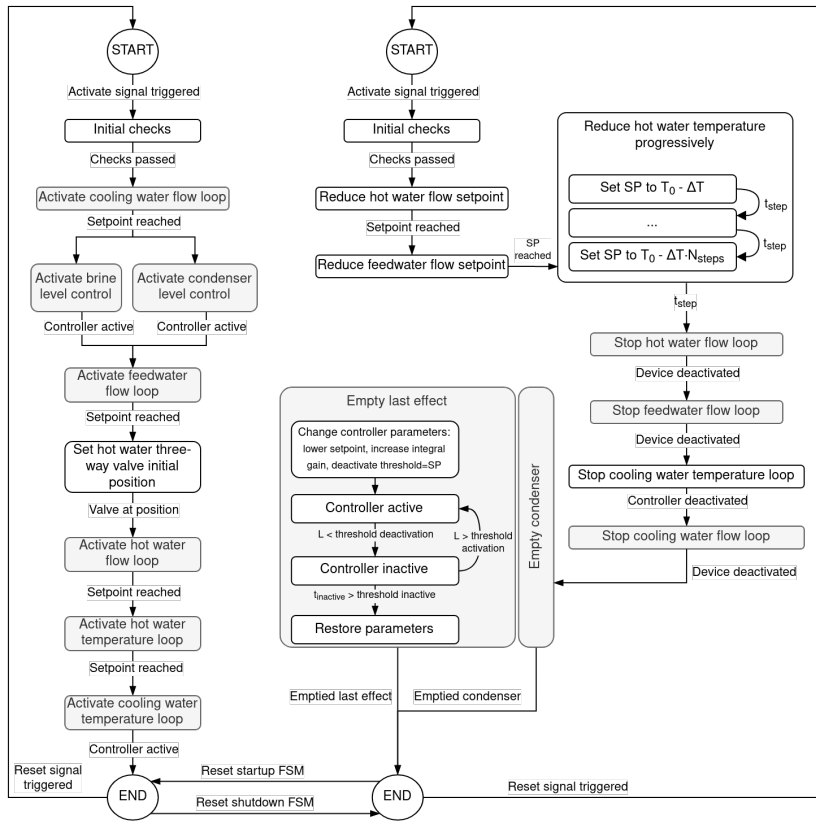


Figure 16.7: Flowchart of finite state machines for plant start-up (left) and shutdown (right)

In Figure 16.9 the activation sequence can be visualized at the beginning of the test (09:49–10:00): extractions → cooling → feedwater and heat source. The Flows are activated in about two minutes followed by another minute for the inlet temperature. Then the system is left to stabilize. At 09:52 the delay between activating the feedwater and it reaching the last effect is completed and the brine extraction pump starts operating. Pressures, temperatures and the distillate level in the system progressively evolve up to 10:00 when the conditions are changed for the first operation point for the day. The distillate level control action is delayed further until 10:04 when the first distillate is produced.

Regarding the shutdown procedure, the two most delicate processes are the cooling of the first effect (which has the highest scaling potential if not done properly) and the complete draining of the last effect and condenser. For the gradual cooling of the first effect, after the plant shutdown signal, the hot water temperature is reduced in 5-minute steps starting from the last recorded value until a final temperature of 50°C is reached. To drain the levels, a reference value well below the normal operating level is set, and the controller parameters are changed to more aggressive ones. Additionally, the device is deactivated each time the reference is reached and is not reactivated until the level reaches a specified value. This activation and deactivation process continues while the feedwater finishes draining from the upper effects of the plant. Once the control system has been deactivated for longer than a preset time, the plant shutdown procedure is considered complete, and the level controller parameters are restored.

This procedure can be observed in Figure 16.9 starting from 13:07. After a decrease in flow rates, the first effect heat load is progressively decreased until 13:34. From this time, pumps are stopped and the extraction cycles begin as can be noted by the high oscillations in the *Electrical consumption – J_b* and *J_d* and *Levels*.

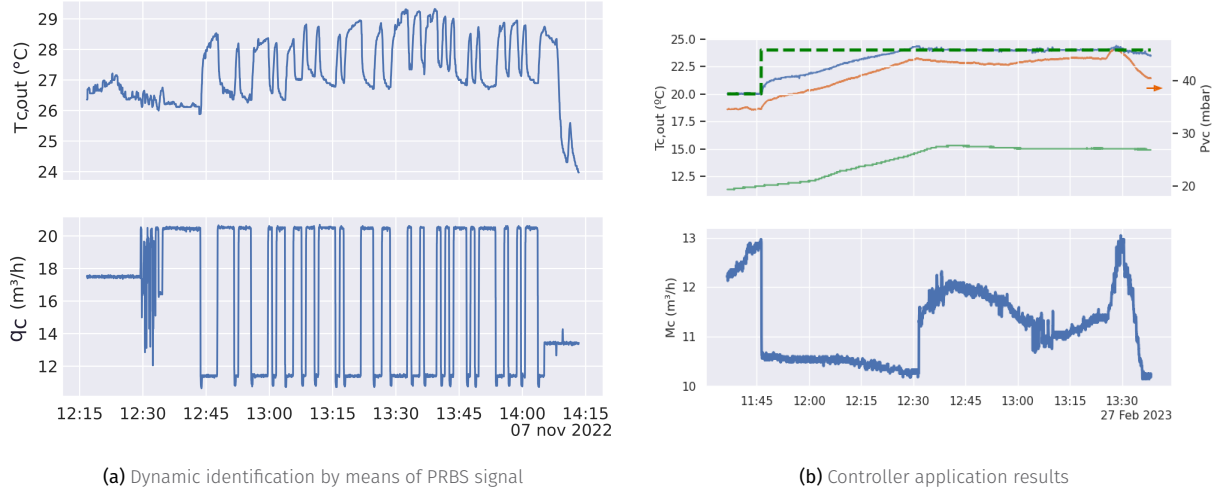


Figure 16.8: Condenser outlet temperature controller implementation. On (b) the perturbation (inlet temperature) is shown with a solid-green line, while the output (condenser outlet temperature) is shown with a solid-blue line. The reference is a thick dashed-green line.

Steady state identification. The steady state identification algorithm has been implemented in the control system. It allows the automatic detection of stable operation points. This is done by monitoring the KPVs and applying the algorithm described in Section 16.4.1. In Figure 16.9, steady state periods are highlighted with a yellow background, which indicates that the algorithm has detected a stable operation point. Two are detected, the first one from 11:00 to 11:55 and the second one from 12:16 to 12:59.

Control. In terms of control, a Proportional-Integral-Derivative controller (PID) control has been implemented to effectively regulate and maintain the desired setpoints of the subsystems mentioned in Section 16.4.2. This approach enables the system to respond quickly to changes, minimize steady state errors, reject disturbances, and enhance overall performance and reliability. Figure 16.8 shows the development procedure for one of the main loops, the condenser outlet temperature control. To tune the controller, the system was excited with a Pseudo-Random Binary Sequence (PRBS) signal (a), obtaining an ARX model ($n_a = 20$, $n_b = 49$, $n_k = 5$, 96.38% fit) using the *System Identification Toolbox* from MATLAB, this allowed to extract an approximate first-order dynamic with which to tune the controller. Figure 16.8 (b) shows the controller performance for a particular test. Initially, the control signal (q_c) increases to compensate for the trend observed in the condenser inlet temperature. At 11:45 the setpoint¹⁴ is changed to 24 °C, to which the controller immediately adapts by decreasing its input and allowing the temperature to increase. The system progressively evolves towards the new setpoint, reached at 12:30 the controller then maintains the desired temperature compensating for other - not shown in the figure - disturbances. A similar situation can be observed in the showcased test of Figure 16.9 – Temperatures and Flows. For the first operation point (11:00 onwards), the continuously increasing inlet temperature ($T_{c,in}$) is compensated by the controller, which increases the cooling flow rate to maintain the condenser outlet temperature at the setpoint. For the second operation point (12:16) the higher outlet temperature setpoint and turning on of the cooling tower allowing the inlet temperature to stabilize permits the controller to reduce the cooling flow rate and remain relatively unchanged.

14: i.e. reference

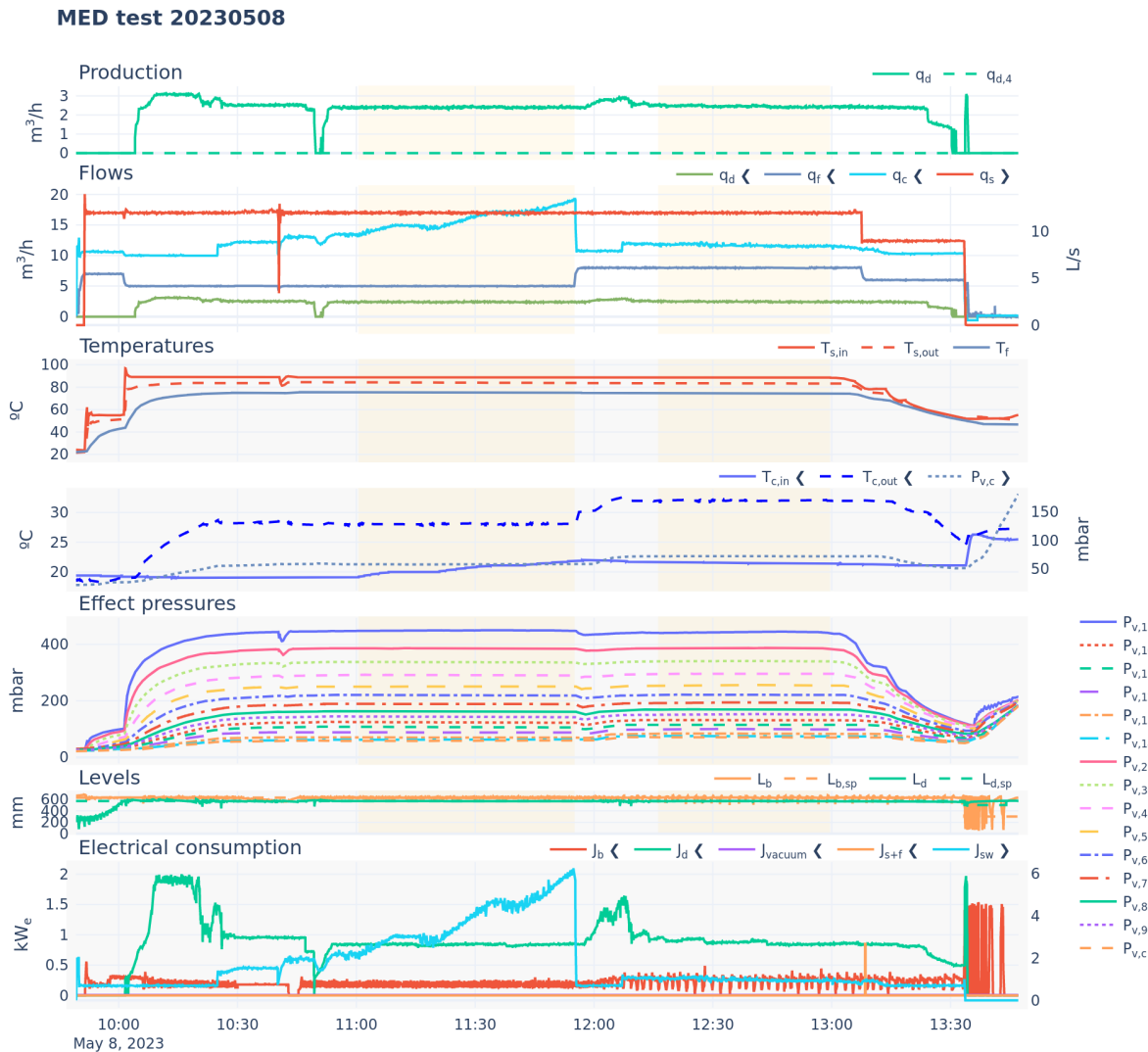


Figure 16.9: Test results. Several days available in interactive version



Reproducibility and the effect of the steady state duration

The operation points pairs 1–2 and 3–4 in Table 16.3 are the same test, *i.e.* the same operating conditions, but performed on different days. Particularly for 1–2, the duration of the steady state is significantly different (16 and 76 minutes, respectively). The obtained performance metrics are similar, with almost identical values for the energetic and separation metrics. Slight differences, but still within the uncertainty margin are observed in metrics influenced by electrical consumption—which vary between tests due to differences in the cooling water inlet temperature: 17 (1) vs 13 (2) m^3/h for the cooling water flow rate, translates into a 0.3% difference in second law efficiency and 0.1 KWh_e for SEEC. Inlet condenser temperature conditions are more similar in 3–4 (22.6 vs

Table 16.3: Measured variables and performance metrics for some operation points of the experimental campaign. The values are expressed as mean \pm standard deviation with a coverage factor of 2 (95% confidence interval). D is the duration of the steady state period.

	Test date (UTC)	D (min)	Performance metrics						
			GOR (-)	STEC (kW _{th})	SEEC (kW _e)	RR (-)	RI (-)	η_{II} (%)	SEXC (kWh _{ex} /m ³)
1	20230331 12:15	16	11 \pm 1	60 \pm 6	3.9 \pm 0.2	29 \pm 1	0.35 \pm 0.02	8.0 \pm 0.6	10.9 \pm 0.8
2	20230418 12:22	76	11 \pm 1	59 \pm 6	4.0 \pm 0.2	29 \pm 2	0.35 \pm 0.02	7.7 \pm 0.6	11.3 \pm 0.9
3	20230329 13:10	24	10.1 \pm 0.7	66 \pm 5	3.9 \pm 0.2	30 \pm 2	0.35 \pm 0.02	6.9 \pm 0.4	12.7 \pm 0.8
4	20230414 12:51	27	10.2 \pm 0.7	65 \pm 5	3.9 \pm 0.2	30 \pm 2	0.36 \pm 0.02	6.8 \pm 0.4	12.8 \pm 0.8
5	20230511 11:23	32	8.1 \pm 0.4	81 \pm 4	3.2 \pm 0.2	44 \pm 2	0.52 \pm 0.02	4.6 \pm 0.3	17.8 \pm 0.9
6	20230414 11:49	18	11 \pm 1	59 \pm 5	3.8 \pm 0.2	47 \pm 3	0.56 \pm 0.03	7.2 \pm 0.5	11.9 \pm 0.9
7	20230508 11:00	54	7.0 \pm 0.4	93 \pm 6	3.7 \pm 0.2	48 \pm 3	0.57 \pm 0.03	3.9 \pm 0.3	21 \pm 1

	Measured variables										
	$T_{c,in}$ (°C)	$T_{c,out}$ (°C)	q_s (L s ⁻¹)	q_f (m ³ h ⁻¹)	q_d (m ³ h ⁻¹)	$T_{s,out}$ (°C)	$T_{c,in}$ (°C)	w_f (mS cm ⁻¹)	w_d (μS cm ⁻¹)	q_c (m ³ h ⁻¹)	J (kW)
1	64.0 \pm 0.8	28.1 \pm 0.6	12.0 \pm 0.2	8.0 \pm 0.1	2.4 \pm 0.1	61.1 \pm 0.7	24.5 \pm 0.7	67.4 \pm 0.7	8.00 \pm 0.08	17 \pm 1	(8.0 \pm 0.2) \times 10 ³
2	64.0 \pm 0.7	28.0 \pm 0.6	12.0 \pm 0.3	8.0 \pm 0.1	2.3 \pm 0.1	61.2 \pm 0.7	23 \pm 1	67.4 \pm 0.7	8.00 \pm 0.08	13 \pm 2	(8.1 \pm 0.2) \times 10 ³
3	68.0 \pm 0.7	28.0 \pm 0.6	12.0 \pm 0.2	8.0 \pm 0.1	2.4 \pm 0.1	64.8 \pm 0.7	22.6 \pm 0.6	67.4 \pm 0.7	8.00 \pm 0.08	13.8 \pm 0.8	(8.1 \pm 0.2) \times 10 ³
4	68.0 \pm 0.7	27.9 \pm 0.8	12.0 \pm 0.3	8.0 \pm 0.1	2.4 \pm 0.1	64.8 \pm 0.6	21.4 \pm 0.8	67.4 \pm 0.7	8.00 \pm 0.08	10.9 \pm 0.9	(8.1 \pm 0.2) \times 10 ³
5	88.9 \pm 0.9	29 \pm 1	12.0 \pm 0.3	7.0 \pm 0.1	3.1 \pm 0.1	83.8 \pm 0.9	22 \pm 1	64.7 \pm 0.6	8.00 \pm 0.08	20.1 \pm 0.3	(7.9 \pm 0.3) \times 10 ³
6	68.0 \pm 0.7	28.0 \pm 0.5	12.0 \pm 0.3	5.0 \pm 0.1	2.4 \pm 0.1	65.2 \pm 0.7	20.8 \pm 0.6	67.4 \pm 0.7	8.00 \pm 0.08	10.1 \pm 0.4	(7.9 \pm 0.3) \times 10 ³
7	89.0 \pm 0.7	28.1 \pm 0.6	12.0 \pm 0.3	5.0 \pm 0.1	2.4 \pm 0.1	84.4 \pm 0.8	21 \pm 2	64.5 \pm 0.7	8.00 \pm 0.08	16 \pm 3	(7.8 \pm 0.3) \times 10 ³

21.4 °C), making differences for all metrics negligible.

Thus, it can be stated that the proposed methodology provides reproducible results and that the quality of stable operation and the ability to correctly identify it are of greater importance than the specific duration of the steady state.

16.5.2 Results analysis

In Table 16.3 operation points 4-5 and 6-7 compare low and high TBT operation. Two of them (4 and 6) receive heat at 68°C, while they differ in the feedwater flow rate (q_f), one (4) with a higher value (8 m³/h) and the other (6) at a lower one (5 m³/h). The other two operation points receive heat at 89°C and similar feedwater flow rate¹⁵. The first two operation points result in an approximate TBT of 61.5°C while the last two operation points have an approximate TBT of 79.2°C. This operation points selection is made to compare the performance of the plant at low and high TBT operation with otherwise equivalent conditions.

Performance analysis. The first immediate observation is that contrary to what stated in the introduction, the performance of the plant does not improve with higher heat source temperatures, on the contrary it decreases: GOR -20% and -36% for the low (4-5) and high (6-7) q_f scenario, respectively. Results are even worse in terms of second law efficiency: -32% and -46%, respectively, since higher quality heat is being destroyed. In summary, more energy, of better quality is being consumed to produce distillate less efficiently

This can be explained by the fact that the increase in the heat source temperature is not taken advantage of by introducing more effects, which would provide the increase in efficiency.

On the other hand, the concentration achieved does increase significantly for the high q_f scenario, with a 47% increase in the recovery ratio. This is not the case for the low q_f scenario, where the recovery ratio is similar to the low temperature operation point. A possible explanation is presented hereinafter.

Using a physical model of the plant¹⁶, a better insight into the inner working of the plant can be obtained. The model is based on the energy and mass balances of the system, and it is used to estimate different outputs at the effect level, such as the temperature and pressure of the vapor, the distillate production, and the brine concentration. This allows to analyze the temperature and concentration

15: Equal between 4 and 5, slightly different but comparable between 6 and 7

comprobar números

16: See Section ??

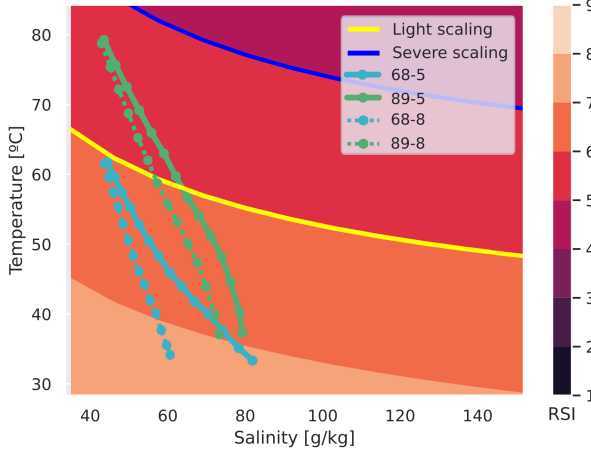


Figure 16.10: Temperature and concentration evolution for operation points at each effect in the MED plant. Surface represents the RSI.

evolution and visualize it as shown in Figure 16.10. According to the RSI, the high temperature operation points (5, 7) do get into the light scaling zone for the first 7 effects, while the low temperature operation points (4, 6) remain in the stable water zone for all effects.

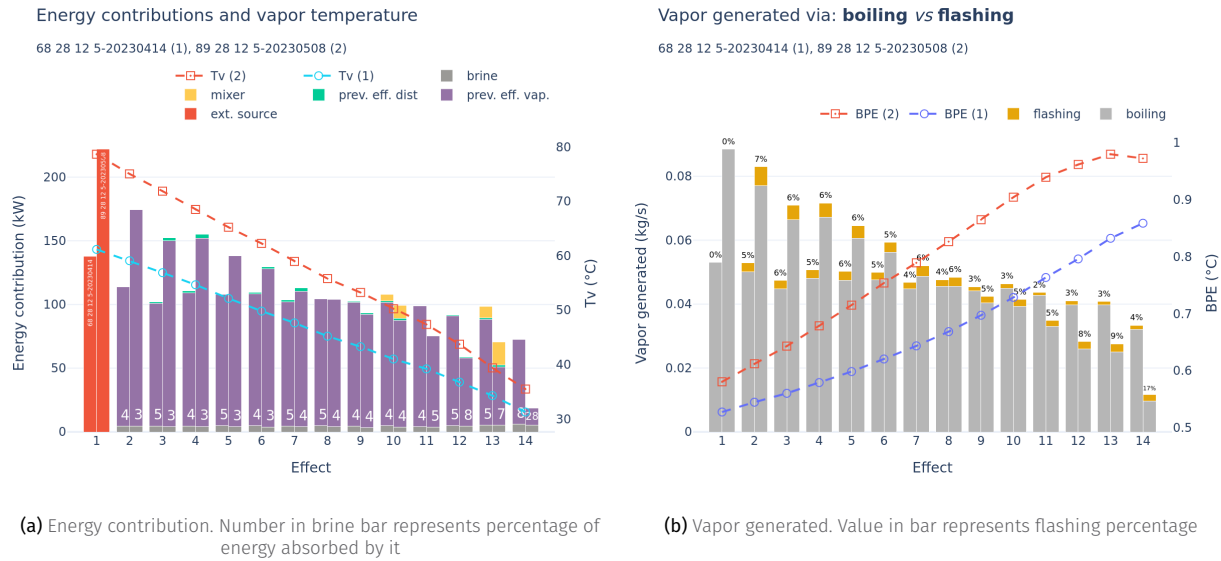


Figure 16.11: Per effect comparison between low and high TBT operation points

A per effect comparison can also be made in terms of energy contribution for vapor generation. This is shown in Figure 16.11 (a) for the low q_f scenario. In the first effect a stark difference between low and high operation can be seen, with almost double the power released, producing almost double the vapor (Figure 16.11 – (b)). However this difference is not maintained in the following effects, but an opposite trend is observed. Effect 8 is the crossing point and from there on the low temperature operation point produces more vapor. Another interesting comparison is the mixer energy contribution, the higher temperature of the distillate produced in the first effects becomes a significant contributor in the later effects, with a greater impact compared to the low temperature operation. Thus, distillate distribution is more effective when

total plant temperature differences are higher.

An explanation as to why vapor generation seems limited and thus the achieved concentration, can be the Boiling Point Elevation (BPE) of the brine (see Figure 16.11 (b)), which is a function of temperature and concentration, increasing with the latter. This means that the temperature difference between the brine and the vapor is reduced, and, which in turn reduces the boiling driving force. In the visualized case, the final BPE value for the low-temperature operation is reached by effect 9 of the high temperature one. In an MED plant, the vapor generated in the previous effect is the driving force for the next effect (Figure 16.11 – (a)), low vapor production on one effect means a diminished force for heat transfer in the next one, which in turn reduces the vapor production on that effect. It is an exponential decay process. That is why despite the larger energy availability in the first effects, the better balanced effects of the low temperature operation turns out to ultimately produce similar levels of separation [79].

[79]: Lienhard V (2019), "Energy Savings in Desalination Technologies"

In this figure, it can be seen than flashing takes a more relevant role in vapor generation in the latter effects of the high temperature alternative, since it is not affected by BPE (8,9 and 17% of the total vapor generated in effects 12, 13 and 14, respectively). This indicates that maybe flashing is a good alternative to increase the vapor production in the latter stages of a thermal brine concentrator plant.

Remark 16.5.1 A MED-MSF hybrid could be a good alternative to increase the brine concentration in the last effects, where the vapor production is limited by the BPE. Another option worth exploring is variable geometry effects, in order to increase temperature differences and maintain vapor production at higher concentrations.

17: Section 14 (Reproducibility and the effect of the steady state duration)

Scaling assessment. To assess whether scaling occurred during high-temperature operation, control tests were conducted both before the high-temperature tests and repeated after about 30 hours of operation. In Table 16.3 the same operation points used to validate the reproducibility¹⁷, i.e.: 1-2 and 3-4 can be used to draw conclusions. Aside from the mentioned differences in metrics influenced by electrical consumption, the performance metrics values are consistent across tests, suggesting that the system is operating efficiently without significant fouling or scaling.

Incluir una gráfica de los coeficientes de transferencia para ambos tests?

CONCLUSIONS AND OUTLOOK

Conclusions

Outlook and future work

Optimal water and electricity management in a combined cooling system

Improved Pareto front computation. In the current optimization implementation, the Pareto front for each step in the optimization horizon is constructed using a grid search over the decision space. This approach can become computationally expensive, especially as the grid resolution increases. Additionally, the Pareto front must be recalculated from scratch at every step, even though the sequential steps are often very similar—cost parameters remain constant, and only the thermal load and weather conditions change, typically with small variations. A more efficient solution would be to use a multi-objective optimization algorithm such as NSGA-II [[<empty citation>](#)], which can transfer evolved populations between successive evaluations, significantly reducing redundant computations.

<empty citation>

Better water management In the current implementation, the primary water source is distributed evenly each day, so the optimization process uses up the entire supply daily. However, a more intelligent daily distribution—essentially, a new optimization problem—could improve water management by allocating different amounts on different days, based on expected weather conditions and predicted generation. This approach would likely be incorporated as a new layer in the hierarchical control structure.¹⁸

Techno-economic analysis. The presented cooling alternatives comparative in this thesis focus on the operation cost of the system, but to get a better picture of the alternatives performance, a techno-economic analysis that includes the capital cost of the system and the expected lifetime of the components should be performed *i.e.* considering all costs associated with the system the plant's lifetime. This is currently being worked on as part of [SOLHycool], where the methodology presented here in terms of operation costs will be integrated in a techno-economic analysis for different case studies.

18: The resulting structure would be: 1. Water allocation, 2. CCS operation optimization, 3. CC regulatory control.

Energy management in MED processes driven by variable energy sources

Alternative configurations for an MED brine concentrator. Configuraciones alternativas para procesos MED para aplicaciones de concentración de salmueras: geometría variable de efectos, fuentes externas en efectos distintos al primero, acoplamiento con MSF para efectos posteriores.

Alternative configurations for solar-driven MED. Configuraciones alternativas para el proceso solar MED (almacenamiento con distintos puntos de carga y descarga, MED con distintos puntos de fuente externa, etc. Incluir diagrama de draw.io con las distintas configuraciones)

Derived scientific contributions

1. Publicaciones en revista
2. Contribuciones a congreso
3. Coloquios doctorales
4. Colaboraciones en proyectos de investigación
5. Estancias de investigación

6. Repositorios de código
7. Repositorios de datos
8. Herramientas interactivas
9. Contribuciones a librerías de código abierto?

Bibliography

Here are the references in citation order.

- [1] Martin T. Hagan et al. *Neural Network Design*. Martin Hagan, 2014. 800 pp. (cited on pages 10, 11).
- [2] Mark Hudson Beale, Martin T Hagan, and Howard B Demuth. "Neural Network Toolbox." In: *User's Guide, MathWorks* 2 (2010), pp. 77–81 (cited on page 11).
- [3] Lonnie Hamm, B. Wade Brorsen, and Martin T. Hagan. "Comparison of Stochastic Global Optimization Methods to Estimate Neural Network Weights." In: *Neural Processing Letters* 26.3 (Dec. 1, 2007), pp. 145–158. doi: [10.1007/s11063-007-9048-7](https://doi.org/10.1007/s11063-007-9048-7). (Visited on 03/16/2024) (cited on page 11).
- [4] Jiri Nossent, Pieter Elsen, and Willy Bauwens. "Sobol'sensitivity Analysis of a Complex Environmental Model." In: *Environmental Modelling & Software* 26.12 (2011), pp. 1515–1525 (cited on page 13).
- [5] Zong Woo Geem, Joong Hoon Kim, and G.V. Loganathan. "A New Heuristic Optimization Algorithm: Harmony Search." In: *SIMULATION* 76.2 (Feb. 1, 2001), pp. 60–68. doi: [10.1177/003754970107600201](https://doi.org/10.1177/003754970107600201). (Visited on 06/16/2025) (cited on page 17).
- [6] Francesco Biscani and Dario Izzo. "A Parallel Global Multiobjective Framework for Optimization: Pagmo." In: *Journal of Open Source Software* 5.53 (2020), p. 2338. doi: [10.21105/joss.02338](https://doi.org/10.21105/joss.02338) (cited on page 17).
- [7] IEA. *Energy Technology Perspectives*. IEA. 2014. URL: <https://www.iea.org/reports/energy-technology-perspectives-2014> (visited on 11/30/2023) (cited on page 27).
- [8] Richard Thonig, Alina Gilmanova, and Johan Lilliestam. *CSP.Guru* 2023-07-01. Zenodo, July 1, 2023. (Visited on 05/31/2025) (cited on pages 27, 68).
- [9] Ebrahim Rezaei, Sorous Shafiei, and Aydin Abdollahnezhad. "Reducing Water Consumption of an Industrial Plant Cooling Unit Using Hybrid Cooling Tower." In: *Energy Conversion and Management* 51.2 (Feb. 1, 2010), pp. 311–319. doi: [10.1016/j.enconman.2009.09.027](https://doi.org/10.1016/j.enconman.2009.09.027). (Visited on 03/10/2023) (cited on page 27).
- [10] Wanchai Asvapoositkul and Mantheerapol Kuansathan. "Comparative Evaluation of Hybrid (Dry/Wet) Cooling Tower Performance." In: *Applied Thermal Engineering* 71.1 (Oct. 5, 2014), pp. 83–93. doi: [10.1016/j.applthermaleng.2014.06.023](https://doi.org/10.1016/j.applthermaleng.2014.06.023). (Visited on 03/10/2023) (cited on page 27).
- [11] Hemin Hu et al. "Thermodynamic Characteristics of Thermal Power Plant with Hybrid (Dry/Wet) Cooling System." In: *Energy* 147 (Mar. 15, 2018), pp. 729–741. doi: [10.1016/j.energy.2018.01.074](https://doi.org/10.1016/j.energy.2018.01.074). (Visited on 03/10/2023) (cited on page 27).
- [12] S. El Marazgioui and A. El Fadar. "Impact of Cooling Tower Technology on Performance and Cost-Effectiveness of CSP Plants." In: *Energy Conversion and Management* 258 (Apr. 15, 2022), p. 115448. doi: [10.1016/j.enconman.2022.115448](https://doi.org/10.1016/j.enconman.2022.115448). (Visited on 03/29/2024) (cited on page 27).
- [13] G. Barigozzi, A. Perdichizzi, and S. Ravelli. "Wet and Dry Cooling Systems Optimization Applied to a Modern Waste-to-Energy Cogeneration Heat and Power Plant." In: *Applied Energy* 88.4 (Apr. 1, 2011), pp. 1366–1376. doi: [10.1016/j.apenergy.2010.09.023](https://doi.org/10.1016/j.apenergy.2010.09.023). (Visited on 03/10/2023) (cited on page 28).
- [14] G. Barigozzi, A. Perdichizzi, and S. Ravelli. "Performance Prediction and Optimization of a Waste-to-Energy Cogeneration Plant with Combined Wet and Dry Cooling System." In: *Applied Energy* 115 (Feb. 15, 2014), pp. 65–74. doi: [10.1016/j.apenergy.2013.11.024](https://doi.org/10.1016/j.apenergy.2013.11.024). (Visited on 03/10/2023) (cited on page 28).
- [15] Patricia Palenzuela et al. "Experimental Assessment of a Pilot Scale Hybrid Cooling System for Water Consumption Reduction in CSP Plants." In: *Energy* 242 (Mar. 1, 2022), p. 122948. doi: [10.1016/j.energy.2021.122948](https://doi.org/10.1016/j.energy.2021.122948). (Visited on 03/10/2023) (cited on page 28).
- [16] Faisal Asfand et al. "Thermodynamic Performance and Water Consumption of Hybrid Cooling System Configurations for Concentrated Solar Power Plants." In: *Sustainability* 12.11 (2020). doi: [10.3390/su12114739](https://doi.org/10.3390/su12114739) (cited on page 28).
- [17] Raniyah Wazirali et al. "State-of-the-Art Review on Energy and Load Forecasting in Microgrids Using Artificial Neural Networks, Machine Learning, and Deep Learning Techniques." In: *Electric Power Systems Research* 225 (Dec. 1, 2023), p. 109792. doi: [10.1016/j.epsr.2023.109792](https://doi.org/10.1016/j.epsr.2023.109792). (Visited on 03/31/2024) (cited on page 28).
- [18] F. Merkel. "Verdunstungskühlung." In: *VDI Zeitschrift Deutscher Ingenieure, Berlin, Alemania* (1925), pp. 123–128 (cited on pages 29, 31).

- [19] C Bourillot. "Hypotheses of Calculation of the Water Flow Rate Evaporated in a Wet Cooling Tower." In: (Aug. 1983) (cited on page 29).
- [20] H. Jaber and R. L. Webb. "Design of Cooling Towers by the Effectiveness-NTU Method." In: *Journal of Heat Transfer* 111.4 (Nov. 1989), pp. 837–843. doi: [10.1115/1.3250794](https://doi.org/10.1115/1.3250794) (cited on page 29).
- [21] M. Poppe and H. Rögener. "Berechnung von Rückkühlwerken." In: *VDI wärmeatlas* (1991), p. Mi 1 (cited on pages 30, 31).
- [22] J.C. Kloppers and D.G. Kröger. "A Critical Investigation into the Heat and Mass Transfer Analysis of Counterflow Wet-Cooling Towers." In: *International Journal of Heat and Mass Transfer* 48.3 (2005), pp. 765–777 (cited on page 30).
- [23] C. G. Cutillas et al. "Energetic, Exergetic and Environmental (3E) Analyses of Different Cooling Technologies (Wet, Dry and Hybrid) in a CSP Thermal Power Plant." In: *Case Studies in Thermal Engineering* 28 (Dec. 1, 2021), p. 101545. doi: [10.1016/j.csite.2021.101545](https://doi.org/10.1016/j.csite.2021.101545). (Visited on 03/27/2024) (cited on page 30).
- [24] M. Hosoz, H. M. Ertunc, and H. Bulgurcu. "Performance Prediction of a Cooling Tower Using Artificial Neural Network." In: *Energy Conversion and Management* 48.4 (Apr. 1, 2007), pp. 1349–1359. doi: [10.1016/j.enconman.2006.06.024](https://doi.org/10.1016/j.enconman.2006.06.024). (Visited on 03/08/2023) (cited on pages 30, 50).
- [25] Ming Gao et al. "Artificial Neural Network Model Research on Effects of Cross-Wind to Performance Parameters of Wet Cooling Tower Based on Level Froude Number." In: *Applied Thermal Engineering* 51.1 (Mar. 1, 2013), pp. 1226–1234. doi: [10.1016/j.applthermaleng.2012.06.053](https://doi.org/10.1016/j.applthermaleng.2012.06.053). (Visited on 03/08/2023) (cited on page 30).
- [26] Jialiang Song et al. "A Novel Approach for Energy Efficiency Prediction of Various Natural Draft Wet Cooling Towers Using ANN." In: *Journal of Thermal Science* 30.3 (May 2021), pp. 859–868. doi: [10.1007/s11630-020-1296-0](https://doi.org/10.1007/s11630-020-1296-0). (Visited on 03/04/2023) (cited on page 30).
- [27] P. Navarro et al. "Critical Evaluation of the Thermal Performance Analysis of a New Cooling Tower Prototype." In: *Applied Thermal Engineering* 213 (2022), p. 118719. doi: [10.1016/j.applthermaleng.2022.118719](https://doi.org/10.1016/j.applthermaleng.2022.118719) (cited on pages 30–32).
- [28] Ashrae. "HVAC Systems and Equipment." In: *Chapter 36 Cooling Towers*. 2004 (cited on pages 32, 49).
- [29] Lidia Martín and Mariano Martín. "Optimal Year-Round Operation of a Concentrated Solar Energy Plant in the South of Europe." In: *Applied Thermal Engineering* 59.1 (Sept. 25, 2013), pp. 627–633. doi: [10.1016/j.applthermaleng.2013.06.031](https://doi.org/10.1016/j.applthermaleng.2013.06.031). (Visited on 06/13/2025) (cited on page 37).
- [30] Mariano Martín. "Optimal Annual Operation of the Dry Cooling System of a Concentrated Solar Energy Plant in the South of Spain." In: *Energy* 84 (May 1, 2015), pp. 774–782. doi: [10.1016/j.energy.2015.03.041](https://doi.org/10.1016/j.energy.2015.03.041). (Visited on 06/12/2025) (cited on page 37).
- [31] David Wales and Jonathan Doye. "Global Optimization by Basin-Hopping and the Lowest Energy Structures of Lennard-Jones Clusters Containing up to 110 Atoms." In: *The Journal of Physical Chemistry A* 101.28 (July 1, 1997), pp. 5111–5116. doi: [10.1021/jp970984n](https://doi.org/10.1021/jp970984n). (Visited on 06/11/2025) (cited on page 43).
- [32] UNE. *Thermal Performance Acceptance Testing of Mechanical Draught Series Wet Cooling Towers*. manual. UNE. 2004 (cited on page 49).
- [33] CTI. *Code Tower, Standard Specifications. Acceptance Test Code for Water Cooling Towers*. manual. Cooling Technology Institute. 2000 (cited on page 49).
- [34] Juan Miguel Serrano et al. "Wet Cooling Tower Performance Prediction in CSP Plants: A Comparison between Artificial Neural Networks and Poppe's Model." In: *Energy* (May 29, 2024), p. 131844. doi: [10.1016/j.energy.2024.131844](https://doi.org/10.1016/j.energy.2024.131844). (Visited on 05/30/2024) (cited on page 49).
- [35] J Meldrum et al. "Life Cycle Water Use for Electricity Generation: A Review and Harmonization of Literature Estimates." In: *Environmental Research Letters* 8.1 (Mar. 2013), p. 015031. doi: [10.1088/1748-9326/8/1/015031](https://doi.org/10.1088/1748-9326/8/1/015031). (Visited on 05/28/2025) (cited on page 67).
- [36] Johan Lilliestam et al. "The Near- to Mid-Term Outlook for Concentrating Solar Power: Mostly Cloudy, Chance of Sun." In: *Energy Sources, Part B: Economics, Planning, and Policy* 16.1 (2021), pp. 23–41. doi: [10.1080/15567249.2020.1773580](https://doi.org/10.1080/15567249.2020.1773580) (cited on page 68).
- [37] Javier Bonilla et al. "CSP Data: A Data Discovery Web Application of Commercial CSP Plants." In: (July 2024) (cited on page 68).
- [38] Chaouki Ghenai et al. "Performance Analysis and Optimization of Hybrid Multi-Effect Distillation Adsorption Desalination System Powered with Solar Thermal Energy for High Salinity Sea Water." In: *Energy* 215 (Jan. 15, 2021), p. 119212. doi: [10.1016/j.energy.2020.119212](https://doi.org/10.1016/j.energy.2020.119212). (Visited on 01/08/2023) (cited on page 85).

- [39] Hyuk Soo Son et al. "Pilot Studies on Synergetic Impacts of Energy Utilization in Hybrid Desalination System: Multi-effect Distillation and Adsorption Cycle (MED-AD)." In: *Desalination* 477 (Mar. 1, 2020), p. 114266. doi: [10.1016/j.desal.2019.114266](https://doi.org/10.1016/j.desal.2019.114266). (Visited on 01/07/2023) (cited on page 85).
- [40] Greg Burgess and Keith Lovegrove. "Solar Thermal Powered Desalination: Membrane versus Distillation Technologies." In: (Jan. 2000) (cited on page 85).
- [41] F. Silva Pinto and R. Cunha Marques. "Desalination Projects Economic Feasibility: A Standardization of Cost Determinants." In: *Renewable and Sustainable Energy Reviews* 78 (Oct. 2017), pp. 904–915. doi: [10.1016/j.rser.2017.05.024](https://doi.org/10.1016/j.rser.2017.05.024). (Visited on 07/27/2023) (cited on page 85).
- [42] Karan H. Mistry et al. "Entropy Generation Analysis of Desalination Technologies." In: *Entropy. An International and Interdisciplinary Journal of Entropy and Information Studies* 13.10 (2011), pp. 1829–1864. doi: [10.3390/e13101829](https://doi.org/10.3390/e13101829) (cited on page 85).
- [43] H. T. El-Dessouky and H. M. Ettouney. *Fundamentals of Salt Water Desalination*. Elsevier, Mar. 20, 2002. 691 pp. (cited on pages 85, 87, 97).
- [44] A. Christ, K. Regenauer-Lieb, and H.T. Chua. "Thermodynamic Optimisation of Multi Effect Distillation Driven by Sensible Heat Sources." In: *Desalination* 336.1 (2014), pp. 160–167. doi: [10.1016/j.desal.2013.12.006](https://doi.org/10.1016/j.desal.2013.12.006) (cited on pages 85, 87).
- [45] John H. Lienhard et al. "Thermodynamics, Exergy, and Energy Efficiency in Desalination Systems." In: *Lienhard via Angie Locknar* (2017). (Visited on 04/04/2022) (cited on pages 85, 86, 91).
- [46] Andrew T. Bouma, Jaichander Swaminathan, and John H. Lienhard V. "Metrics Matter: Accurately Defining Energy Efficiency in Desalination." In: *Journal of Heat Transfer* 142.12 (Oct. 7, 2020). doi: [10.1115/1.4048250](https://doi.org/10.1115/1.4048250). (Visited on 03/22/2023) (cited on pages 85, 87, 91).
- [47] M. A. Darwish, Faisal Al-Juwayhel, and Hassan K. Abdulraheim. "Multi-Effect Boiling Systems from an Energy Viewpoint." In: *Desalination* 194.1 (June 10, 2006), pp. 22–39. doi: [10.1016/j.desal.2005.08.029](https://doi.org/10.1016/j.desal.2005.08.029). (Visited on 06/01/2022) (cited on pages 86, 91).
- [48] Muhammad Wakil Shahzad, Muhammad Burhan, and Kim Choom Ng. "A Standard Primary Energy Approach for Comparing Desalination Processes." In: *npj Clean Water* 2.1 (Jan. 7, 2019), pp. 1–7. doi: [10.1038/s41545-018-0028-4](https://doi.org/10.1038/s41545-018-0028-4). (Visited on 07/23/2024) (cited on page 86).
- [49] Doriano Brogioli, Fabio La Mantia, and Ngai Yin Yip. "Thermodynamic Analysis and Energy Efficiency of Thermal Desalination Processes." In: *Desalination* 428 (Feb. 15, 2018), pp. 29–39. doi: [10.1016/j.desal.2017.11.010](https://doi.org/10.1016/j.desal.2017.11.010). (Visited on 01/05/2023) (cited on pages 86, 97).
- [50] K.S. Spiegler and Y.M. El-Sayed. "El-Sayed, Y.M.: The Energetics of Desalination Processes. Desalination 134, 109–128." In: *Desalination* 134 (Apr. 1, 2001), pp. 109–128. doi: [10.1016/S0011-9164\(01\)00121-7](https://doi.org/10.1016/S0011-9164(01)00121-7) (cited on page 86).
- [51] Mostafa H. Sharqawy, John H. Lienhard V, and Syed M. Zubair. "On Exergy Calculations of Seawater with Applications in Desalination Systems." In: *International Journal of Thermal Sciences* 50.2 (Feb. 1, 2011), pp. 187–196. doi: [10.1016/j.ijthermalsci.2010.09.013](https://doi.org/10.1016/j.ijthermalsci.2010.09.013). (Visited on 03/22/2023) (cited on pages 86, 90).
- [52] Mostafa H. Sharqawy, Syed M. Zubair, and John H. Lienhard. "Formulation of Seawater Flow Exergy Using Accurate Thermodynamic Data." In: *Prof. Lienhard via Angie Locknar* (Nov. 2010). (Visited on 04/13/2023) (cited on page 86).
- [53] Karan H. Mistry and John H. Lienhard V. "Effect of Nonideal Solution Behavior on Desalination of a Sodium Chloride (NaCl) Solution and Comparison to Seawater." In: *Karan Mistry* (Nov. 2012). (Visited on 04/22/2023) (cited on page 86).
- [54] Karan H. Mistry and John H. Lienhard. "Generalized Least Energy of Separation for Desalination and Other Chemical Separation Processes." In: *Entropy. An International and Interdisciplinary Journal of Entropy and Information Studies* 15.6 (2013), pp. 2046–2080. doi: [10.3390/e15062046](https://doi.org/10.3390/e15062046) (cited on page 86).
- [55] Gregory P. Thiel et al. "Energy Consumption in Desalinating Produced Water from Shale Oil and Gas Extraction." In: *Desalination. Energy and Desalination* 366 (June 15, 2015), pp. 94–112. doi: [10.1016/j.desal.2014.12.038](https://doi.org/10.1016/j.desal.2014.12.038). (Visited on 03/06/2023) (cited on pages 86, 89, 91).
- [56] Loreto Valenzuela, Rafael López-Martín, and Eduardo Zarza. "Optical and Thermal Performance of Large-Size Parabolic-Trough Solar Collectors from Outdoor Experiments: A Test Method and a Case Study." In: *Energy* 70 (June 1, 2014), pp. 456–464. doi: [10.1016/j.energy.2014.04.016](https://doi.org/10.1016/j.energy.2014.04.016). (Visited on 07/17/2024) (cited on page 86).
- [57] Christoph Prahl, Christoph Happich, and Jesús Fernández. *Protocol for Characterization of Complete Solar Concentrators Using Photogrammetry or Deflectometry*. WP14 – Task 14.2. DLR, Feb. 2018 (cited on page 86).

- [58] Rocío Bayón and Esther Rojas. "Development of a New Methodology for Validating Thermal Storage Media: Application to Phase Change Materials." In: *International Journal of Energy Research* 43.12 (2019), pp. 6521–6541. doi: [10.1002/er.4589](https://doi.org/10.1002/er.4589). (Visited on 07/17/2024) (cited on page 86).
- [59] Karan H. Mistry and John H. Lienhard. "An Economics-Based Second Law Efficiency." In: *Entropy* 15.7 (7 July 2013), pp. 2736–2765. doi: [10.3390/e15072736](https://doi.org/10.3390/e15072736). (Visited on 03/22/2023) (cited on page 87).
- [60] Alexander Christ et al. "Techno-Economic Analysis of Geothermal Desalination Using Hot Sedimentary Aquifers: A Pre-Feasibility Study for Western Australia." In: *Desalination* 404 (Feb. 17, 2017), pp. 167–181. doi: [10.1016/j.desal.2016.11.009](https://doi.org/10.1016/j.desal.2016.11.009). (Visited on 01/05/2023) (cited on page 87).
- [61] Alexander Christ, Klaus Regenauer-Lieb, and Hui Tong Chua. "Application of the Boosted MED Process for Low-Grade Heat Sources — A Pilot Plant." In: *Desalination. Energy and Desalination* 366 (June 15, 2015), pp. 47–58. doi: [10.1016/j.desal.2014.10.032](https://doi.org/10.1016/j.desal.2014.10.032). (Visited on 01/04/2023) (cited on page 87).
- [62] Alexander Christ, Klaus Regenauer-Lieb, and Hui Tong Chua. "Boosted Multi-Effect Distillation for Sensible Low-Grade Heat Sources: A Comparison with Feed Pre-Heating Multi-Effect Distillation." In: *Desalination. Energy and Desalination* 366 (June 15, 2015), pp. 32–46. doi: [10.1016/j.desal.2014.12.047](https://doi.org/10.1016/j.desal.2014.12.047). (Visited on 01/04/2023) (cited on page 87).
- [63] Edward Jones et al. "The State of Desalination and Brine Production: A Global Outlook." In: *Science of The Total Environment* 657 (Mar. 20, 2019), pp. 1343–1356. doi: [10.1016/j.scitotenv.2018.12.076](https://doi.org/10.1016/j.scitotenv.2018.12.076). (Visited on 06/29/2022) (cited on page 88).
- [64] Patricia Palenzuela, Diego-César Alarcón-Padilla, and Guillermo Zaragoza. *Concentrating Solar Power and Desalination Plants*. Oct. 9, 2015 (cited on pages 88, 92).
- [65] John H. Lienhard V et al. "SOLAR DESALINATION." In: *Annual Review of Heat Transfer* 15 (2012). doi: [10.1146/annurevheattransfer.2012.004659](https://doi.org/10.1146/annurevheattransfer.2012.004659). (Visited on 10/17/2024) (cited on page 89).
- [66] Qian Chen et al. "A Zero Liquid Discharge System Integrating Multi-Effect Distillation and Evaporative Crystallization for Desalination Brine Treatment." In: *Desalination* 502 (Apr. 2021), p. 114928. doi: [10.1016/j.desal.2020.114928](https://doi.org/10.1016/j.desal.2020.114928) (cited on page 90).
- [67] Adrian Bejan. *Advanced Engineering Thermodynamics*. John Wiley & Sons, 2016 (cited on page 90).
- [68] JCGM 100:2008. *GUM 1995 with Minor Corrections. Evaluation of Measurement Data — Guide to the Expression of Uncertainty in Measurement*. Joint Committee for Guides in Metrology, 2008. URL: https://www.bipm.org/documents/20126/2071204/JCGM_101_2008_E.pdf/325dcaad-c15a-407c-1105-8b7f322d651c (cited on page 94).
- [69] Ralph C. Smith. *Uncertainty Quantification: Theory, Implementation, and Applications*. SIAM, Dec. 2, 2013. 400 pp. (cited on page 94).
- [70] nist. "NIST Guidelines for Evaluating and Expressing the Uncertainty of NIST Measurement Results Cover." In: *NIST* (). (Visited on 06/16/2023) (cited on page 95).
- [71] JCGM101:2008. *Evaluation of Measurement Data — Supplement 1 to the "Guide to the Expression of Uncertainty in Measurement"—Propagation of Distributions Using a Monte Carlo Method*. Joint Committee for Guides in Metrology, 2008. URL: https://www.bipm.org/documents/20126/2071204/JCGM_101_2008_E.pdf/325dcaad-c15a-407c-1105-8b7f322d651c (cited on page 95).
- [72] Ulli Wolff. "Monte Carlo Errors with Less Errors." In: *Computer Physics Communications* 176.5 (Mar. 2007), p. 383. doi: [10.1016/j.cpc.2006.12.001](https://doi.org/10.1016/j.cpc.2006.12.001). (Visited on 06/19/2023) (cited on page 95).
- [73] Milan Korbel et al. "Steady State Identification for On-Line Data Reconciliation Based on Wavelet Transform and Filtering." In: *Computers & Chemical Engineering* 63 (Apr. 17, 2014), pp. 206–218. doi: [10.1016/j.compchemeng.2014.02.003](https://doi.org/10.1016/j.compchemeng.2014.02.003). (Visited on 12/14/2022) (cited on page 95).
- [74] Taiwen Jiang et al. "Application of Steady-State Detection Method Based on Wavelet Transform." In: *Computers & Chemical Engineering* 27.4 (Apr. 15, 2003), pp. 569–578. doi: [10.1016/S0098-1354\(02\)00235-1](https://doi.org/10.1016/S0098-1354(02)00235-1). (Visited on 01/03/2023) (cited on page 95).
- [75] Taiwen Jiang, Bingzhen Chen, and Xiaorong He. "Industrial Application of Wavelet Transform to the On-Line Prediction of Side Draw Qualities of Crude Unit." In: *Computers & Chemical Engineering* 24.2 (July 15, 2000), pp. 507–512. doi: [10.1016/S0098-1354\(00\)00520-2](https://doi.org/10.1016/S0098-1354(00)00520-2). (Visited on 12/27/2022) (cited on page 95).
- [76] Karl Johan Åström and Tore Hägglund. *PID Controllers: Theory, Design, and Tuning*. ISA - The Instrumentation, Systems and Automation Society, 1995 (cited on page 96).

- [77] Karan H. Mistry, Mohamed A. Antar, and John H. Lienhard V. "An Improved Model for Multiple Effect Distillation." In: *Desalination and Water Treatment* 51.4–6 (Jan. 1, 2013), pp. 807–821. doi: [10.1080/19443994.2012.703383](https://doi.org/10.1080/19443994.2012.703383). (Visited on 06/01/2022) (cited on page 97).
- [78] John W Ryznar. "A New Index for Determining Amount of Calcium Carbonate Scale Formed by a Water." In: *Journal-American Water Works Association* 36.4 (1944), pp. 472–483 (cited on page 97).
- [79] John H. Lienhard V. "Energy Savings in Desalination Technologies: Reducing Entropy Generation by Transport Processes." In: *Journal of Heat Transfer* 141.7 (May 17, 2019). doi: [10.1115/1.4043571](https://doi.org/10.1115/1.4043571). (Visited on 03/30/2023) (cited on page 104).

